



UNIVERSIDADE D
COIMBRA

Zoé Ladieu Arcas Arnaut Moreira

**DEVELOPMENT OF CATIONIC PHOTOSENSITIZERS FOR
PHOTOINACTIVATION OF MICROORGANISMS**

**Dissertação no âmbito do Mestrado em Química Medicinal orientada pela
Professora Doutora Maria Miguéns Pereira coorientada pela Doutora Sara
Martinho Almeida Pinto e apresentada ao Departamento de Química da Faculdade
de Ciências e Tecnologia da Universidade de Coimbra**

Junho de 2021

Faculdade de Ciências e Tecnologia

Development of cationic photosensitizers for photoinactivation of microorganisms

Zoé Ladieu Arcas Arnaut Moreira

Dissertação de Mestrado na área científica de Química Medicinal orientada pela Senhora Professora Doutora Maria Miguéns Pereira, coorientada pela Doutora Sara Martinho Almeida Pinto e apresentada ao Departamento de Química da Faculdade de Ciências e Tecnologia da Universidade de Coimbra

Junho de 2021



UNIVERSIDADE D
COIMBRA

In memory of my godfather.

Acknowledgments

A work of science requires teamwork, and this Thesis is not an exception. In this sense, I would like to acknowledge all those who have, in a way, made this project happen.

To Professor Mariette Pereira, for all the opportunities given, for supporting me to follow my ideas, even when the success was to find things that did not work and for encouraging me to think out-of-the box to find solutions and participate on other scientific projects to expand my horizons.

To Professor Alberto Canelas Pais, for allowing this project to be multidisciplinary so that I could acquire knowledge in areas complementary to organic chemistry.

To Doctor Sara Pinto, for helping me in my first steps in porphyrin synthesis, for the patience in showing me the techniques and for taking the time to answer my many questions.

To Doctor Sandra Nunes, for the support on the computational analysis, showing me how to use the several programs used throughout this thesis and help in understanding the results obtained.

To Doctor Fábio Schaberle, for the support in the photochemical characterization of the compounds.

To my colleagues from the Catalysis and Fine Chemistry group, for the good moments in the laboratory, for showing me how to use the equipment and new synthetic techniques. A special thanks to Doctor Fábio Rodrigues for helping me with the Flash chromatography optimizations, to Giusi Piccirillo for her guidance in the analytical HPLC optimizations and Rafael Aroso for showing me how to perform the *in vitro* studies on bacteria.

To my colleagues from the Medicinal Chemistry group of CQC, specially to Doctor Catarina Lobo, for testing the compounds on viral samples and sharing her results with me.

To PorphyChem, for accepting me for a two-month internship, where not only did I learn how to use equipment for multi-gram scale processes, but I also acquired knowledge on how to work in an industry setting.

To the Centro de Química de Coimbra for the “Bolsa Lic. CQC SER C3_4” financed by FCT/MCTES.

To my friends, who helped me get through the Pandemic without feeling lonely. For having my back in the laboratory, in life and while playing. Without you all, the past year would not have been the same.

Finally, none of this would have been possible without my family. For showing me the importance of hard work, friendship and overall balance in life. For their unconditional love and support throughout this year and supporting me in my decisions.

Index

Abbreviations and symbols.....	i
Resumo.....	iii
Abstract.....	v
Nomenclature.....	vii
1. Introduction.....	1
1.1. Computational analysis.....	5
1.2. aPDI- The light at the end of the tunnel?.....	7
1.3. PDI <i>in vitro</i> and <i>in vivo</i> bacteria tests.....	9
1.4. Synthesis of <i>meso</i> -aryl porphyrins.....	21
1.5. Goals.....	27
1.6. References.....	28
2. Computational analysis of chlorin photosensitizers.....	33
2.1. Conformational analysis using DFT calculations.....	38
2.2. Conclusions.....	48
2.3. References.....	49
3. Development of a scalable synthetic process of <i>meso</i> -imidazolyl porphyrins and derivatives.....	51
3.1. Tetra-substituted imidazolyl-porphyrins.....	53
3.2. Scale-up of 5,15-bis-imidazolyl porphyrins.....	61
3.3. Photophysical studies of 5,15-bis imidazolyl porphyrins.....	69
3.4. Conclusions.....	74
3.5. References.....	76
4. Cationic photosensitizers for photoinactivation of pathogens.....	77
4.1. Synthesis, purification and characterization of chlorins.....	78
4.2. Biological studies.....	90
4.3. Conclusions.....	94
4.4. References.....	95
5. Experimental section.....	96
5.1. Computational analysis.....	96
5.2. Solvents and reagents.....	96
5.3. Instrumentation.....	97
5.4. Porphyrin synthesis.....	99
5.5. Chlorin synthesis.....	104
5.6. Photochemical characterization studies:.....	106
5.7. Bibliography.....	108

Abbreviations and symbols

ϵ	Molar absorption coefficient
λ	Wavelength
δ	Chemical shift
η	Yield/refraction index
ϕ_F	Fluorescence quantum yield
ϕ_Δ	Singlet oxygen quantum yield
ϕ_{Pd}	Photostability quantum yield
#	Entry number
1O_2	Singlet oxygen
$O_2^{\cdot-}$	Superoxide radical
OH^{\cdot}	Hydroxyl radical
A/Abs	Absorbance
aPDI	Antimicrobial Photodynamic Inactivation
API	Active Pharmaceutical Ingredient
CADD	Computer Aided Drug Design
CFU	Colony Forming Units
COVID-19	Coronavirus Disease 2019
DFT	Density Functional Theory
EMA	European Medicines Agency
ESBL	Extended-spectrum beta-lactamases
FDA	Food and Drug Administration

GLP	Good Laboratory Practice
GMP	Good Manufacturing Practice
HPLC	High Performance Liquid Chromatography
IUPAC	International Union of Pure and Applied Chemistry
MAOS	Microwave-assisted Organic Synthesis
MBC	Minimum bactericidal Concentration
MIC	Minimum Inhibitory Concentration
PS	Photosensitizer
ROS	Reactive Oxygen Species
WHO	World Health Organization

Resumo

Segundo a Organização Mundial de Saúde um dos maiores problemas da medicina atual está associado à falta de medicamentos e/ou tratamentos eficazes para doenças infecciosas, provocadas por bactérias multirresistentes ou vírus, incluindo o SARS-CoV-2. Em linha com esta preocupação o objetivo global dos estudos descritos nesta Tese de mestrado centra-se na modulação computacional e otimização de processos de síntese, em escala multi-grama, de *meso*-imidazolil porfirinas e clorinas catiónicas e anfífilas, para desenvolvimento de fotossensibilizadores para fotoinativação de agentes patogénicos responsáveis por doenças infecciosas. O trabalho encontra-se dividido em 5 Capítulos.

No Capítulo 1 – Introdução, descreve-se uma revisão crítica da problemática associada às infeções resultantes de micro-organismos e apresentam-se algumas soluções alternativas. De entre elas, e por ser o objetivo central da Tese, apresenta-se uma revisão da literatura relativa à estrutura e atividade das diferentes famílias de fotossensibilizadores para inativação fotodinâmica de bactérias e de vírus responsáveis por infeções respiratórias. Adicionalmente, é apresentada uma discussão geral da utilização de micro-ondas na síntese de fotossensibilizadores da família das porfirinas. O Capítulo 1 termina com a descrição dos objetivos do trabalho experimental desenvolvido e descrito nesta Tese.

O Capítulo 2 inicia-se com uma introdução geral sobre os diferentes métodos de cálculo computacional e suas aplicações em Química Medicinal. Segue-se a apresentação dos resultados dos cálculos computacionais relativos à análise conformacional *meso*-imidazolil-clorinas nomeadamente, 5,15-bis(4-etil-1-metilimidazol-2-il) clorina, 5,15-bis(4-(1,1,1-trifluoro)etil-1-metilimidazol-2-il) clorina, 5,10,15,20-tetra(4-etil-1-metilimidazol-2-il) clorina e 5,10,15,20-tetra(4-(1,1,1-trifluoro)etil-1-metilimidazol-2-il) clorina catiónica. São ainda apresentados os mapas de potencial eletrostático de conformémeros selecionados. Da análise crítica destes resultados, surgem orientações para a síntese que irá ser otimizada experimentalmente e ainda sobre a problemática da existência de atropisómeros no desenvolvimento de um novo medicamento.

No Capítulo 3 descreve-se, em primeiro lugar, o processo de otimização à escala laboratorial do processo de síntese de *meso*-tetra-imidazolil porfirina e de 5,15-bis-imidazolil porfina, seguido da sua transposição para uma escala de multi-grama. No primeiro caso concluiu-se que o método de um só passo, nitrobenzeno/propiónico, sob

irradiação de micro-ondas, é o processo de síntese mais apropriado para efetuar a transposição de escala, tendo-se obtido a porfirina **1** com um rendimento de 21%. A porfirina 5,15-bis(1-metilimidazol-2-il) foi preparada em maior escala nos laboratórios da empresa PorphyChem. Esta porfirina **2** foi isolada com um rendimento de 17%. A porfirina **2** foi selecionada para preparar os respetivos derivados catiónicos tendo-se obtido as porfirinas **4**, **5** e **6** com rendimentos de 82%, 79% e 84%, respetivamente. Para avaliar as suas potencialidades como fotossensibilizados, para além das técnicas habituais de caracterização para comprovar a pureza (RMN, e espetrometria de massa), neste capítulo foram ainda efetuados estudos para determinar as propriedades fotofísicas dos compostos sintetizados (coeficiente de absorção molar, rendimento quântico de fluorescência e de oxigénio singuleto e fotodegradação).

Tendo como objetivo otimizar as propriedades deste tipo de fotossensibilizadores catiónicos e orientados pelos cálculos computacionais, no Capítulo 4 apresentam-se os resultados de otimização da reação de redução de porfirina à respetiva clorina, seguida da sua cationização (Estes resultados estão protegidos por propriedade intelectual). Descreve-se a otimização do método analítico por HPLC e sua purificação por cromatografia de flash. A pureza e propriedades fotofísicas da clorina catiónica são também descritas e discutidas. Por fim, apresentam-se estudos preliminares, mas muito promissores, da comparação da utilização das novas imidazolil porfirinas e clorina catiónicas na fotoinativação de agentes patogénicos de doenças infecciosas.

No Capítulo 5 apresenta-se a descrição experimental detalhada referente a todos os Capítulos da Tese e ainda a caracterização química completa de todas as porfirinas e clorinas sintetizadas no decorrer do trabalho. Descrevem-se também detalhadamente os métodos computacionais utilizados.

Abstract

According to the World Health Organization, one of the main challenges of modern medicine is associated with the lack of efficient drugs and treatments against infectious diseases caused by multi-resistant bacteria or viruses, including SARS-CoV-2. Taking these concerns into account, the overall goal of the studies described in this master's Thesis is centered on the computational analysis and optimization of synthetic methods in a multi-gram scale for *meso*-imidazolyl cationic and amphiphilic porphyrins and chlorins, for the development of photosensitizers for photoinactivation of disease-causing pathogens. The present work is divided into five Chapters.

In Chapter 1-Introduction, a critical review of the problems associated with infections caused by micro-organisms is described and alternative solutions are presented, namely, antimicrobial photodynamic inactivation. In accordance with the goals of this project, a review of the literature about the structure and activity of several families of photosensitizers used for inactivation of bacteria and viruses responsible for respiratory tract infections is presented. Additionally, a general discussion on the use of microwave assisted porphyrin synthesis is presented. Chapter 1 finishes with the main goals of the work developed in this Thesis.

Chapter 2 begins with a general introduction of computational methods and their applications in Medicinal Chemistry. Then, the experimental results on the conformational analysis of *meso*-imidazolyl cationic chlorins (5,15-bis(4-ethyl-1-methylimidazol-2-yl) chlorin, 5,15-bis(4-(1,1,1-trifluoro)ethyl-1-methylimidazol-2-yl) chlorin, 5,10,15,20-tetra(4-ethyl-1-methylimidazol-2-yl) chlorin and 5,10,15,20-tetra(4-(1,1,1-trifluoro)ethyl-1-methylimidazol-2-yl) chlorin). The electrostatic maps of selected conformers are also presented. The results obtained in this Chapter give us an insight on possible experimental challenges and the problem of having atropisomers in a new drug.

Chapter 3 describes the optimization process for scale-up of *meso*-tetra-imidazolyl and 5,15-bis-imidazolyl porphyrins and their transposition to a larger scale. In the first case, the best synthetic process was the one-step nitrobenzene/propionic acid method under microwave irradiation, where porphyrin **1** was obtained with 21% yield. For the 5,15-bis(1-methylimidazol-2-yl) porphyrin **2**, the best scale-up method was performed at PorphyChem, where, it was possible to obtain in a multi-gram scale porphyrin **2** with a yield of 17%. Porphyrin **2** was selected to prepare the cationic derivatives **4**, **5** and **6** with 82%, 79% and 84% yields. To evaluate the use of these porphyrins as photosensitizers,

they were characterized not only using NMR and mass spectrometry, but also through their photophysical properties (molar absorption coefficient, fluorescence, and singlet oxygen quantum yield and photodegradation) which are described and discussed.

Aiming the optimization of the properties of these photosensitizers and based on the results obtained with computational analysis, Chapter 4 presents the results of the optimization of the reduction of porphyrin to the corresponding chlorin followed by its cationization. The optimization of the analytical method HPLC and purification through flash chromatography is also described. (These results are protected by intellectual property). The purity and photophysical properties of the cationic chlorin are also described and discussed. Lastly, preliminary studies with very promising results are presented comparing the use of the new cationic imidazolyl porphyrins and chlorin in the photoinactivation of pathogens that cause infectious diseases.

Chapter 5 contains the detailed description of the synthesis and characterization of all the compounds described in this work. Computational methods are also described in this Chapter.

Nomenclature

In this MSc Thesis, in most of the cases, International Union of Pure and Applied Chemistry (IUPAC) guidelines regarding numbering and naming of compounds were followed, except some exceptions promptly referred in this section.

Porphyrins

For the designation of the synthesized porphyrins in this Thesis, IUPAC¹ numbering system was used, which consists in the numbering of all the carbon atoms from the macrocycle from 1 to 20 and the internal nitrogen from 21 to 24 (Figure I). Sometimes, Fischer's terminology² which designate the positions 5, 10, 15, 20 as *meso* and the positions 2, 3, 7, 8, 12, 13, 17 and 18 as positions β (beta) will be adopted.

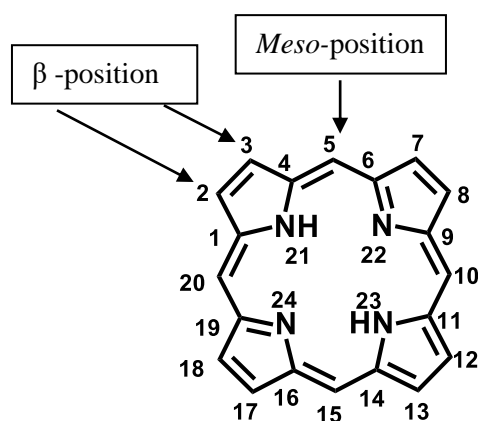


Figure I– IUPAC numbering system used for porphyrins and their respective designations according to Fischer's terminology.

Hydroporphyrins

Regarding the porphyrin's reduced derivatives (Figure II), they are designated by 2,3-dihydroporphyrin when the saturated carbons are in one of the pyrrolic rings, throughout this Thesis, their trivial name "chlorin" will be used. When the saturated carbons are found in two diametrically opposite pyrrolic rings, they are designated by 7,8,17,18-tetrahydroporphyrins or their trivial name "bacteriochlorin".

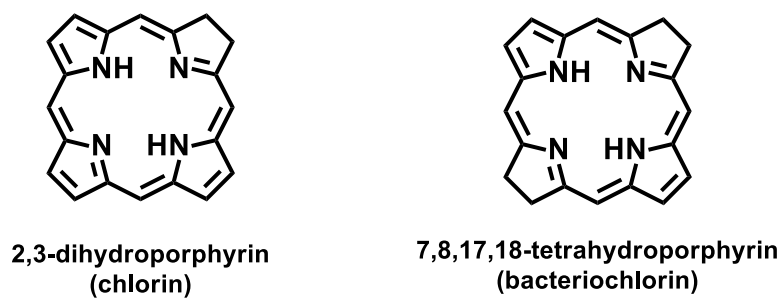


Figure II– IUPAC names of the reduced derivatives of the porphyrins and their respective trivial designation.

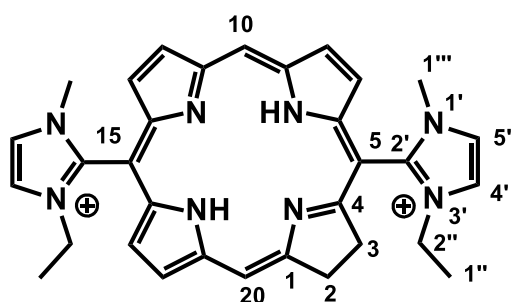
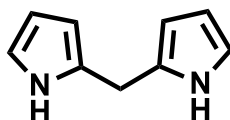


Figure III- IUPAC nomenclature for di-substituted chlorin derivatives¹

Dipyrromethane



5,10- Dihydrodipyrin
Dipyrromethane

Figure IV- IUPAC nomenclature of dipyrromethane

Isomers

Conformer: One of a set of stereoisomers, each of which is characterized by a conformation corresponding to a distinct potential energy minimum.

Atropisomer: A subclass of conformers which can be isolated as separate chemical species, and which arise from restricted rotation about a single bond.³

References

1. Moss, G. P., Nomenclature of tetrapyrroles (Recommendations 1986). In *Pure & Applied Chemistry*, **1987** 59, 779-832.
2. Fischer, H.; Orth, H., *Die Chemie des Pyrrols*. Akad. Verlagsges: Leipzig, **1934**
3. McNaught, A. D., Wilkinson, A., Basic terminology of stereochemistry in Compendium of Chemical Terminology, 2nd ed. (the "Gold Book"), *Blackwell Scientific Publications, Oxford*: Online version (2019-) created by S. J. Chalk. **1996** 68, 2193.

1. Introduction

Microbes such as viruses, bacteria and fungi can have dire consequences in our community. One of the most recent examples of how microbes can influence our daily lives is the Coronavirus disease 2019 (COVID-19). There are several short-term health and social consequences, which are already visible in our daily lives, such as the widespread use of antimicrobial gels for hand hygiene, social distancing, and self-isolation. The longer-term consequences are very concerning, namely the possibility of propagation of antimicrobial resistance due to improper use of antimicrobials in this crisis.¹ Although some bacterial and fungal co-infections in patients with COVID-19 are possible, the prescription rate of broad-spectrum antimicrobial agents is high.² This could worsen a problem that has been rising in the past few years and that scientists have made efforts to counteract: the development of resistant strains of bacteria.

Antibiotic resistance is a phenomenon that was first reported as early as 1940.³ Since then, several strategies have been adopted to tackle this problem, from slight changes in the structure of antibiotic drugs, to using new bacterial targets. The financial rewards associated to these findings along with the relative ease of the early antibiotic discovery led to indiscriminate use of these drugs in several industries. After this “golden era of antibiotics”, pharmaceutical companies started facing scientific challenges in searching for new antibiotics, namely efflux pumps and the difficulty of penetrating Gram-negative cell walls. These problems lead pharmaceutical companies to abandon this path and search for new and more profitable ones in the 1980s. Although there was this loss of interest, new resistant strains of bacteria continue to develop, especially in places such as hospitals, where antibacterial drugs are used daily. It is estimated that 700 000 deaths, per year, are caused by resistant strains of bacteria⁴. This concerning number is expected to increase to 10 million by 2050. To mitigate this issue, the World Health Organization (WHO) has made a priority list of twelve bacteria for which novel antibiotics are needed. The list is divided according to the priority level. Of the twelve bacteria listed, nine are Gram-negative and the three bacteria listed on the critical level are all Gram-negative, one of which is *Enterobacteriaceae* carbapenem-resistant, extended-spectrum beta-lactamases (ESBL) producing bacteria, which includes *Escherichia Coli*.⁵, one of the targets of these studies.

The drug discovery pipeline is a multi-step interdisciplinary process that can take about a decade and an investment of about one million euros.⁶ This process needs to be undertaken to get new drugs on the market. It typically starts with the identification of a key target that is crucial for disease progression.⁶ Then, chemical compounds are designed to interact with this target and the most promising ones are synthesized. Once the initial compounds are obtained, some structure-activity relationships may be studied and *in silico* studies can be performed for further insights.⁷ Once a library of compounds is available, *in vitro* studies may start, using the most promising molecules. At this stage, it is necessary to obtain a proof of concept before advancing into the next step, *in vivo* studies. Once the lead compound has been optimized and characterized to an acceptable level, using good laboratory practices (GLP), *in vivo* studies may begin. In this step, the appropriate animal model must be chosen, and several variables must be studied. Once thorough *in vivo* studies have been performed, the drug regulatory agencies (e.g. Infarmed in Portugal) may give authorization for the start of clinical trials. For these trials, it is necessary that the lead molecule is synthesized under good manufacturing practices (GMP). There are three phases that the drug must pass before it can be considered for Food and Drug Administration (FDA) and European Medicines Agency (EMA) approval. Phases I, II and III have different endpoint objectives that must be met. Finally, for a drug to become commercially available, it must be approved by the FDA to be sold in the USA and EMA to be sold in Europe. Once these approvals are obtained, it becomes commercially available for purchase and continues under vigilance to see if there are any adverse effects that were not previously detected. Figure 1.1 summarizes this information.

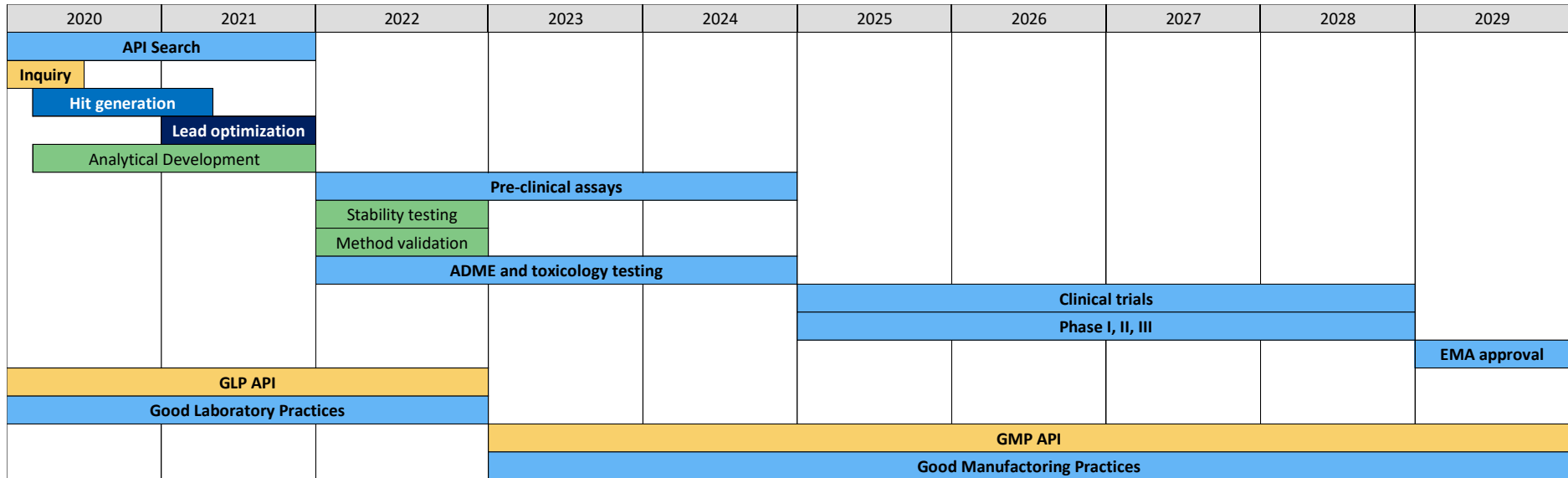


Figure 1.1: Drug discovery pipeline

Nowadays, most institutions involved in pre-clinical discovery and development of antibacterial drugs are small and medium sized companies, located mainly in the United States of America, Germany, United Kingdom and France.⁸ Many drugs that are being developed are direct acting antibiotics, which can further push bacteria to develop new mechanisms of resistance.⁹⁻¹¹ An alternative method that has been brought to light recently is the use of antimicrobial photodynamic inactivation (aPDI).¹² Research regarding aPDI indicates that it is highly unlikely for bacteria to develop mechanisms of resistance against it as it involves damaging many microbial biomolecules lethally.¹³⁻¹⁶ Cationic *meso*-aryl porphyrins have been described in the literature as good photosensitizers in aPDI for photoinactivation of Gram-negative bacteria (Table 1.1). Computational modelling can be used to better understand these mechanisms as well as interpret how molecules may interact with cell membranes according to their charge distribution. It can also help visualize how the molecule would interact with a bacterial wall and rationalize the modulation of these molecules to understand what kind of structural modifications can be done to improve the interaction between the macrocycles and their target.¹⁷

The aim of this project is to develop synthetic processes to prepare and characterize cationic *meso*-imidazolyl porphyrins and derivatives (chlorin) to use as photosensitizers in aPDI. To perform this, it is necessary to start by optimizing the structures of tetra-substituted and di-substituted *meso*-aryl porphyrins and their derivatives to try and understand which atropisomers are most likely to exist and which would have the best affinity towards Gram-negative bacterial membranes. From these optimizations, we will try to synthesize and characterize the most promising derivatives in a quantity and purity that is enough to be used for photophysical characterization and *in vitro* testing.

1.1. Computational analysis

Computational methods are increasingly relevant in science and society. Until recent times, the development of new drugs was performed through several approximations, including trial-and-error efforts, where it was necessary to synthesize many compounds that would then be tested *in vitro*, making it a long and costly process. Despite advances in biotechnology and in our understanding of biological systems, drug discovery is still a lengthy, costly, difficult, and inefficient process with a high attrition rate for new medicines. More recently, computational chemistry evolved to change this paradigm. Nowadays, drug discovery uses a combination of computational, experimental, translational, and clinical models to identify new therapeutic entities.^{18,19} Drug design is the inventive process of finding new drugs based on the knowledge of a biological target. Most often, it involves the design of molecules that are complementary in shape and charge to the molecular target with which they interact and bind. Drug design frequently relies on computer modeling techniques and bioinformatic approaches. Modern drug discovery involves the identification of screening hits and optimization of those hits to increase the affinity, selectivity (to reduce the potential of side effects), efficacy/potency, metabolic stability (to increase the half-life), and oral bioavailability. Once a compound that fulfills all these requirements is identified, it will begin the process of drug development prior to clinical trials. Subsequent drug development includes preclinical research on cell-based and animal models, clinical trials on humans, and finally the step of obtaining regulatory approval to market the drug.

Nowadays, computational methods are important in drug development, helping reduce the cost of selecting the lead compound. There are various types of computational methods available to address chemical problems, namely, (i) electronic structure calculations, such as DFT and *ab initio* methods (ii) computer aided drug design, and (iii) artificial intelligence. Each method answers different questions. Next, meaningful examples of how these methods have helped identifying drugs that were later approved by the FDA are presented. Computer aided drug design (CADD) can be classified into two groups, structure based and ligand-based drug discovery, depending on what type of information there is about the target and its structure. In the literature, it is possible to find some examples where using CADD aided the discovery of pharmaceutical drugs that were approved by the FDA and EMA.¹⁹ One example is Aliskiren (Tekturna®, Novartis), a human renin inhibitor approved by the FDA in 2007. This drug is key to help regulate

blood pressure through the regulation of angiotensin II. Molecular modelling methods were used to design a pharmacophore to obtain a lead compound.²⁰ From there, X-ray structure analysis helped identify a previously unknown site in the target, where hydrophobic interactions dramatically improved the binding affinity and selectivity of the drug. Further structure-based analysis led to the development of the final compound Aliskiren, a first-in-class drug that is still under use.¹⁹

A recent example where artificial intelligence was used to reposition a drug is the discovery of a potential antiviral drug against SARS-CoV-2. Due to the most recent pandemic, there is a global need to find an efficient antiviral against COVID-19. Because of the large library of compounds that could be studied against this virus, it was necessary to use machine learning techniques to search for the most promising drugs that were preferentially already in use to find a solution to this problem. Using BenevolentAI's knowledge graph, it was possible to identify Baricitinib, an antiviral, that could reduce the infectivity of the virus in the lungs.²¹

Recently, the use of DFT methods to understand the charge distribution of photosensitizers that showed strong activity in antimicrobial-PDI (aPDI) of Gram-negative bacteria was described.¹⁷ This will be further detailed below, since this work further explores this approach.

The absence of specific interactions between the PS and biological targets in microorganisms has consequences that extend well beyond the choice of the computational method to aid in the selection of the best drug candidate. The indirect connection, through reactive oxygen species, from the PS to the biological targets, makes it more difficult for the microorganisms to develop drug resistance. The microorganisms are killed by oxidative stress that affects a large diversity of biomolecules in different locations. It is known that many cycles of aPDI can be repeated under subtherapeutic conditions before drug resistance is observed.²²⁻²⁴ This also addresses the concerns of the World Health Organization over drug resistant microorganisms, which are increasingly worrisome and lead scientists to develop alternative therapeutics to efficiently kill microorganisms, without the risk of inducing resistances. *In vitro* studies of aPDI, have shown that the structure and especially the amphiphilicity of the photosensitizer is a challenge that needs to be overcome to promote a good translation into clinical settings²⁵. It is known that functionalization of drugs with fluorine, including antibiotics, can cause dramatic changes in the interaction of these compounds with the biological environment.²⁶ In the literature, we can also

find promising fluorinated PS such as redaporfin.²⁷ In this work we also aim to develop the synthesis of a biocompatible cationic fluorinated porphyrin-based photosensitizer.

1.2. aPDI- The light at the end of the tunnel?

aPDI uses a PS to form reactive oxygen species (ROS) capable of damaging many types of biomolecules, causing cell death.²⁸⁻²⁹ The PS absorbs a photon of light which leads to its excited singlet electronic state. An intersystem crossing can then occur, leading to the triplet state of the PS, which in turn reacts with ground state oxygen.³⁰ There are two types of photochemical pathways that this species can undergo. Type 1 involves the production of superoxide radicals via electron transfer, while Type 2 produces excited singlet oxygen species ($^1\text{O}_2$) by energy transfer. Both types of reactive oxygen species can damage biomolecules and cause cell death.²⁸⁻²⁹ Figure 1.2 shows a simplified Jablonski diagram depicting the photochemical production of ROS using a PS.

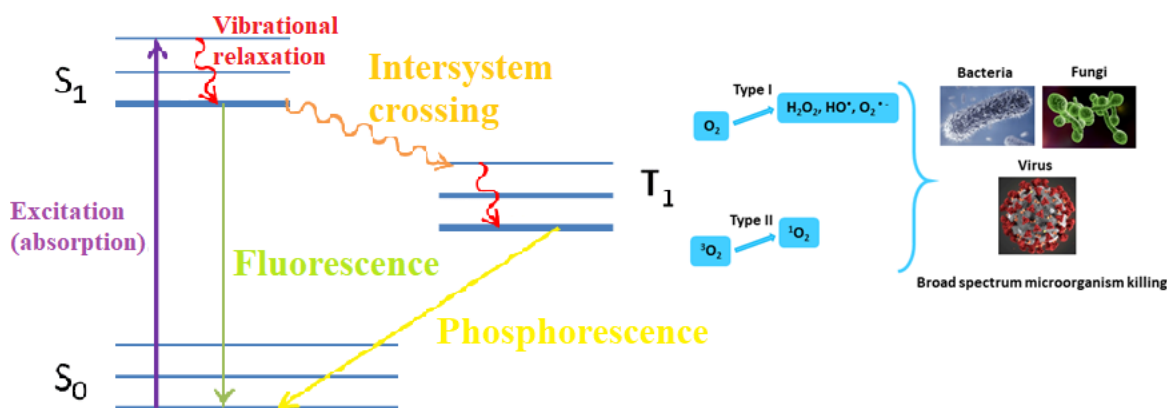


Figure 1.2: Simplified Jablonski diagram showing how a photosensitizer (PS) can cause broad spectrum microorganism death. Adapted from the literature.²³

Ideally, a photosensitizer must:^{12, 31}

1. Have high purity.
2. Have an easy synthesis with high yields.

3. Have low toxicity in the dark, especially towards mammalian cells.
4. Show selectivity for microbial cells over mammalian cells.
5. Have a high molar absorption coefficient in the therapeutic window (600 - 850 nm)
6. Have the appropriate photophysical properties, including:
 - a. Low fluorescence yield
 - b. High singlet oxygen yield
 - c. Long triplet state half-life
7. Have an appropriate partition coefficient according to the intended administration route and good dissolution in biocompatible formulations.

Bringing together all these parameters can be a challenge, one worth overcoming to avoid the development of antibacterial resistance. Other advantages of using aPDI include the possibility of applying the PS directly into the infected area, their broad-nature, their anti-biofilm action and the fast action, important for fast spreading infections.¹² Some challenges include the difficulty of accessing infections deep inside the body and the selectivity for mammalian cells over bacterial cells. To overcome the first obstacle, the PS and light can be delivered using endoscopes and narrow diameter interstitially inserted needles and fiber optics. For the latter, positively charged photosensitizers were developed and have shown good selectivity for bacterial cells who tend to have a more electronegative membrane than mammalian cells, allowing positively charged PS to bind selectively to them.¹² It has also been shown that the binding of PS to microbial cells is faster than their uptake by the mammalian cells, which makes them ideal when there is a short time lapse between the delivery of the drug and the light irradiation. Examples of PS that can be used for aPDI include polycationic conjugates, fullerenes, phthalocyanines, porphyrins and their derivatives, among others.^{12, 32-33}

Although many studies have shown that bacteria are unlikely to develop resistance to aPDI, further investigation on this thematic is encouraged.¹² After the patient is treated using aPDI and the PS washed out, it is likely that small amounts of PS stay on the patient, attached to their cells. As the patient goes about their daily life, they will be subjected to light. This means that the PS

that stays on the patient can still be activated by this light and proceed its action at sub-lethal levels, allowing the remaining bacterial population to become more tolerant to higher concentrations of these antimicrobial agents. Therefore, more studies where bacterial cells are exposed to sub-lethal levels of PS and light are still needed.^{12-16, 33}

As mentioned above, porphyrins and their derivatives can be used as PSs for aPDI. These tetrapyrrolic macrocycles have an 18-electron aromatic ring, which allows them to absorb light in the therapeutic window (600-850nm). Bacteriochlorins have a very high absorbance in this area of the spectrum but are often difficult to synthesize and are not very stable in solution. Chlorins have a high absorbance band at 650nm, are easier to synthesize and are more stable than bacteriochlorins. Porphyrins have a lower absorbance band in this window but are much more stable than their derivatives. These compounds are particularly relevant when their structure encompasses positive charges, allowing them to get closer to the negatively charged Gram-negative bacteria and virus membrane targets. This is also one of the main goals of our studies.

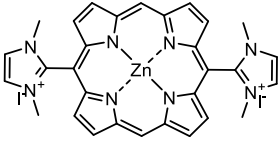
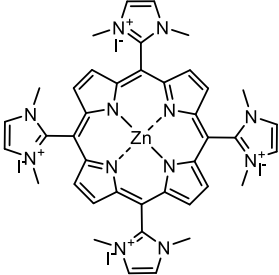
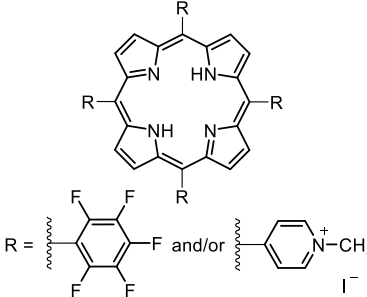
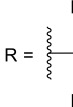
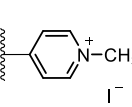
1.3. PDI *in vitro* and *in vivo* bacteria tests

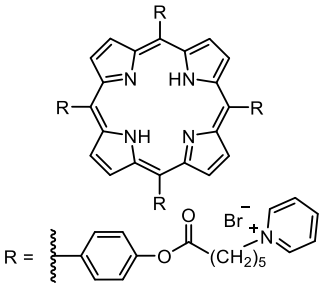
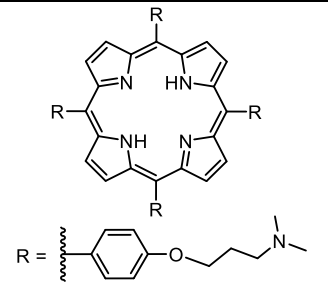
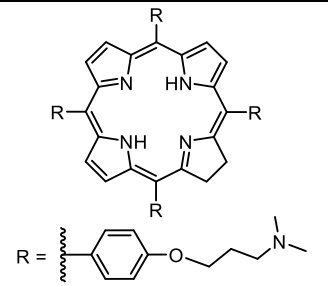
As previously discussed, the goal of aPDI is to cure local infections. When dealing with bacterial infections, it is important to distinguish between the bacteriostatic (agents that prevent the growth of bacteria) from the bactericidal effect where the agent kills the bacteria.²⁸ The potency of antibiotics is characterized in two ways: i) their minimum inhibitory concentration (MIC), *i.e.*, the lowest concentration that results in inhibition of bacterial growth after 24h incubation; ii) their minimum bactericidal concentration (MBC), *i.e.*, by the lowest concentration that results in 3 log of colony forming units (CFU) reduction. This measure is not entirely adequate for photosensitizers because lower drug concentrations can be partially compensated by higher light doses, and the incubation times relevant for photosensitizers (less than 1 h) and for antibiotics (18 to 24 h) are widely different. Nevertheless, photosensitizers with bactericidal effects that require photosensitizer concentrations higher than 50 μ M are likely to be difficult to translate to clinical

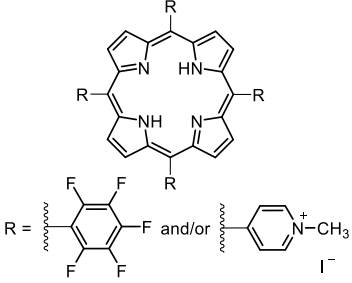
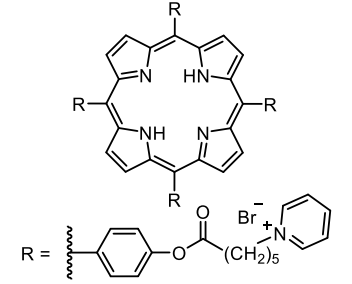
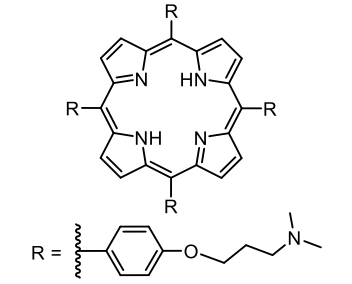
practice because such high concentrations will be difficult to achieve in the whole infected region and may be toxic to human cells.²³

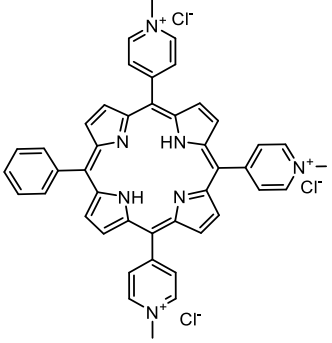
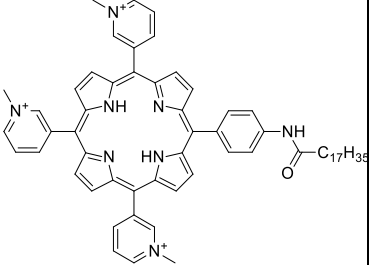
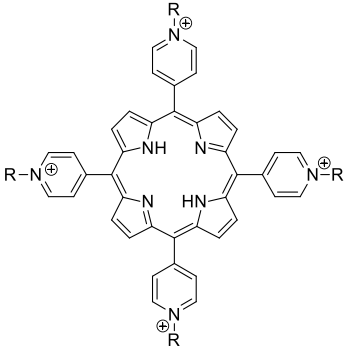
Table 1.1 summarizes selected recent studies on photoinactivation of i) Gram-positive bacteria in biofilms (entries 1 to 6); ii) Gram-negative bacteria in biofilms (entries 7 to 9); iii) *in vitro*, *in vivo* and *ex vivo* pre-clinical studies for the treatment of infections by Gram-positive bacteria (entries 10-12) and iv) Gram-negative bacteria (entries 13 to 16).

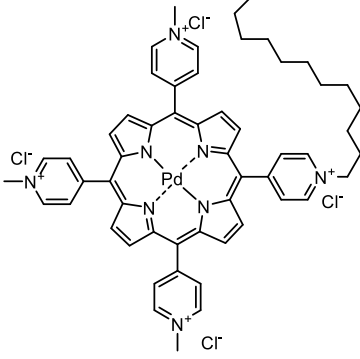
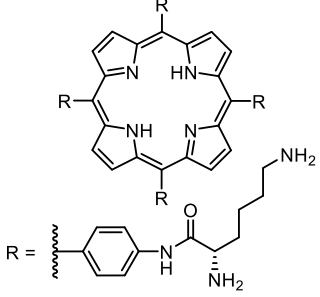
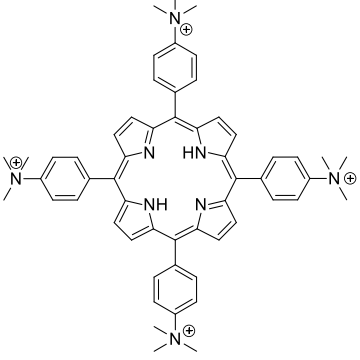
Table 1.1: Chemical properties and biological activity of photosensitizers studied in the literature.

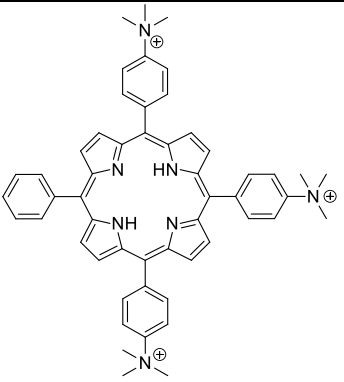
#	Structure	Biofilm strain/model	Results
1	 <p>IP-2-Zn (PS1) Charge: +2 Mw: 592 Da</p>	<i>S. aureus</i> ATCC 25925 ¹⁷	<p>Outcome: 7 log CFU reduction [PS] = 5.2 nM Light dose: 5 J/cm² (Biotable λ=400–650 nm)</p>
2	 <p>IP-4-Zn (PS2) Charge: +4 MW = 754 Da</p>	<i>S. aureus</i> ATCC 25925 ¹⁷	<p>Outcome: 6 log CFU reduction [PS] = 1.0 μM Light dose: 12 J/cm² (Biotable λ=400–650 nm)</p>
3	 <p>R =  and/or  I⁻</p> <p>Porphyrin Mixture FORM (PS3)</p>	MRSA DSM 25693 ³⁴	<p>Outcome: ~7 log CFU reduction [PS] = 1.0 μM (in combination with 100 mM KI) Light dose: 9 J/cm² (White fluorescent lamp λ=380–700 nm)</p>

	<p>Charge: +1 to +4 <i>MW</i> = 679 to 900 Da</p>		
4	 <p>PS4 (in polymeric micelles of Pluronic F-127)</p> <p>Charge: +4 <i>MW</i> = 1384 Da</p>	<i>S. aureus</i> 209P ³⁵	<p>Outcome: >99% bacterial death</p> <p>[PS] = 10 μM</p> <p>Light dose: 128 J/cm² (500 W halogen lamp with filter λ=420–1000 nm)</p>
5	 <p>TAPP (PS5)</p> <p>Charge: 0 to +4 (pH dependent)</p> <p><i>MW</i> = 1019 Da</p>	<i>S. aureus</i> RN6390 ³⁶	<p>Outcome: 4 log CFU reduction</p> <p>[PS] = 50 μM</p> <p>Light dose: 180 J/cm² (Tungsten Halogen lamps 500 W)</p>
6	 <p>TAPC (PS6)</p> <p>Charge: 0 to +4 (pH dependent)</p> <p><i>MW</i> = 1021 Da</p>	<i>S. aureus</i> ATCC 25923 ³⁷	<p>Outcome: 4 log CFU reduction</p> <p>[PS] = 10 μM</p> <p>Light dose: 108 J/cm² (Novamat 130 AF slide projector 150 W lamp, using optical filters λ = 350-800 nm)</p>

7	 <p>Porphyrin Mixture FORM (PS3)</p> <p>Charge: +1 to +4</p> <p>MW = 679 to 900 Da</p>	<p>Bioluminescent <i>E. coli</i>³⁴</p>	<p>Outcome ~7 log CFU reduction</p> <p>[PS] = 1.0 μM (in combination with 100 mM KI)</p> <p>Light dose: 9 J/cm² (White fluorescent lamp λ=380–700 nm)</p>
8	 <p>PS4 (in polymeric micelles of Pluronic F-127)</p> <p>Charge: +4</p> <p>MW = 1384 Da</p>	<p><i>E. coli</i> C600³⁵</p>	<p>Outcome: 0.5 log CFU reduction</p> <p>[PS] = 10 μM</p> <p>Light dose: 128 J/cm² (500 W halogen lamp with filter λ=420–1000 nm)</p>
9	 <p>TAPP (PS5)</p> <p>Charge: 0</p> <p>MW = 1019 Da</p>	<p><i>P. aeruginosa</i> (clinical isolate)³⁶</p>	<p>Outcome: 3 log CFU reduction</p> <p>[PS] = 30 μM</p> <p>Light dose: 180 J/cm² (Tungsten Halogen lamps 500 W)</p>

10	 <p>PTMPP (PS7) Charge: +3 Mw: 663 Da</p>	<p><i>In vivo:</i> Male BALB/c with third degree burns infected with <i>S. aureus</i> 8325-4³⁸</p>	<p>Outcome: 1.7 log CFU reduction (7th day) [PS] = 500 μM Light dose: 210 J/cm² (Light λ=635± 15 nm)</p>
11	 <p>PS8 Charge: +3 MW = 944 Da</p>	<p><i>L. pneumophila</i> AA100³⁹</p>	<p>Outcome: >99% bacterial death [PS] = 24 nM Light dose: 12 J/cm² (violet light λ = 394 nm)</p>
12	 <p>PS9 Charge: +4 MW = 734 to 855 Da</p> <p>R₁ = CH₂CH₃ R₂ = CH₂CH₂CH₃ R₃ = CH₂CH₂CH₂OH</p>	<p><i>S. aureus</i> ATTC 29213⁴⁰</p>	<p>Outcome: >6,33 log reduction [PS] = 12.5 μM Light dose: 150 J/cm² (Diode laser λ = 655nm)</p>

13	 <p>FS111-Pd (PS10) Charge: +4 Mw: 938</p>	<p><i>In vivo:</i> Adult female BALB/c mice with wound infection by <i>E. coli</i>⁴¹</p>	<p>Outcome: 4 log CFU reduction initially. Complete inactivation 4 days after treatment [PS] = 50 μM (50+20+20 μL) Light dose: 80 J/cm² (Light λ=415nm)</p>
14	 <p>Tetra-lysine porphyrin (PS11) Charge: 0 to +8 (pH dependent) Mw: 1188 Da</p>	<p><i>In vivo:</i> Sprague–Dawley rats with wound infected by mixed bacteria (<i>E. coli</i>, <i>S. aureus</i>, <i>P. aeruginosa</i>)⁴²</p>	<p>Outcome: 5 log CFU reduction, 7 days after treatment [PS] = 40 μM Light dose: 100 J/cm² (Laser λ=650nm)</p>
	<p><i>In vivo:</i> Adult female BALB/c mice wound infected with multi-resistant <i>A. baumannii</i> (clinical isolate)⁴³</p>	<p>Outcome: 4 log CFU reduction, 4 days after treatment [PS] = 40 μM Light dose: 50 J/cm² (Laser λ =650nm)</p>	
15	 <p>(PS12)</p>	<p><i>E. Coli</i>⁴⁴</p>	<p>Outcome: 4 log CFU reduction [PS] = 0.1 μM Light dose: 44 J/cm² (White light λ =400-700nm)</p>

	<p>Charge: +4 Mw: 847 Da</p>		
16	 <p>(PS13) Charge: +3 Mw: 789 Da</p>	<i>E. Coli</i> ⁴⁴	<p>Outcome: 7 log CFU reduction [PS] = 1.0 μM Light dose: 44 J/cm² (White light λ =400-700nm)</p>

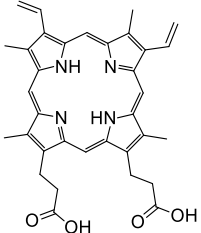
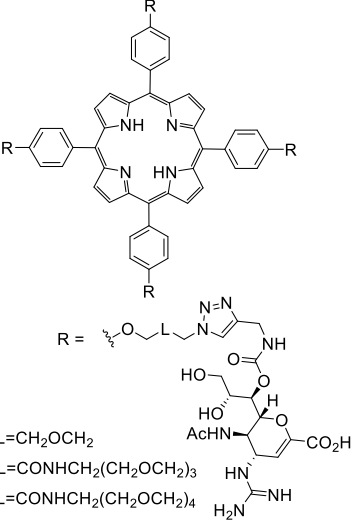
For photoinactivation of Gram-positive bacteria photosensitizers PS4 does not reach a bactericidal effect under the reported conditions. The critical analysis of these results points out that the photosensitizers that reach a most promising bactericidal effect are PS1-3, PS6, PS9, PS11-13. PS1 and PS2 are cationic imidazolyl porphyrins that gave the best results against Gram-positive and Gram-negative planktonic bacteria and against biofilms of Gram-positive bacteria (>6 log reduction of *S. aureus* biofilms with 5.2 nM at 5 J/cm² and 1 μM at 12 J/cm² for PS1 and PS2, respectively). Confocal microscopy revealed that PS1 could successfully permeate biofilms, while most of PS2 remained in the planktonic part.¹⁷ The matrix that composes bacterial biofilms hampers antimicrobial diffusion. This means that amphiphilic and low molecular weight photosensitizers may diffuse more readily inside biofilms. Moreover, the anionic nature of the components of this matrix must also be taken into account. While it can lead to favorable electrostatic interactions with cationic photosensitizers, coulombic forces in the periphery of biofilm may trap the photosensitizers with too many cationic charges.

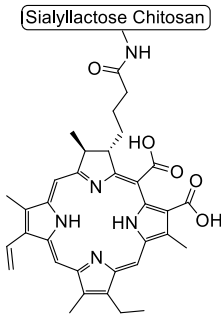
PS5, PS7 and PS10 need a concentration of ≥50 μM. At these concentrations, it is likely that they will present toxicity in human cells and will have a more difficult translation into a clinical setting. PS4, PS5, PS7, PS9-11, and PS13 report the use of light doses that are quite high, which also complicates the translation into a clinical setting.

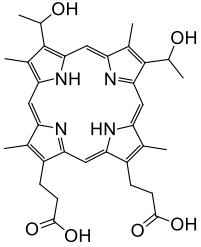
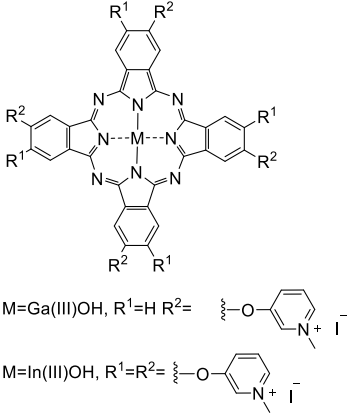
The strong bactericidal effects found for PS1 and PS2 suggest that low molecular weight photosensitizers with cationic charges are more promising for aPDI of bacterial biofilms and therefore its synthetic large-scale development is one of the main goals of this work.

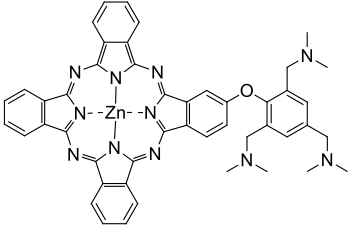
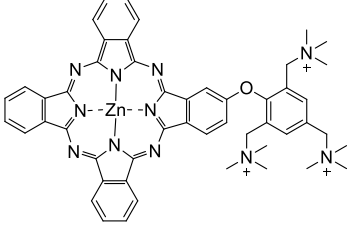
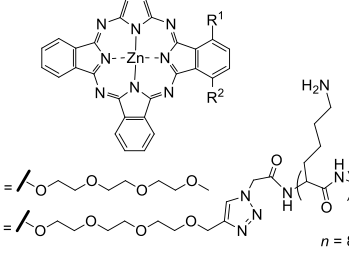
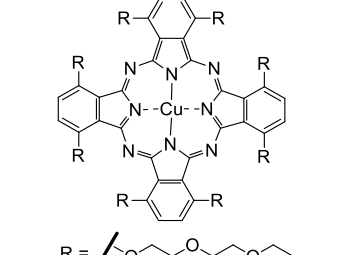
aPDI can also be used in the fight against viral infections. As such, it can be a very important tool to fight the current pandemic. Table 1.2 shows some photosensitizers that are currently being studied for aPDI of influenza viruses. SARS-Cov-2 is an upper respiratory tract infection, similarly to the influenza virus. Hopefully, studying what has been done on the latter virus will give us some insight on how to fight the current pandemic.

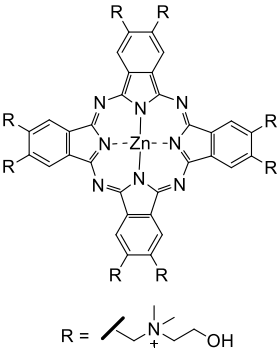
Table 1.2: *In vitro* and *in vivo* assays using photodynamic inactivation on influenza viruses.

#	Structure	Study type	Protocol and outcome	ROS
1	 <p>Protoporphyrin IX (PS13) Charge: -2</p>	<p><i>In vitro:</i> NCI cells inoculated with H1N1 strain X- 31⁴⁵</p>	<p>Outcome: 78-fold decrease of NCI cells infection rate compared with dark control. [PS] = 1.0 mg/mL Light dose: after 90 min of Visible light irradiation, $\lambda = 300$- 425 nm</p>	<p>$^1\text{O}_2$ $\text{O}_2^{\cdot-}$</p>
2	 <p>a L=CH₂OCH₂ b L=CONHCH₂(CH₂OCH₂)₃ c L=CONHCH₂(CH₂OCH₂)₄</p>	<p><i>In vitro:</i> MDCK cells infected with H1N1 and H5N1 virus⁴⁶</p>	<p>Outcome: 50% inhibition of infectivity (EC₅₀). [PS] = 0.1-2.1 nM (PS14c); 2-8 nM (PS14a) Light dose: after 1h of illumination with laboratory light (~850 lx)</p>	<p>-^a</p>

	PS14 Charge: 0			
3	 <p>Sialyllactose Chitosan</p>	<p><i>In vitro:</i> MDCK cells infected with H1N1 and Influenza B⁴⁷</p>	<p>Outcome: Reduction of infectivity (plaque reduction assay) to 23% for H1N1 and 50% for influenza B virus, when compared with antiviral oseltamivir.</p> <p>[PS] = 0.01 µg/mL Light dose: 1 J/cm² (laser, λ = 671 nm)</p>	¹ O ₂
4		<p>SCC (PS15) Charge: -2</p>	<p><i>In vivo:</i> Mice (BALB/c, male, 8 weeks old, n = 7) infected with H1N1⁴⁷</p>	<p>Outcome: Pre-treatment of H1N1 with PDI before inoculation in mice resulted in 100% survival, compared to 0% in control, after 14 days.</p> <p>[PS] = 5.0 mg/kg Light dose: 15 J/cm² (laser, λ = 671 nm)</p>
5		<p><i>In vitro:</i> CEF cells were infected with Influenza virus A strains WSN (H0N1), PR8</p>	<p>Outcome: ≥ 4 log₁₀ reduction of infectivity.</p> <p>[PS] = 2.5 µg/mL Light dose: visible light (15 minutes)</p>	¹ O ₂

		(H0N1), and Aichi (H3N2) ⁴⁸		
6	 <p>Hematoporphyrin (PS16) Charge: -2</p>	<i>In vivo:</i> embryonated chicken eggs infected with H0N1 ⁴⁸	Outcome: Total virus inactivation and reduction of egg mortality from 5/8 to 1/7 [PS] = 1.0 mg/mL Light dose: visible light	¹ O ₂
7		<i>In vitro:</i> MDCK cells infected with influenza H3N2 (Aichi/2/68) ⁴⁹	Outcome: Virus infectivity reduced by 1.5 log ₁₀ CCID ₅₀ /0.1 mL, when compared to the control. [PS] = 10 μM Light dose: 50 J/cm ² (red LED, λ= 635 nm)	¹ O ₂
8	 <p>PS17 Charge: +4 or +8</p>	<i>In vitro:</i> MDCK cells infected with influenza H3N2 (Aichi/2/68) ⁴⁹	Outcome: No reduction of virus infectivity. [PS] =10 μM Light dose: 50 J/cm ² (red LED, λ= 635 nm)	- ^a

9	 <p>PS18 Charge: 0 (Up to +3 at pH = 7)</p>	<p><i>In vitro:</i> HEp-2 and</p>	<p>Outcome: 50% inhibition of infectivity (IC₅₀). [PS] = 0.001 nM Light dose: 48 J/cm² (red visible light, λ > 610 nm)</p>	<p>¹O₂ (Φ_Δ=0.54, DMF)</p>
10	 <p>PS19 Charge: +3</p>	<p>MDCK infected by H1N1 virus⁵⁰</p>	<p>Outcome: 50% inhibition of infectivity (IC₅₀). [PS] = 0.087 nM Light dose: 48 J/cm² (red visible light, λ > 610 nm)</p>	<p>¹O₂ (Φ_Δ=0.63, DMF)</p>
11	 <p>PS20 Charge: 0 (Up to +8 at pH = 7)</p>	<p><i>In vitro:</i> HEp-2 and MDCK infected by H1N1 virus⁵¹</p>	<p>Outcome: 50% inhibition of infectivity (IC₅₀). [PS] = 0.05 nM Light dose: 48 J/cm² (red light, λ > 610 nm)</p>	<p>¹O₂ (Φ_Δ=0.86 -0.89, DMF)</p>
12	 <p>PS21 Charge: 0</p>	<p><i>In vitro:</i> MDCK cells infected with influenza virus A (H1N1, H3N2)⁵²</p>	<p>Outcome: Virus infectivity of Influenza A H1N1, H3N2 and Influenza B reduced to <1.6%, <3.3% and 30% of the control, respectively. [PS] = 100 μM</p>	<p>-^a</p>

			Light dose: 8.1 J/cm ² (red light, $\lambda = 735$ nm)	
13	 <p>PS22 Charge: +8</p>	<i>In vitro:</i> MDCK cells infected by Avian H5N8 Influenza virus ⁵³	Outcome: After treatment, H5N8 virions were unable to infect MDCK cells (lgTCID ₅₀ /mL = 0). [PS] = 2 μ M Light dose: 12 J/cm ² (halogen lamp)	- ^a

^a – not reported

Overall, there are interesting results involving the application of porphyrins and phthalocyanines as photosensitizers in aPDI. The benefits of using cationic photosensitizers for the treatment of influenza are not as clear as for Gram-negative bacteria. In some cases, namely PS18 and PS19, it seems like having non-permanent positive charges increases the photosensitizer's activity. This may be because influenza virus acquires its envelope from the host, containing less negatively charged residues when compared to other microorganisms. This means that having a high number of positive charges around the photosensitizer is not entirely beneficial, and other features should be taken into account, such as lipophilicity and ability to generate reactive oxygen species.

Although there are good prospects for widespread use of PDI for the prevention and clinic treatment of influenza infections, there is still much to be done regarding the transition of *in vitro* and *in vivo* studies to human trials. This may include the optimization of aPDI protocols for the irradiation of upper and lower respiratory tract, and widespread development and production of anti-influenza photosensitizer-coated materials. Indeed, the multi-targeted ROS-mediated mechanism of aPDI makes it suitable not only for inactivation of influenza or SARS-Cov-2 but

also for other current respiratory infections and may play a significant role in the protection and treatment of incoming, yet unknown, pandemics.

One of the most encouraging efforts comes from Weber *et al*, who evaluated the effects of aPDI on twenty patients who tested positive for COVID-19 and displayed mild symptoms. Using riboflavin as the photosensitizer and UV-blue light, with 10-20 min irradiation of oral and nasal cavities, they found that it was possible to significantly reduce the viral load in the upper respiratory tract, with 70% of the patients having a negative QPCR test 5 days after PDI treatment. This is also translated into a significant reduction of clinical symptoms like fever, dry cough, and chest pain. In comparison, the control group, who was given conventional treatment, and did not experience any significant improvements over this period of time.⁵⁴ We aim that the new chlorin-based photosensitizers developed in this study (Chapter 4) may give a relevant contribution for Sars-CoV-2 photoinactivation at nasal level, in the future.

1.4. Synthesis of *meso*-aryl porphyrins

Throughout the years, many synthetic methods have been developed for *meso*-aryl porphyrins. The first description of the synthesis of those porphyrins was done by Rothemund in 1935.⁵⁵ In this reaction, pyrrole was condensed with the appropriate aldehyde in an inert atmosphere at 100 °C for 48h, using pyridine as solvent. In 1967, Adler and Longo⁵⁶ modified this reaction using propionic acid in an aerobic media, obtaining higher yields but also some chlorin contamination. Later, Pereira⁵⁷ followed by Lindsey and co-workers⁵⁸ developed a two-step method with milder conditions, where the cyclization step occurred, at room temperature, before oxidation of the porphyrinogen. This methodology uses very diluted solutions, an acid catalyst and toxic and expensive quinones as oxidants. In 1991, Gonsalves and Pereira⁵⁹ described an alternative one-pot synthesis, where nitrobenzene is used as both solvent and oxidant. This methodology is more concentrated than the one described by Adler-Longo and has, in general, higher yields, particularly for *ortho*-disubstituted aromatic aldehydes and the porphyrins are not contaminated with chlorin.

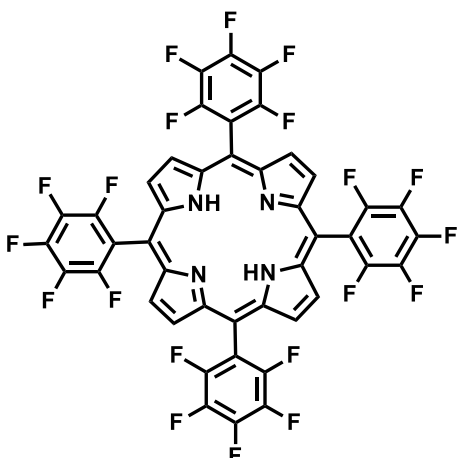
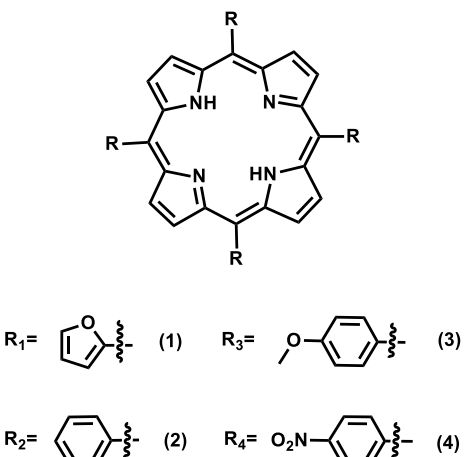
Additionally, we should highlight the Lindsey two step methodology for the synthesis of 1,15-disubstituted porphyrins, that starts with the condensation of dipyrromethane with the desired aldehyde, followed by oxidation with quinones (DDQ or chloranil).⁶⁰

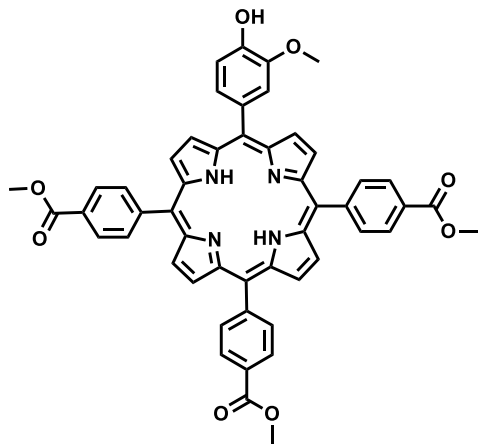
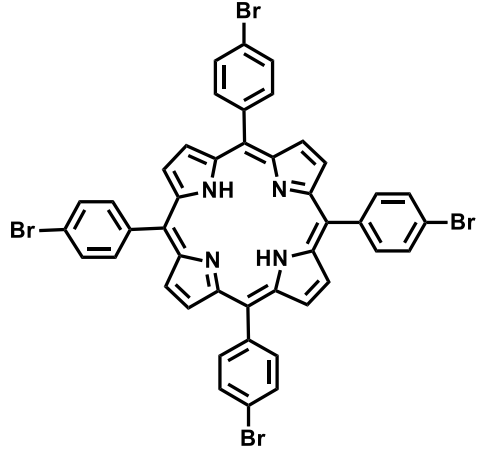
As a greener approach, microwave-assisted organic synthesis (MAOS) has gained some attention over the last few years. This technology has been used since the mid-1980s.⁶¹⁻⁶² Petit et al first described the synthesis of porphyrins using microwave irradiation in 1992.⁶³ The decrease in reaction times, improvement of yields, simplified treatment and purification and versatility of this method, have led scientists to fully recognize that MAOS is a useful alternative tool in medicinal synthetic chemistry and drug development, including porphyrin synthesis.⁶⁴

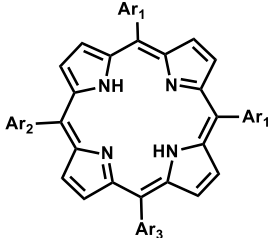
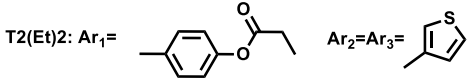
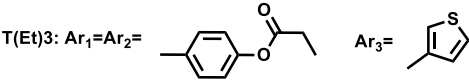
In 2007, Pineiro and Gonsalves reported an adaptation of the classical one-step nitrobenzene method to microwave technology.⁶⁵ Using a domestic microwave equipment, with a power of 640 W, they tested the use of pyrrole in a mixture of propionic acid and nitrobenzene with 13 different aryl aldehydes, irradiated for 5 minutes, obtaining the correspondent porphyrins with low to moderate yields.⁶⁵ Later, Pineiro and Gonsalves revisited this methodology using a single-mode microwave reactor.⁶⁶ The aryl aldehyde and pyrrole were added to the propionic acid/nitrobenzene mixture at 200 °C for 5 minutes using only 250 W as the initial power setting. The yields obtained ranged from 5% to 55% and the mass obtained from 0.5 to 1.1 g.⁶⁶

In 2016, a review⁶⁷ was written describing the most relevant synthetic methods of *meso*-substituted aryl porphyrins, under microwave irradiation developed so far. Table 1.3 summarizes *meso*-substituted aryl porphyrins synthesized between 2016 and 2021, using microwave irradiation.

Table 1.3: Microwave assisted synthesis of *meso* aryl tetra-substituted porphyrins.

#	Porphyrin	Reagents	Time	Temperature	Power	Yield	Reference
1		Pyrrole Acetic acid Nitrobenzene 2,3,4,5,6-Pentafluorobenzaldehyde	15 min	120°C	650W	19%	68
2		1 Pyrrole Furfural SiO ₂ /Al ₂ O ₃ or Al ₂ O ₃ a) 2, 3, 4 Pyrrole	20 min	170°C	1000W	2-5%	69

		aryl-aldehyde in dioxane Amberlyst \5 b)					
3		4-hydroxy-3- methoxybenzaldehyde Methyl 4-formyl benzoate Pyrrole Al ₂ O ₃	9 min	Not referred	650W	38%	70
4		4-bromobenzaldehyde Pyrrole CH ₂ Cl ₂ Propionic Acid	20 min	Not referred	300W	78%	71

		c)					
5	  	Thiophene-2-carboxaldehyde 4-hydroxybenzaldehyde Propionic acid Propionic anhydride Pyrrole	8 min	135°C	800W	T2(Et)2 10% T(Et)3 11%	72

a) Porphyrinogen is isolated, and oxidation is performed with DDQ. b) It is not clear how oxidation is performed. c) It is not clear how oxidation is performed. It seems that they perform the synthesis of porphyrinogen and then perform oxidation with p-chloranil.

The recent literature review clearly highlights that the use of microwaves in the synthesis of substituted *meso*-aryl porphyrins has contributed to improve the sustainability of the process. However, as observed with synthetic processes obtained by conventional heating, the final porphyrin yields are highly dependent on the aldehyde structure, reaction temperature, solvent and irradiation power used.

The results presented in Table 1.3 show that most authors are using one-step porphyrin synthesis and very high irradiation powers (650-1000 W), except in entry 4 where the irradiation power was only 300 W. It should be noted that in the last methodology the authors used, they obtained 78% of *meso*-tetra-(4-bromophenyl)porphyrin in only 20 min (Table 1.3, entry 4). The synthesis of *meso*-tetrapentafluorophenyl porphyrin was achieved with 19% yield, using one-pot nitrobenzene method (acetic acid/nitrobenzene mixture), under 650W, at 120 °C within just 15 minutes of reaction time (Table 1.3, entry 1). The synthesis of non-symmetric *meso*-substituted porphyrins with 38% yield in only 9 minutes using Al₂O₃ as catalyst (Table 1.3, entry 3) was remarkable.

The use of microwaves was also evaluated in the synthesis of porphyrins containing heteroaromatics in the *meso* positions (furan and thiophene) using very high irradiation powers (1000 and 800 W, respectively), but the yields obtained were always less than 15%. (Table 1.3 entries 2 and 5)

Overall, the use of microwave irradiation for porphyrin synthesis is still under study and can achieve very interesting yields with low reaction times. MAOS can also be used to obtain other derivatives, such as chlorins, bacteriochlorins and to introduce substituents in the porphyrin periphery in order to modulate their functionalization.⁶⁴

To our knowledge, this methodology has never been applied to the synthesis of porphyrins containing imidazolyl groups in the *meso* positions and, therefore, the transposition of classic porphyrin synthetic methodologies to this alternative and more sustainable technology is one of the main goals of this project.

1.5. Goals

The use of porphyrin and their derivatives in clinical trials requires the development of simple synthetic processes, economically viable, with few side reactions and that can be easily scalable. From critical analysis of literature, we hypothesized that *meso*-substituted porphyrins are more in sync with these goals than the beta-substituted ones, which generally requires multi-step synthetic approaches. Therefore, our first hypothesis to use porphyrins in Medicinal Chemistry, particularly for aPDI applications, was the development of *meso*-substituted imidazolyl-porphyrin synthetic methods in a multi-gram scale.

Among the various computational tools available, we have chosen conformational analysis as a tangible goal for a one-year MSc. project. It was hypothesized that the size and structure of the cationic side chain and high absorption in the therapeutical window of imidazolyl cationic macrocycles may have a significant effect for future development of ideal photosensitizers for aPDI. This can be obtained with the development of imidazolyl cationic chlorins. (Figure 1.3).

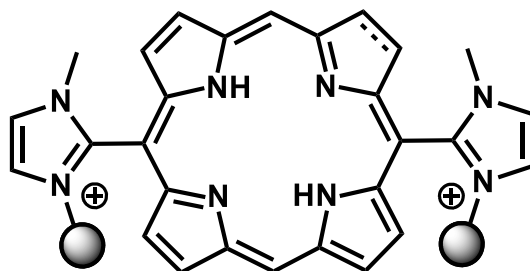


Figure 1.3: Example of cationic *meso*-bis-imidazolyl photosensitizer studied. ----- with double bond porphyrin; single bond, chlorin.

The specific goals of this work are:

- i) To perform computational conformational analysis of *meso*-imidazolyl cationic chlorins – modulation of potential photosensitizers for aPDI.
- ii) To develop scalable processes for synthesis of *meso*-imidazolyl porphyrin-based photosensitizer.
- iii) To synthesize a set of cationic *meso*-imidazolyl based porphyrins for potential aPDI applications.
- iv) To synthesize cationic *meso*-imidazolyl based chlorins for potential aPDI clinical transposition.

1.6. References

1. Rawson, T. M.; Ming, D.; Ahmad, R.; Moore, L. S. P.; Holmes, A. H., Antimicrobial use, drug-resistant infections and COVID-19. *Nature Reviews Microbiology* **2020**, *18* (8), 409-410.
2. Rawson, T. M.; Moore, L. S. P.; Zhu, N.; Ranganathan, N.; Skolimowska, K.; Gilchrist, M.; Satta, G.; Cooke, G.; Holmes, A., Bacterial and fungal coinfection in individuals with coronavirus: a rapid review to support COVID-19 antimicrobial prescribing. *Clinical Infectious Diseases* **2020**, *71* (9), 2459-2468.
3. Abraham, E. P.; Chain, E., An Enzyme from Bacteria Able to Destroy Penicillin. *Nature* **1940**, *146* (3713), 837-837.
4. Ruckert, A.; Fafard, P.; Hindmarch, S.; Morris, A.; Packer, C.; Patrick, D.; Weese, S.; Wilson, K.; Wong, A.; Labonté, R., Governing antimicrobial resistance: a narrative review of global governance mechanisms. *Journal of Public Health Policy* **2020**, *41* (3), 515-528.
5. Chioro, A.; Coll-Seck, A. M.; Hoie, B.; Moeloek, N.; Motsoaledi, A.; Rajatanavin, R.; Touraine, M., Antimicrobial resistance: a priority for global health action. *Bulletin World Health Organization* **2015**, *93* (7), 439.
6. Grey, J. L.; Thompson, D. H., Challenges and opportunities for new protein crystallization strategies in structure-based drug design. *Expert Opinion on Drug Discovery* **2010**, *5* (11), 1039-1045.
7. Leach, A. R.; Gillet, V. J.; Lewis, R. A.; Taylor, R., Three-dimensional pharmacophore methods in drug discovery. *Journal of Medicinal Chemistry* **2010**, *53* (2), 539-558.
8. Theuretzbacher, U.; Outterson, K.; Engel, A.; Karlén, A., The global preclinical antibacterial pipeline. *Nature Reviews Microbiology* **2020**, *18* (5), 275-285.
9. World-Health-Organization, WHO report on surveillance of antibiotic consumption:2016-2018 early implementation. **2019**.
10. Blair, J. M. A.; Webber, M. A.; Baylay, A. J.; Ogbolu, D. O.; Piddock, L. J. V., Molecular mechanisms of antibiotic resistance. *Nature Reviews Microbiology* **2015**, *13* (1), 42-51.
11. Butler, M. S.; Paterson, D. L., Antibiotics in the clinical pipeline in October 2019. *The Journal of Antibiotics* **2020**, *73* (6), 329-364.
12. Hamblin, M. R.; Hasan, T., Photodynamic therapy: a new antimicrobial approach to infectious disease? *Photochemical and Photobiological Sciences* **2004**, *3* (5), 436-450.
13. Casas, A.; Venosa, G. D.; Hasan, T.; Al, B., Mechanisms of resistance to photodynamic therapy. *Current Medicinal Chemistry* **2011**, *18* (16), 2486-2515.
14. Dai, T.; Huang, Y. Y.; Hamblin, M. R., Photodynamic therapy for localized infections—State of the art. *Photodiagnosis and Photodynamic Therapy* **2009**, *6* (3), 170-188.
15. Maisch, T., Resistance in antimicrobial photodynamic inactivation of bacteria. *Photochemical and Photobiological Sciences* **2015**, *14* (8), 1518-1526.
16. Soares, J. M.; Inada, N. M.; Bagnato, V. S.; Blanco, K. C., Evolution of surviving *Streptococcus pyogenes* from pharyngotonsillitis patients submit to multiple cycles of antimicrobial photodynamic therapy. *Journal of Photochemistry and Photobiology B: Biology* **2020**, *210*, 111985.
17. Vinagreiro, C. S.; Zangirolami, A.; Schaberle, F. A.; Nunes, S. C. C.; Blanco, K. C.; Inada, N. M.; Da Silva, G. J.; Pais, A. A. C. C.; Bagnato, V. S.; Arnaut, L. G.; Pereira, M. M., Antibacterial photodynamic inactivation of antibiotic-resistant bacteria and biofilms with nanomolar photosensitizer concentrations. *ACS Infectious Diseases* **2020**, *6* (6), 1517-1526.
18. Berman, J.; Krysan, D. J., Drug resistance and tolerance in fungi. *Nature Reviews Microbiology* **2020**, *18* (6), 319-331.
19. Talele, T. T.; Khedkar, S. A.; Rigby, A. C., Successful applications of computer aided drug discovery: moving drugs from concept to the clinic. *Current Topics in Medicinal Chemistry* **2010**, *10* (1), 127-141.

20. Rahuel, J.; Rasetti, V.; Maibaum, J.; Rüeger, H.; Göschke, R.; Cohen, N. C.; Stutz, S.; Cumin, F.; Fuhrer, W.; Wood, J. M.; Grütter, M. G., Structure-based drug design: the discovery of novel nonpeptide orally active inhibitors of human renin. *Chemistry & biology* **2000**, *7* (7), 493-504.
21. Richardson, P.; Griffin, I.; Tucker, C.; Smith, D.; Oechsle, O.; Phelan, A.; Rawling, M.; Savory, E.; Stebbing, J., Baricitinib as potential treatment for 2019-nCoV acute respiratory disease. *Lancet (London, England)* **2020**, *395* (10223), e30-e31.
22. Kashef, N.; Hamblin, M. R., Can microbial cells develop resistance to oxidative stress in antimicrobial photodynamic inactivation? *Drug Resistance Updates : Reviews and Commentaries in Antimicrobial and Anticancer Chemotherapy* **2017**, *31*, 31-42.
23. Hamblin, M. R., Antimicrobial photodynamic inactivation: a bright new technique to kill resistant microbes. *Current Opinion Microbiology* **2016**, *33*, 67-73.
24. Malik, Z., Photodynamic inactivation of antibiotic-resistant Gram-positive bacteria: challenges and opportunities. *Translational Biophotonics* **2020**, *2* (1-2), e201900030.
25. Xuan, W.; Huang, L.; Wang, Y.; Hu, X.; Szewczyk, G.; Huang, Y.-Y.; El-Hussein, A.; Bommer, J. C.; Nelson, M. L.; Sarna, T.; Hamblin, M. R., Amphiphilic tetracationic porphyrins are exceptionally active antimicrobial photosensitizers: In vitro and in vivo studies with the free-base and Pd-chelate. *Journal of Biophotonics* **2019**, *12* (8), e201800318.
26. Kessel, D., Photodynamic therapy: from the beginning. *Photodiagnosis and Photodynamic Therapy* **2004**, *1* (1), 3-7.
27. Luis Guilherme Da Silva Arnaut Moreira, Maria Miguéns Pereira, Sebastião José Formosinho Sanches Simões, Sérgio Paulo Magalhães Simões, Grazyna Stochel, Krystyna Urbanska. Process for preparing chlorins and their pharmaceutical uses. US 9,670,217 B2, 6 June 2017
28. Donohoe, C.; Senge, M. O.; Arnaut, L. G.; Gomes-da-Silva, L. C., Cell death in photodynamic therapy: from oxidative stress to anti-tumor immunity. *Biochimica et Biophysica Acta (BBA) - Reviews on Cancer* **2019**, *1872* (2), 188308.
29. Silva, E. F. F.; Serpa, C.; Dąbrowski, J. M.; Monteiro, C. J. P.; Formosinho, S. J.; Stochel, G.; Urbanska, K.; Simões, S.; Pereira, M. M.; Arnaut, L. G., Mechanisms of singlet-oxygen and superoxide-ion generation by porphyrins and bacteriochlorins and their implications in photodynamic therapy. *Chemistry – A European Journal* **2010**, *16* (30), 9273-9286.
30. Dąbrowski, J. M.; Arnaut, L. G., Photodynamic therapy (PDT) of cancer: from local to systemic treatment. *Photochemical & Photobiological Sciences* **2015**, *14* (10), 1765-1780.
31. Frochet, C.; Mordon, S., Update of the situation of clinical photodynamic therapy in Europe in the 2003–2018 period. *Journal of Porphyrins and Phthalocyanines* **2019**, *23* (04n05), 347-357.
32. Pérez-Laguna, V.; Gilaberte, Y.; Millán-Lou, M. I.; Agut, M.; Nonell, S.; Rezusta, A.; Hamblin, M. R., A combination of photodynamic therapy and antimicrobial compounds to treat skin and mucosal infections: a systematic review. *Photochemical and Photobiological Sciences* **2019**, *18* (5), 1020-1029.
33. Wainwright, M., The emerging chemistry of blood product disinfection. *Chemical Society Reviews* **2002**, *31* (2), 128-136.
34. Vieira, C.; Santos, A.; Mesquita, M. Q.; Gomes, A. T. P. C.; Neves, M. G. P. M. S.; Faustino, M. A. F.; Almeida, A., Advances in aPDT based on the combination of a porphyrinic formulation with potassium iodide: effectiveness on bacteria and fungi planktonic/biofilm forms and viruses. *Journal of Porphyrins and Phthalocyanines* **2019**, *23* (04n05), 534-545.
35. Zhdanova, K. A.; Savelyeva, I. O.; Ignatova, A. A.; Gradova, M. A.; Gradov, O. V.; Lobanov, A. V.; Feofanov, A. V.; Mironov, A. F.; Bragina, N. A., Synthesis and photodynamic antimicrobial activity of amphiphilic meso-arylporphyrins with pyridyl moieties. *Dyes and Pigments* **2020**, *181*.
36. Mamone, L.; Ferreyra, D. D.; Gandara, L.; Di Venosa, G.; Vallecorsa, P.; Saenz, D.; Calvo, G.; Batlle, A.; Buzzola, F.; Durantini, E. N.; Casas, A., Photodynamic inactivation of planktonic and biofilm growing bacteria mediated by a meso-substituted porphyrin bearing four basic amino groups. *Journal of Photochemistry and Photobiology B* **2016**, *161*, 222-229.

37. Reynoso, E.; Ferreyra, D. D.; Durantini, E. N.; Spesia, M. B., Photodynamic inactivation to prevent and disrupt *Staphylococcus aureus* biofilm under different media conditions. *Photodermatology Photoimmunology and Photomedicine* **2019**, *35* (5), 322-331.
38. Lambrechts, S. A. G.; Demidova, T. N.; Aalders, M. C. G.; Hasan, T.; Hamblin, M. R., Photodynamic therapy for *Staphylococcus aureus* infected burn wounds in mice. *Photochemical & Photobiological Sciences* **2005**, *4* (7), 503-503.
39. Lesar, A.; Begić, G.; Malatesti, N.; Gobin, I., Innovative approach in *Legionella* water treatment with photodynamic cationic amphiphilic porphyrin. *Water Supply* **2019**, *19* (5), 1473-1479.
40. Tasli, H.; Akbiyik, A.; Topaloglu, N.; Alptuzun, V.; Parlar, S., Photodynamic antimicrobial activity of new porphyrin derivatives against methicillin resistant *Staphylococcus aureus*. *Journal of microbiology (Seoul, Korea)* **2018**, *56* (11), 828-837.
41. Xuan, W.; Huang, L.; Wang, Y.; Hu, X.; Szewczyk, G.; Huang, Y. Y.; El-Hussein, A.; Bommer, J. C.; Nelson, M. L.; Sarna, T.; Hamblin, M. R., Amphiphilic tetracationic porphyrins are exceptionally active antimicrobial photosensitizers: in vitro and in vivo studies with the free-base and Pd-chelate. *Journal of Biophotonics* **2019**, *12* (8), 1-13.
42. Xu, Z.; Gao, Y.; Meng, S.; Yang, B.; Pang, L.; Wang, C.; Liu, T., Mechanism and in vivo evaluation: photodynamic antibacterial chemotherapy of lysine-porphyrin conjugate. *Frontiers in Microbiology* **2016**, *7*, 242.
43. Yuan, Y.; Liu, Z. Q.; Jin, H.; Sun, S.; Liu, T. J.; Wang, X.; Fan, H. J.; Hou, S. K.; Ding, H., Photodynamic antimicrobial chemotherapy with the novel amino acid-porphyrin conjugate 4I: in vitro and in vivo studies. *PLoS One* **2017**, *12* (5), e0176529.
44. Hurst, A. N.; Scarbrough, B.; Saleh, R.; Hovey, J.; Ari, F.; Goyal, S.; Chi, R. J.; Troutman, J. M.; Vivero-Escoto, J. L., Influence of cationic *meso*-substituted porphyrins on the antimicrobial photodynamic efficacy and cell membrane interaction in *Escherichia coli*. *International journal of molecular sciences* **2019**, *20* (1), 134.
45. Banerjee, I.; Douaisi, M. P.; Mondal, D.; Kane, R. S., Light-activated nanotube-porphyrin conjugates as effective antiviral agents. *Nanotechnology* **2012**, *23* (10), 105101.
46. Wen, W. H.; Lin, M.; Su, C. Y.; Wang, S. Y.; Cheng, Y. S. E.; Fang, J. M.; Wong, C. H., Synergistic effect of zanamivir-porphyrin conjugates on inhibition of neuraminidase and inactivation of influenza virus. *Journal of Medicinal Chemistry* **2009**, *52* (15), 4903-4910.
47. Jeong, H.; Lee, J. J.; Lee, J.; Na, K., A multiligand architectural photosensitizer that targets hemagglutinin on envelope of influenza virus for photodynamic inactivation. *Small* **2020**, *16* (20), 2000556.
48. Perlin, M.; Mao, J. C. H.; Otis, E. R.; Shipkowitz, N. L.; Duff, R. G., Photodynamic inactivation of influenza and herpes viruses by hematoporphyrin. *Antiviral Research* **1987**, *7* (1), 43-51.
49. Nikolaeva-Glomb, L.; Mukova, L.; Nikolova, N.; Kussovski, V.; Doumanova, L.; Mantareva, V.; Angelov, I.; Wöhrle, D.; Galabov, A. S., Photodynamic effect of some phthalocyanines on enveloped and naked viruses. *Acta virologica* **2017**, *61* (3), 341-346.
50. Ke, M. R.; Eastel, J. M.; Ngai, K. L. K.; Cheung, Y. Y.; Chan, P. K. S.; Hui, M.; Ng, D. K. P.; Lo, P. C., Photodynamic inactivation of bacteria and viruses using two monosubstituted zinc(II) phthalocyanines. *European Journal of Medicinal Chemistry* **2014**, *84*, 278-283.
51. Ke, M. R.; Eastel, J. M.; Ngai, K. L. K.; Cheung, Y. Y.; Chan, P. K. S.; Hui, M.; Ng, D. K. P.; Lo, P. C., Oligolysine-conjugated zinc(II) phthalocyanines as efficient photosensitizers for antimicrobial photodynamic therapy. *Chemistry – An Asian Journal* **2014**, *9* (7), 1868-1875.
52. Sobotta, L.; Wierzchowski, M.; Mierzwicki, M.; Gdaniec, Z.; Mielcarek, J.; Persoons, L.; Goslinski, T.; Balzarini, J., Photochemical studies and nanomolar photodynamic activities of phthalocyanines functionalized with 1,4,7-trioxanonyl moieties at their non-peripheral positions. *Journal of Inorganic Biochemistry* **2016**, *155*, 76-81.
53. Korneev, D.; Kurskaya, O.; Sharshov, K.; Eastwood, J.; Strakhovskaya, M., Ultrastructural aspects of photodynamic inactivation of highly pathogenic avian H5N8 influenza virus. *Viruses* **2019**, *11*, 955 (10), 1-11.

54. Weber, H. M.; Mehran, Y. Z.; Orthaber, A.; Saadat, H. H.; Weber, R.; Wojcik, M., Successful reduction of SARS-CoV-2 viral load by photodynamic therapy (PDT) verified by QPCR – a novel approach in treating patients in early infection stages. *Medical and Clinical Research*. **2020**, *5* (11), 311-325.
55. Rothemund, P., Formation of Porphyrins from Pyrrole and Aldehydes. *Journal of the American Chemical Society* **1935**, *57* (10), 2010–2011.
56. Adler, A. D.; Longo, F. R.; Finarelli, J. D.; Goldmacher, J.; Assour, J.; Korsakoff, L., A simplified synthesis for meso-tetraphenylporphine. *The Journal of Organic Chemistry* **1967**, *32* (2), 476-476.
57. Gonsalves, A. M. D. A. R.; Pereira, M. M., A new look into the rothemund meso-tetraalkyl and tetraarylporphyrin synthesis. *Journal of Heterocyclic Chemistry* **1985**, *22* (3), 931-933.
58. Lindsey, J. S.; Hsu, H. C.; Schreiman, I. C., Synthesis of tetraphenylporphyrins under very mild conditions. *Tetrahedron Letters* **1986**, *27* (41), 4969-4970.
59. Gonsalves, A. M. D. A. R.; Varejão, J. M. T. B.; Pereira, M. M., Some new aspects related to the synthesis of meso-substituted porphyrins. *Journal of Heterocyclic Chemistry* **1991**, *28* (3), 635-640.
60. Littler, B. J.; Ciringh, Y.; Lindsey, J. S., Investigation of Conditions Giving minimal scrambling in the synthesis of trans-porphyrins from dipyrromethanes and aldehydes. *The Journal of organic chemistry* **1999**, *64* (8), 2864-2872.
61. Giguere, R. J.; Bray, T. L.; Duncan, S. M.; Majetich, G., Application of commercial microwave ovens to organic synthesis. *Tetrahedron Letters* **1986**, *27* (41), 4945-4948.
62. Gedye, R.; Smith, F.; Westaway, K.; Ali, H.; Baldisera, L.; Laberge, L.; Rousell, J., The use of microwave ovens for rapid organic synthesis. *Tetrahedron Letters* **1986**, *27* (3), 279-282.
63. Petit, A.; Loupy, A.; Maiuardb, P.; Momenteaub, M., Microwave irradiation in dry media: a new and easy method for synthesis of tetrapyrrolic compounds. *Synthetic Communications* **1992**, *22* (8), 1137-1142.
64. Pineiro, M., Microwave-assisted synthesis and reactivity of porphyrins. *Current Organic Synthesis* **2014**, *11* (1), 89-109.
65. Nascimento, B. F. O.; Pineiro, M.; Gonsalves, A. M. D. A. R.; Silva, M. R.; Beja, A. M.; Paixão, J. A., Microwave-assisted synthesis of porphyrins and metalloporphyrins: a rapid and efficient synthetic method. *Journal of Porphyrins and Phthalocyanines* **2007**, *11* (02), 77-84. ₂
66. Nascimento, B. F. O.; Rocha Gonsalves, A. M. d. A.; Pineiro, M., MnO instead of quinones as selective oxidant of tetrapyrrolic macrocycles. *Inorganic Chemistry Communications* **2010**, *13* (3), 395-398.
67. Pinto, S. M. A.; Henriques, C. A.; Tomé, V. A.; Vinagreiro, C. S.; Calvete, M. J. F.; Dąbrowski, J. M.; Pineiro, M.; Arnaut, L. G.; Pereira, M. M., Synthesis of meso-substituted porphyrins using sustainable chemical processes. *Journal of Porphyrins and Phthalocyanines* **2016**, *20* (01n04), 45-60.
68. Rebelo, S. L. H.; Silva, A. M. N.; Medforth, C. J.; Freire, C., Iron(III) fluorinated porphyrins: greener chemistry from synthesis to oxidative catalysis reactions. *Molecules* **2016**, *21* (4), 481-481.
69. Bosca, F.; Tagliapietra, S.; Garino, C.; Cravotto, G.; Barge, A., Extensive methodology screening of meso-tetrakis-(furan-2-yl)-porphyrin microwave-assisted synthesis. *New Journal of Chemistry* **2016**, *40* (3), 2574-2581.
70. Boscencu, R.; Socoteanu, R. P.; Manda, G.; Radulea, N.; Anastasescu, M.; Gama, A.; Machado, I. F.; Ferreira, L. F. V., New A3B porphyrins as potential candidates for theranostic. Synthesis and photochemical behaviour. *Dyes and Pigments* **2019**, *160*, 410-417.
71. Matamala-Cea, E.; Valenzuela-Godoy, F.; González, D.; Arancibia, R.; Dorcet, V.; Hamon, J.-R.; Novoa, N., Efficient preparation of 5,10,15,20-tetrakis(4-bromophenyl)porphyrin. Microwave assisted v/s conventional synthetic method, X-ray and hirshfeld surface structural analysis. *Journal of Molecular Structure* **2020**, *1201*, 127139.
72. Mazumdar, Z. H.; Sharma, D.; Mukherjee, A.; Basu, S.; Shukla, P. K.; Jha, T.; Sengupta, D., meso-thiophenium porphyrins and their Zn(II) complexes: a new category of cationic photosensitizers. *ACS Medicinal Chemistry Letters* **2020**, *11* (10), 2041-2047.

2. Computational analysis of chlorin photosensitizers

Computational methods are nowadays regularly used to accelerate the process of drug discovery. Once the drug discovery target is selected, the identification of the active pharmaceutical ingredient (API), goes through essentially three phases: i) Inquiry phase, that aims to identify chemical compounds with promising activity towards the target, ii) Hit generation phase, wherein hit compounds are improved in potency against the target and iii) lead optimization phase, in which lead compounds are optimized, generating molecules that will ultimately have a beneficial pharmacological effect on patients (Figure 2.1). Computational methods can help in these drug discovery activities, from target identification to giving an insight on small molecules that can interact with the target and their properties. It is also possible to predict absorption, distribution, metabolism, elimination (ADME) and toxicology parameters of drugs candidates, limiting failures in costly pre-clinical and clinical trials

2020	2021	2022	2023	2024	2025	2026	2027	2028	2029
API Search									
Inquiry (docking, virtual screening)									
Hit generation (QSAR, <i>de novo</i> design)									
	Lead optimization (QSAR, molecular dynamics)								
		Pre-clinical assays							
		ADME and toxicology testing							
					Clinical trials				
					Phase I, II, III				
									EMA approval
GLP API									
Good Laboratory Practices									
			GMP API						
			Good Manufacturing Practices						

Figure 2.1: Drug Discovery pipeline highlighted with the phases where computational methods can give insights.

Ab initio methods that give a very precise electronic structure of the molecules are scarcely incorporated in drug discovery, mainly because such methods are difficult to apply to proteins and, in general, to the study of intermolecular interactions. However, *Ab initio* calculations become more relevant for aPDI because it is not the specific interaction of the PS with the biological target that kills the microorganisms but its reactivity with the oxygen molecules around it. In this sense, *ab initio* calculations are more interesting to assess the properties, namely the charge distribution of the proposed PS to predict its suitability in aPDI.

Given the positions of a set of atomic nuclei, and the total number of electrons in the system, the electronic energy, electron density, and other properties are calculated using a well-defined automated approximation. The ability to obtain approximate solutions to the electronic Schrödinger equation for systems containing up to hundreds of atoms has revolutionized the ability of theoretical chemistry to address important problems in a wide range of subjects; the Nobel Prize awarded to John Pople and Walter Kohn in 1998 reflects this observation.¹

Density Functional Theory Methods (DFT) have been considered to achieve a particular level of accuracy at relatively low cost in the determination of the molecular geometry and spectroscopic (IR, Raman, and UV-vis spectra and ¹H and ¹³C NMR chemical shifts), thermodynamic, and electronic properties (HOMO, LUMO, NLO, and MEP) of polyatomic molecules.²

Hybrid functionals are a class of approximations to the exchange–correlation energy functional in DFT that incorporate a portion of exact exchange from Hartree–Fock theory with the rest of the exchange–correlation energy from other sources (*ab initio* or empirical). The exact exchange energy functional is expressed in terms of the Kohn–Sham orbitals. One of the most used versions is B3LYP, (Becke, 3-parameter, Lee–Yang–Parr).³ If sufficient electronic correlation effects are considered and a suitable basis sets is chosen, it is usually possible to predict reliable optimized geometric parameters and vibrational frequencies of molecules.⁴⁻⁷ Among the many DFT methods, the hybrid functional B3LYP, first developed to study vibrational absorption and circular dichroism, has been shown to be a good compromise between computational cost and accuracy of results. It has become a standard method to study organic molecules in the gas phase.

As mentioned above, a very important feature for the interaction of molecules with bacterial membranes is the charge distribution.⁸⁻⁹ which can be evaluated calculating the Electrostatic potential maps of the molecules. In short, this can be obtained moving a

positively charged test charge along the spherical isosurface of an atom or molecule. The positively charged nucleus emits a radially constant electric field. A region of higher-than-average electrostatic potential energy indicates the presence of a stronger positive charge or a weaker negative charge. Given the consistency of the nuclei positive charge, the higher potential energy value indicates the absence of negative charges, which would mean that there are fewer electrons in this region. The converse is also true. Thus, a high electrostatic potential indicates the relative absence of electron density, and a low electrostatic potential indicates an abundance of electrons.¹⁰

Our starting point are the cationic porphyrins PS developed in the catalysis & fine chemistry research group that have proved to be highly efficient against biofilms.⁹ These di-imidazolyl cationic zinc porphyrins are highly symmetrical due to their 1,3-disubstituted imidazolyl groups. As a matter of fact, Hamblin et al observed that a change in the symmetry of the molecule is an interesting feature to enhance bacterial membrane permeation, resulting in an improved aPDI efficacy Figure 2.2.¹¹

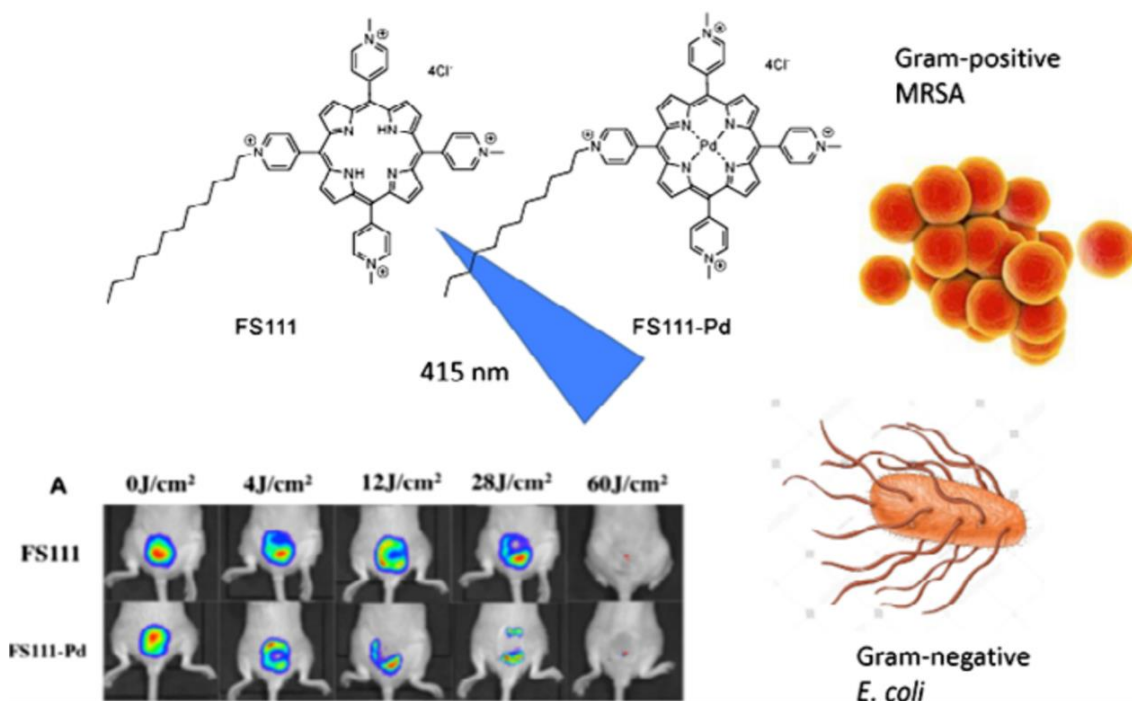
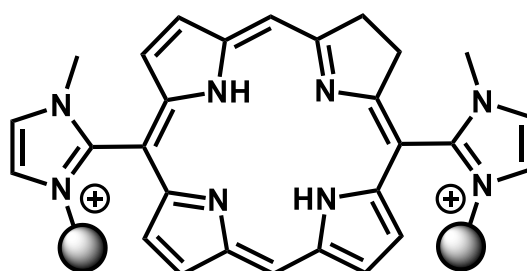


Figure 2.2 Improved aPDI due to changes in the symmetry of the molecule to enhance bacterial membrane permeation. Where MRSA means methicillin-resistant *Staphylococcus aureus*. Adapted from the literature.¹¹

In this sense, we chose to evaluate the effect of inserting groups with different chains in the symmetry of the molecule and modulate the charge distribution throughout the molecule with groups of varying polarities.

Among the various computational tools available, we have chosen conformational analysis as a tangible goal for a one-year M.Sc. project. It was hypothesized that the size and structure of the side chain and high absorption in the therapeutic window of imidazolyl cationic macrocycles may have a significant effect for future development of ideal photosensitizers for aPDI. This can be solved with the development of imidazolyl cationic chlorins. Therefore, in this chapter, we describe our preliminary and introductory results of computational analysis of imidazolyl di-cationic chlorins containing methyl, ethyl and trifluoro ethyl chains (Scheme 2.1).

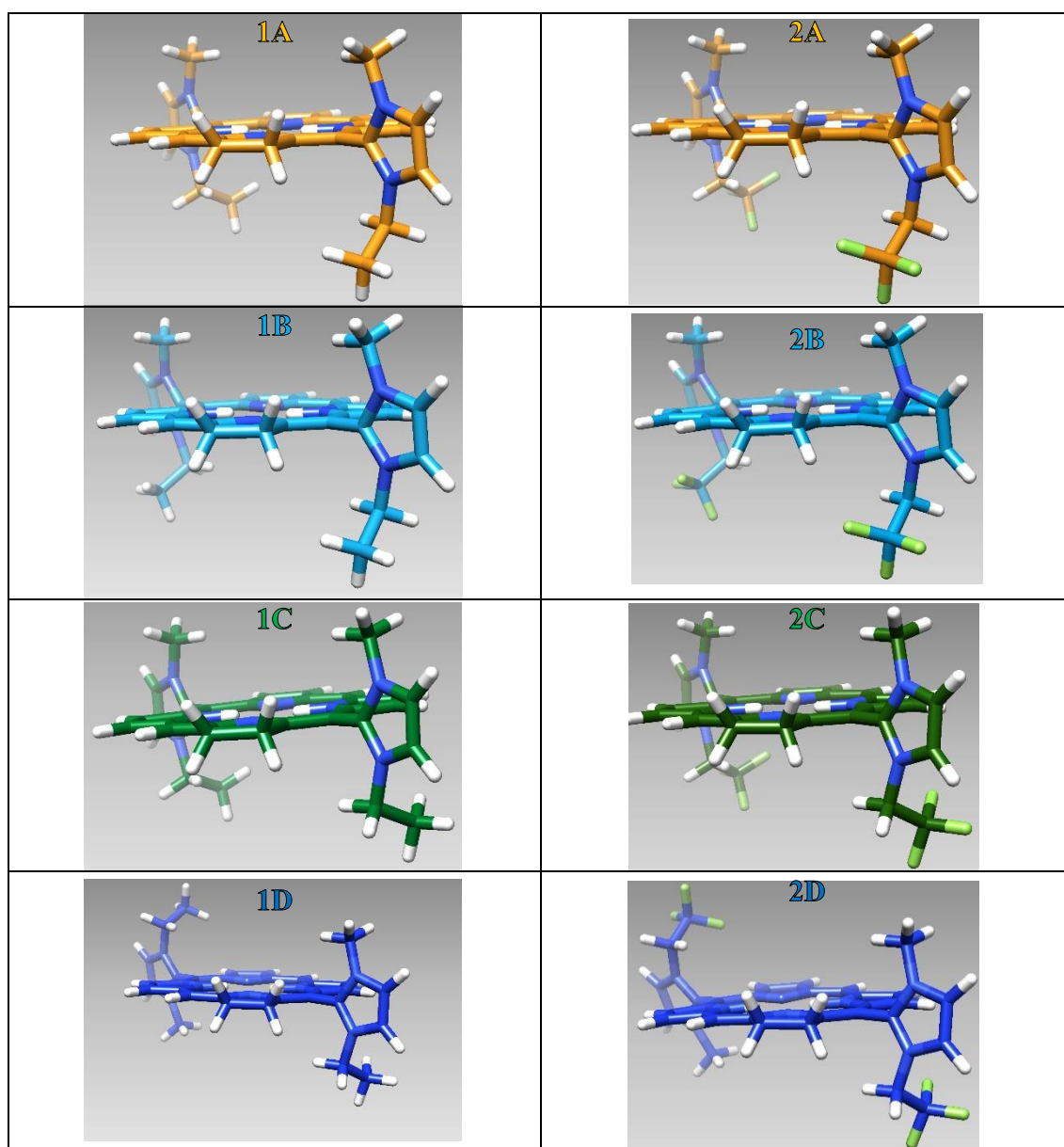


Scheme 2.1: non-symmetrical di-imidazolyl cationic chlorin

Herein we aim to use computational calculations to give an insight on i) charge distribution in chlorins and in di and tetra substituted derivatives different from the porphyrin derivatives ii) the effect of substituents on the charge distribution iii) whether we will obtain stable atropisomers and iv) whether we will obtain different conformers. In an attempt to answer these points, the following section presents the results of a conformational analysis on the di and tetra substituted chlorins together with the density distribution maps on some selected optimized structures.

2.1. Conformational analysis using DFT calculations

First, we started with the structure optimization, at the DFT level, of different conformers of the cationic di-imidazolyl chlorins. The literature suggests that these molecules may be interesting due to their charge distribution⁹ and the presence of groups with different electronegativities. On the left column of Figure 2.3 are presented the conformers of the chlorin with ethyl cationic side-chains and on the right the conformers of the chlorin with fluorinated ethyl ones.



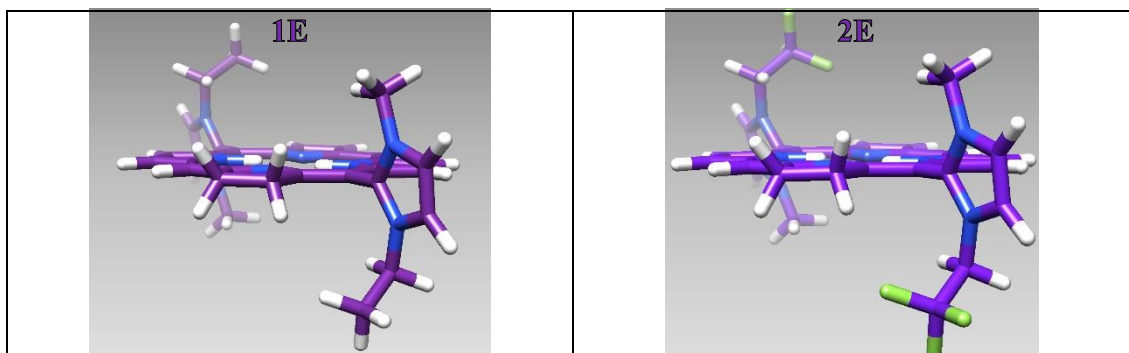
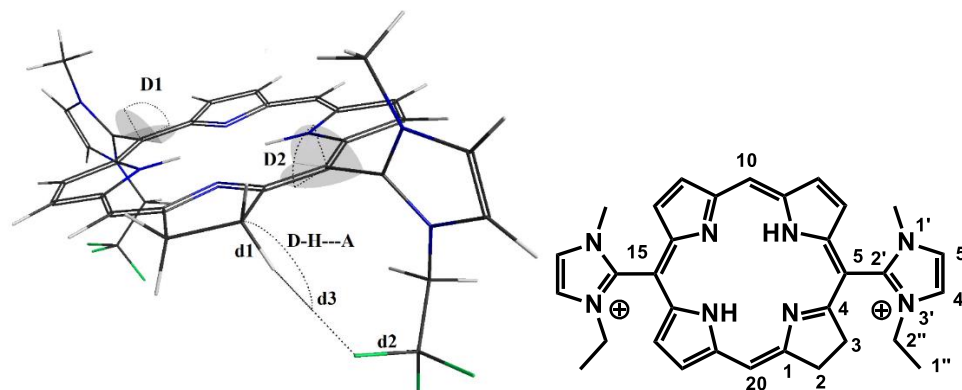


Figure 2.3: Structures of some selected conformers of ethyl and 1,1,1-trifluorethyl-5,15-bisimidazol-2-yl chlorins optimized at the B3LYP/6-31G(d,p) level. Color code: blue stands for nitrogen, white for hydrogen and green for the fluorine atoms. Carbon atoms are represented by orange, light blue, green and violet.

Table 2.1 contains a compilation of the energy difference between conformers together with structural features considered more relevant to characterize the optimized structure of the molecules presented in Figure 2.3.

Table 2.1: Energy difference (kJmol^{-1}) of the conformers of cationic ethyl and 1,1,1-trifluorethyl 5,15-bis-imidazol-2-yl chlorins relatively to the most stable structure and structural features considered to be more relevant for the discrimination between conformers. D stands for angles, in degrees, while d stands for distance between selected atoms, in Angstroms, according to the scheme included in the top of the table.



Conform. Label	ΔE (kJ/mol)	D1	D2	d1 (Å)	d2 (Å)	d3 (Å)	D-H...A
		Dihedral angle ($^{\circ}$) ($\text{N}_1\text{C}_2\text{C}_{15}\text{C}_{14}$)	Dihedral angle ($^{\circ}$) ($\text{N}_1\text{C}_2\text{C}_5\text{C}_4$)	($\text{C}_3\text{-H}_3$)	($\text{C}_1\cdots\text{F}_{1\cdots}$)	($\text{H}_3\text{-F}_{1\cdots}$)	Angle ($^{\circ}$) ($\text{C}_3\text{H}_3\text{F}_{1\cdots}$)
1A	1.9	89.8	84.8				
1B	2.1	99.2	85.4				
1C	0.4	88.0	94.0				
1D	0.0	98.8	93.1				
1E	1.7	100.2	85.2				
2A	2.6	90.4	84.2	1.09	1.35	2.36	154.3
2B	0.0	100.6	84.6	1.09	1.35	2.36	155.4
2C	6.4	87.3	97.77	1.10	1.35	-	-
2D	6.1	106.4	98.22	1.10	1.35	-	-
2E	2.0	104.8	84.08	1.09	1.35	2.37	154.5

From Table 2.1, it is possible to observe that:

1. Generally, the differences in energy between the conformers are not very large.
 - a. The energy differences in the fluorinated conformers (**2A-2E**) are larger than in the alkyl ones (**1A-1E**), mainly due to the stabilization promoted by the intramolecular CF...H hydrogen bonds observed in conformers **2A**, **2B** and **2E**.
2. The minimum energy in the alkyl compounds corresponds, as could be expected, to the conformer with the substituted groups in a *trans* arrangement, **1D**.
3. The minimum energy in the fluorinated compounds corresponds to conformer **2B**, in which there is a possibility of hydrogen bonding from the fluorine atom of the substituent with the hydrogen atom of the chlorine as in conformers **2A** and **2E**.
 - a. The distance d_3 between H_3 and F_1 is similar to the one found in the literature for hydrogen bonding.
4. For the fluorinated compounds, the conformers that have the groups pointing away from the chlorine hydrogens **2C** and **2D**, have a greater d_1 (C_3-H_3) than when the fluorinated group is facing these hydrogens (**2A**, **2B** and **2E**).

The small energy difference between the *trans* conformers **2A-2C** and *cis* conformers **2D-2E**, called by IUPAC atropisomers, (resultant from the hindered rotation around the C_5-C_2 single bond)¹² suggests that both atropisomers can be obtained experimentally with similar probabilities. Complementary studies on rotational barriers around the single-bond C_5-C_2 would give further insight.

Figure 2.4 shows a comparison of the electrostatic potential maps from selected chlorine conformers.

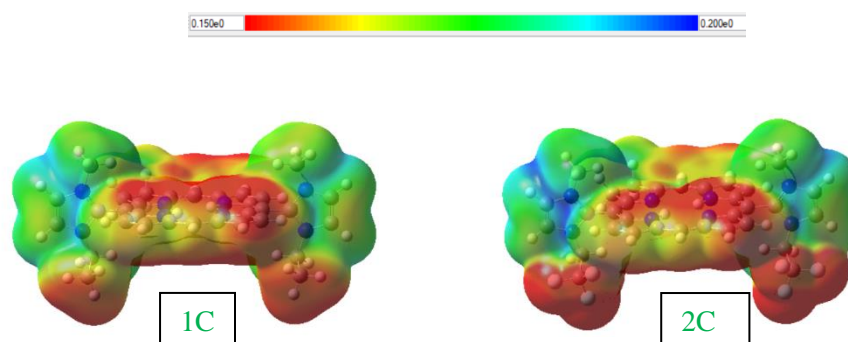


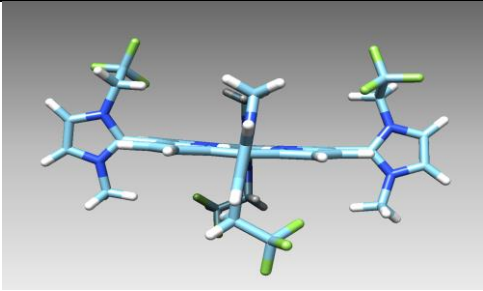
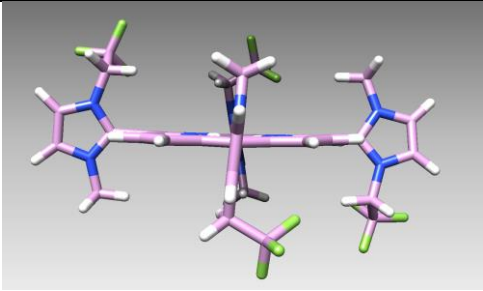
Figure 2.4: Electronic density maps of the *cis* ethyl derivative conformer **1C** and the fluorinated ethyl conformer **2C**, without counterions, from total self-consistent field density mapped with electrostatic potential, isovalue = 0.0004 at the B3LYP/6-31G(d,p) level in atomic units (e/a_0^3).

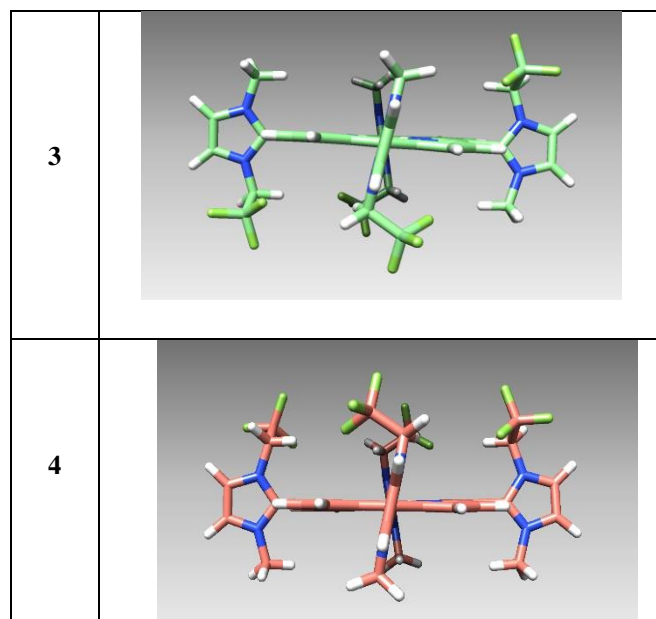
When analyzing the electrostatic potential maps, we can observe that in the fluorinated compound **2C**, there seems to be a region containing the fluorine groups (dark red) that is more electronegative than when the alkyl group is present (**1C**-orange). The asymmetry in the charge distribution could be beneficial in the interaction with Gram-negative bacteria.^{11,13} The experimental separation of this particular atropisomer could be of interest as the photosensitizer may be able to tether to the Gram-negative membrane through both of the longer chains.

It is known from experimental results, that 5,15-bis(1-methyl)imidazol-2-yl porphyrins have excellent results on inactivation of Gram-positive bacteria inside biofilms, while 5,10,15,20-tetra (1-methyl)imidazol-2-yl porphyrins have great results on photoinactivation of planktonic bacteria.⁹ Both can be interesting in the combat against bacterial resistance. Therefore, to give an insight on these differences, a similar analysis was performed for selected conformers of the tetrasubstituted imidazolyl chlorin.

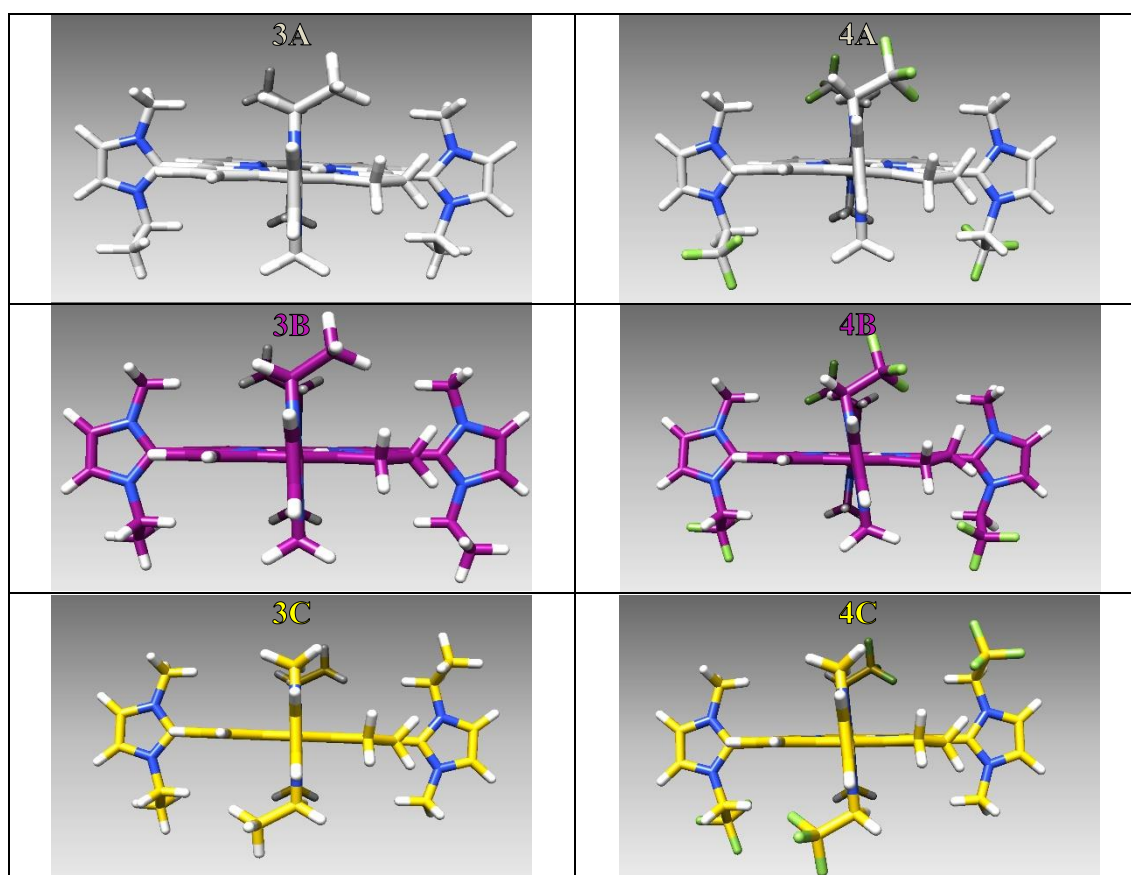
Table 2.2 summarizes the possible geometrical arrangements for the tetra-substituted compounds resultant from the hindered rotation around the single-bonds C₅-C_{2'}; C₁₀-C_{2'}; C₁₅-C_{2'} and C₂₀-C_{2'} of porphyrin-imidazolyl rings (atropisomers).

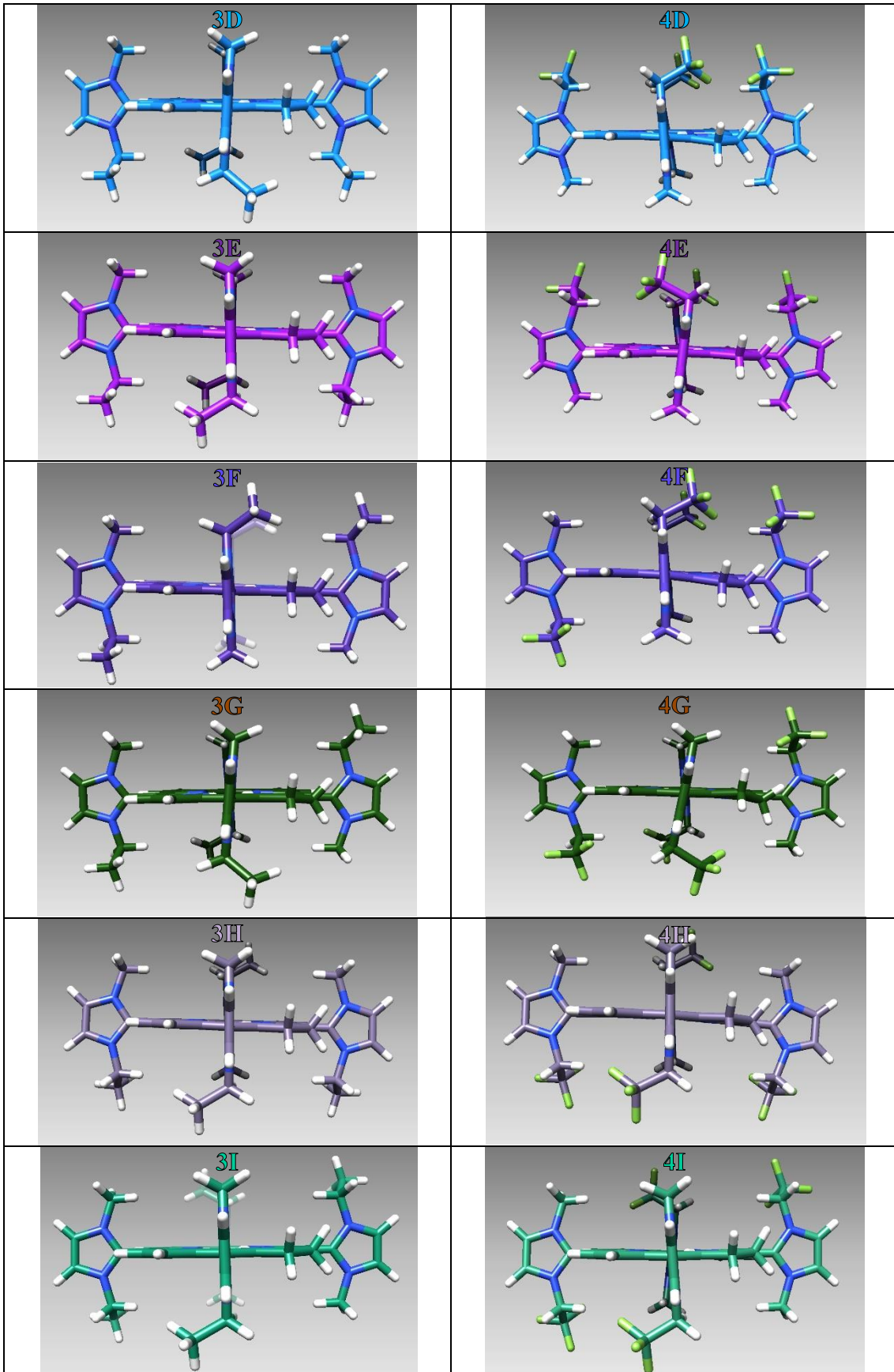
Table 2.2 Atropisomers of the tetra-substituted compounds.

#	Atropisomer
1	
2	



The structures of the conformers of the ethyl and fluoro-ethyl tetra-imidazolyl chlorins optimized at the DFT level are depicted in Figure 2.5.





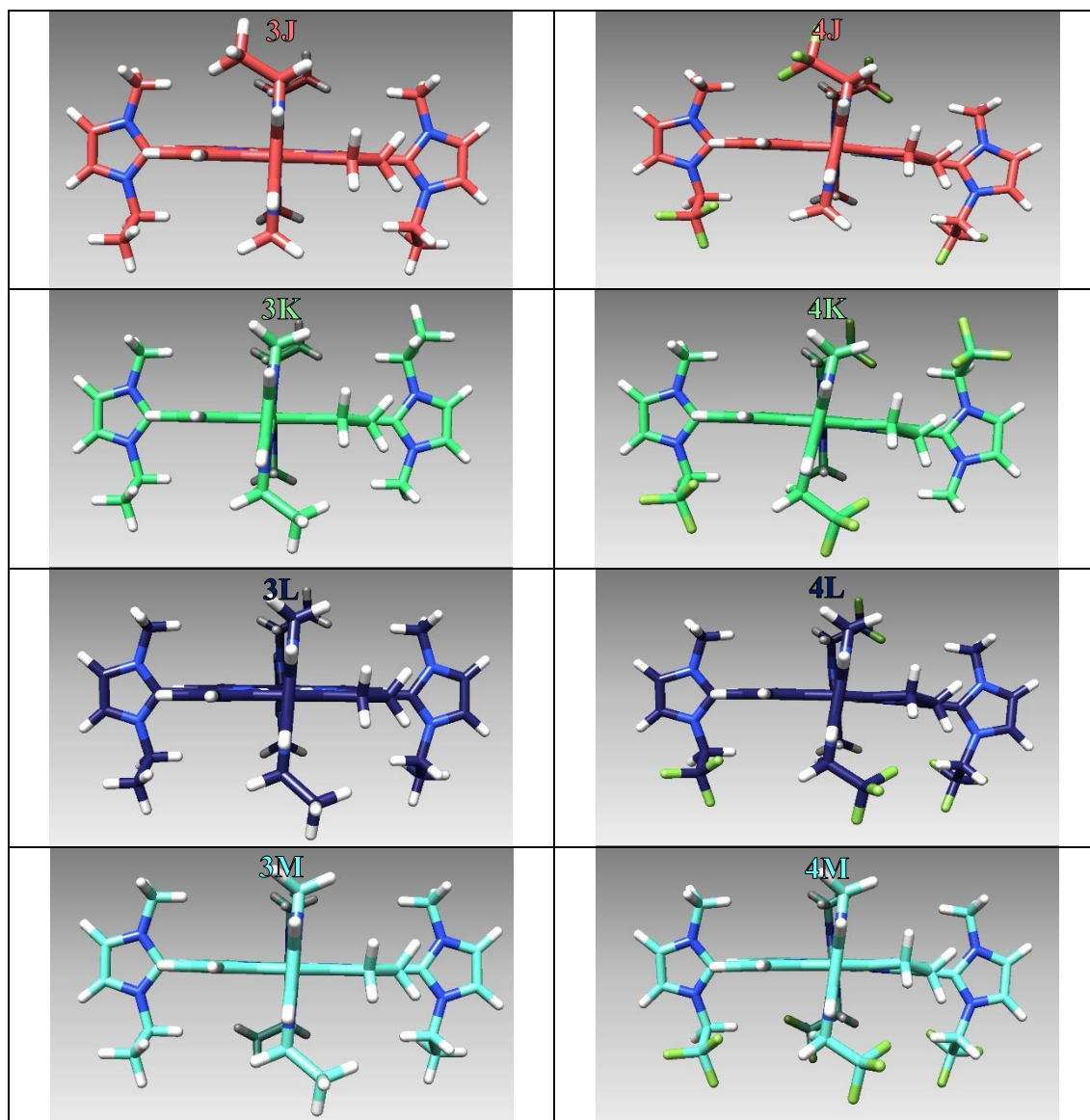


Figure 2.5: Structures of the conformers of ethyl and 1,1,1-trifluorethyl-5,10,15,20-tetraimidazol2-yl chlorins optimized at the B3LYP/6-31G(d,p) level. Color code: blue stands for nitrogen, white for hydrogen and green for the fluorine atoms. Carbon atoms are represented by light brown, light grey, dark purple, yellow, light blue, purple, blue, dark green, gray, emerald, red, light green, dark blue, teal.

The relative energies and the most relevant dihedral angles defining the position of the substituents are, in turn, presented in Table 2.3.

Table 2.3: Energy difference (kJmol⁻¹) of the conformers of cationic ethyl and 1,1,1-trifluorethyl 5,10,15,20-tetraimidazol-2-yl chlorins relatively to the most stable structure and structural features considered to be more relevant for the discrimination between conformers. D stands for angles, in degrees, while d stands for distance between selected atoms, in Angstroms, according to the scheme included in the top of the table.

Conformer label	ΔE (kJ/mol)	D1	D2	D3	D4
		Dihedral angle (°) (N ₁ ·C ₂ ·C ₁₅ C ₁ 4)	Dihedral angle (°) (N ₁ ·C ₂ ·C ₁₀ C 9)	Dihedral angle (°) (N ₁ ·C ₂ ·C ₁₅ C ₁ 4)	Dihedral angle (°) (N ₁ ·C ₂ ·C ₂₀ C ₁ 9)
3A	0.9	94.0	87.4	92.4	86.9
3B	1.7	94.3	92.2	92.7	93.5
3C	1.3	95.0	93.6	85.8	87.2
3D	2.2	93.9	86.3	87.6	89.2
3E	0.3	88.2	93.4	87.6	89.3
3F	3.0	92.3	92.5	95.2	86.8
3G	2.6	95.2	91.4	94.8	95.6
3H	0.7	86.3	92.4	94.7	86.2
3I	0.0	89.1	87.4	87.4	88.3
3J	0.3	88.4	87.4	87.1	87.0
3K	2.4	95.7	92.9	91.4	92.4
3L	2.5	94.9	93.9	91.5	96.3
3M	1.2	94.4	92.8	91.1	92.8
4A	6.3	97.0	86.3	97.1	84.5
4B	3.1	98.6	97.4	98.0	98.6
4C	6.3	97.7	83.6	81.9	96.6
4D	3.4	81.3	81.3	78.7	85.6
4E	10.6	85.5	95.5	79.8	80.5
4F	1.9	97.9	81.9	81.6	83.0
4G	2.1	98.0	98.0	98.2	99.7
4H	9.8	83.7	93.6	103.5	82.5
4I	11.2	89.5	85.9	81.4	84.7
4J	7.2	85.8	89.9	83.9	81.0
4K	0.0	98.3	97.5	96.0	96.7
4L	2.9	97.5	97.7	97.1	98.7
4M	5.4	96.9	96.2	98.6	100.4

Overall, it is possible to note that:

1. Generally, the differences in energy between the conformers are not very large.
 - a. The energy differences in the fluorinated compounds are larger than in the alkyl ones, as observed in the di-substituted compounds, due to the presence of intramolecular CH...F hydrogen bonds in the lowest energy conformers.
 - b. The atropisomer **2** (Table 2.2), shows the largest energy difference between the fluorinated compounds with the groups facing towards the hydrogens of the chlorine (**4K**) and the one with the fluorinated groups facing away from the hydrogens of the chlorine (**4I**) (Table 2.3).
 - c. Generally, the lower energy conformers have the fluorinated groups facing the chlorine hydrogens (**4B, 4D, 4F, 4G, 4L**).
2. The minimum energy in the alkyl compounds corresponds to the arrangement with the ethyl groups facing away from each other, with two ethyl groups on the same side (**3I**- atropisomer **2**).
3. The average of the dihedral angles (D1) of the fluorinated conformers is 94.2° while for the alkyl conformers it is 92.8°. This suggests that the presence of the fluorinated side chain causes some distortion in the overall structure, which can be relevant for biological applications.

These results suggest that, similarly to what happens to the di-substituted compounds, a mixture of four atropisomers (Table 2.2) should be obtained experimentally.

Finally, Figure 2.6 shows a comparison of the electrostatic potential maps from the 5,10,15,20-tetra(1-methyl)imidazol-2-yl porphyrin precursor and corresponding chlorine.

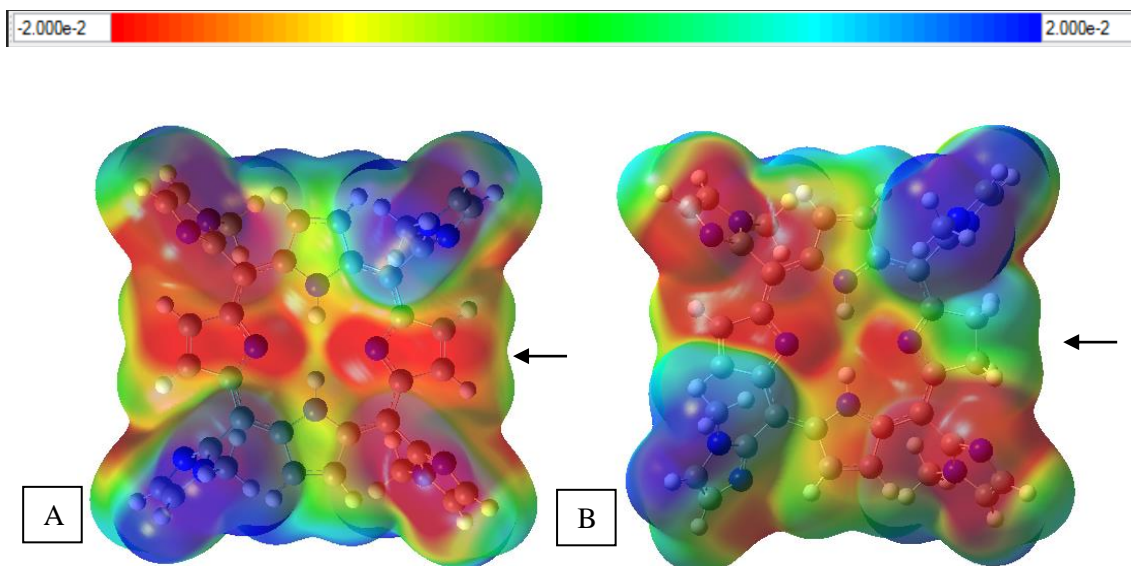


Figure 2.6: Electronic density maps of the tetrasubstituted imidazolyl porphyrin (A) and chlorin (B) without counterions, from total self-consistent field density mapped with electrostatic potential, isovalue = 0.0004 at the B3LYP/6-31G(d,p) level in atomic units (e/a_0^3).

The analysis of Figure 2.6 puts in evidence that the charge distribution near the sp^3 carbons of the chlorin is less electronegative (green) than the equivalent position of the porphyrin ring (red). This small structural difference is predicted to have consequences on the absorption spectra (different HOMO-LUMO energy differences) but will certainly be less relevant for the interaction with biological membranes.

2.2. Conclusions

Overall, conformational analysis is useful to identify conformers, predict atropisomers and evaluate asymmetric charge distribution which are structural features that can lead to very different photodynamic efficacies.¹⁴

From these results, it is possible to observe that i) the charge distribution of the central ring of the chlorin and the porphyrin is slightly different in the sp^3 carbons, which leads to a better absorption of the chlorins in the therapeutic window; ii) the substituents ethyl and fluorinated have similar charge distributions, although the fluorinated compound is more electronegative and iii) conformers should interconvert experimentally. It is necessary to test experimentally if the separation of the atropisomers is possible, as they

can have different interactions with the membrane which could lead to having certain atropisomers with more activity than others.

Overall, these results suggest a different conformation of the fluorinated relative to the alkylated molecule that seems to distort to allow the fluorine groups to be closer to the hydrogens of the chlorin. This conformational flexibility may lead to different intermolecular interactions with consequent different solid-state packing, which can result in changes of the photosensitizers' solubility and aPDI activity.

From the electrostatic potential maps, we can conclude that the fluorinated compounds seem to have a region that has more electron density than when the alkyl group is present. This asymmetry in the charge distribution could be valuable to interact with the membrane of bacteria. In sum, these conformational analysis, showed that the atropisomers have similar energies, both in *di* and *tetra*-substituted chlorins, which indicates that they can be experimentally separated, which can be relevant for aPDI applications.

2.3. References

1. Cramer, C. J., *Essentials of Computational Chemistry, Theories and Models* 2nd ed.; Wiley: 2004; p 618.
2. Leach, A. R., *Molecular modelling : principles and applications*. Prentice Hall: Harlow, England; New York, 2001.
3. Lee, C.; Yang, W.; Parr, R. G., Development of the Colle-Salvetti correlation-energy formula into a functional of the electron density. *Physical Review B* **1988**, *37* (2), 785-789.
4. Perdew, J. P.; Wang, Y., Accurate and simple analytic representation of the electron-gas correlation energy. *Physical review. B, Condensed matter* **1992**, *45* (23), 13244-13249.
5. Seminar, W. E. H.; Ziesche, P.; Eschrig, H.; Technische Universität, D.; Institut für Theoretische, P.; European Physical, S.; International Symposium on Electronic Structure of, S.; Dresdener Seminar für Theoretische, P., Electronic structure of solids '91 : proceedings of the 75. WE-Heraeus-Seminar and 21st Annual International Symposium on Electronic Structure of Solids held in Gaussig (Germany), March 11-15, 1991. **1991**.
6. Jensen, F., *Introduction to Computational Chemistry*. 3rd ed.; Wiley: 2017; p 660.
7. Dobson, J. F. V. g., Mukunda P. Das, *Electronic Density Functional Theory: Recent Progress and New Directions*. 1st ed.; 1998.
8. Cieplik, F.; Späth, A.; Regensburger, J.; Gollmer, A.; Tabenski, L.; Hiller, K.-A.; Bäumler, W.; Maisch, T.; Schmalz, G., Photodynamic biofilm inactivation by SAPYR—An exclusive singlet oxygen photosensitizer. *Free Radical Biology and Medicine* **2013**, *65*, 477-487.
9. Vinagreiro, C. S.; Zangirolami, A.; Schaberle, F. A.; Nunes, S. C. C.; Blanco, K. C.; Inada, N. M.; da Silva, G. J.; Pais, A. A. C. C.; Bagnato, V. S.; Arnaut, L. G.; Pereira, M. M.,

Antibacterial Photodynamic Inactivation of Antibiotic-Resistant Bacteria and Biofilms with Nanomolar Photosensitizer Concentrations. *ACS Infectious Diseases* **2020**, *6* (6), 1517-1526.

10. Electrostatic Potential maps <https://chem.libretexts.org/@go/page/1987> (accessed Jul 14, 2021).

11. Xuan, W.; Huang, L.; Wang, Y.; Hu, X.; Szewczyk, G.; Huang, Y.-Y.; El-Hussein, A.; Bommer, J. C.; Nelson, M. L.; Sarna, T.; Hamblin, M. R., Amphiphilic tetracationic porphyrins are exceptionally active antimicrobial photosensitizers: In vitro and in vivo studies with the free-base and Pd-chelate. *Journal of Biophotonics* **2019**, *12* (8), e201800318.

12. IUPAC, *Basic terminology of stereochemistry (IUPAC Recommendations 1996)*. 1996.

13. Arnaut, L. G.; Pereira, M. M.; Dąbrowski, J. M.; Silva, E. F. F.; Schaberle, F. A.; Abreu, A. R.; Rocha, L. B.; Barsan, M. M.; Urbańska, K.; Stochel, G.; Brett, C. M. A., Photodynamic Therapy Efficacy Enhanced by Dynamics: The Role of Charge Transfer and Photostability in the Selection of Photosensitizers. *Chemistry – A European Journal* **2014**, *20* (18), 5346-5357.

14. Rocha, L. B.; Gomes-da-Silva, L. C.; Dąbrowski, J. M.; Arnaut, L. G., Elimination of primary tumours and control of metastasis with rationally designed bacteriochlorin photodynamic therapy regimens. *European journal of cancer (Oxford, England : 1990)* **2015**, *51* (13), 1822-30.

3. Development of a scalable synthetic process of *meso*-imidazolyl porphyrins and derivatives

As previously portrayed in Chapter 1 the main synthetic processes of *meso*-aryl chlorins use porphyrins as starting materials. Therefore, based on the computational modulation of the cationic *meso*-imidazolyl chlorins, the studies herein described began with the optimization of the synthetic processes of the porphyrinic precursors. The use of porphyrin and their derivatives in clinical trials requires the development of simple, economically viable, synthetic processes with few side reactions and that can be easily scalable. The critical analysis of porphyrin synthetic methods described in the literature so far, led us to conclude that *meso*-substituted porphyrins are more in sync with these parameters than the beta-substituted ones, which generally requires multi-step synthetic approaches.¹ Therefore, our first hypothesis to use porphyrins in Medicinal Chemistry, particularly for aPDI applications, was the development of *meso*-substituted porphyrin synthetic methods in a multigram scale.

The development of a lead molecule for pre-clinical *in vitro* and *in vivo* studies requires the optimization of its synthesis under a pilot scale aiming the future transposition for Good Laboratory Practices (GLP) synthesis (Figure 3.1). With the overall goal of developing synthetic methods for cationic photosensitizers derived from *meso*-imidazolyl porphyrins, the studies began with the optimization of a scalable process of the core porphyrin. As described in Figure 3.1, this is the first step for API search once the inquiry phase is completed. Once the process is optimized, it is possible to obtain a pilot lot that will allow the start of the pre-clinical assays. During these assays, more process optimization is required to start using Good Manufacturing Practices (GMP) so that other lots can be made for the clinical trials and later for commercial use. GMP is necessary for products that are developed for use by human beings while GLP is applied for non-clinical laboratory studies.²

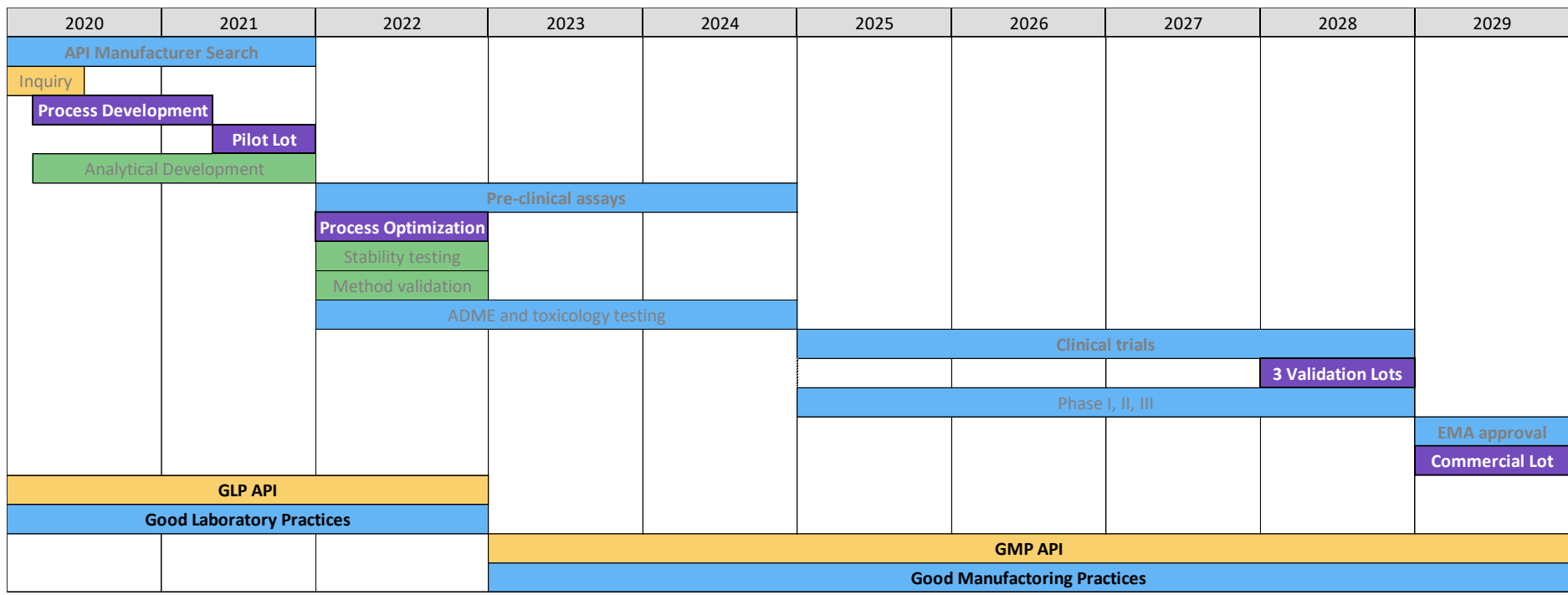


Figure 3.1: Drug discovery pipeline. In purple, the scale-ups necessary before transposition to the market.

As discussed in Chapter 1, the synthesis of *meso*-aryl porphyrins can be performed using essentially one of the following methods: i) one-pot pyrrole condensation with the aldehyde;³⁻⁴ ii) two-step pyrrole condensation with the aldehyde, followed by oxidation⁵⁻⁶ iii) condensation of dipyrromethane with the aldehyde, followed by oxidation (two-step synthesis).⁷ It is also established that these synthetic processes are not directly applicable for all the aldehydes. This becomes particularly relevant for 1-methylimidazolyl aldehyde, due to its specific reactivity accordingly to the solution pH.

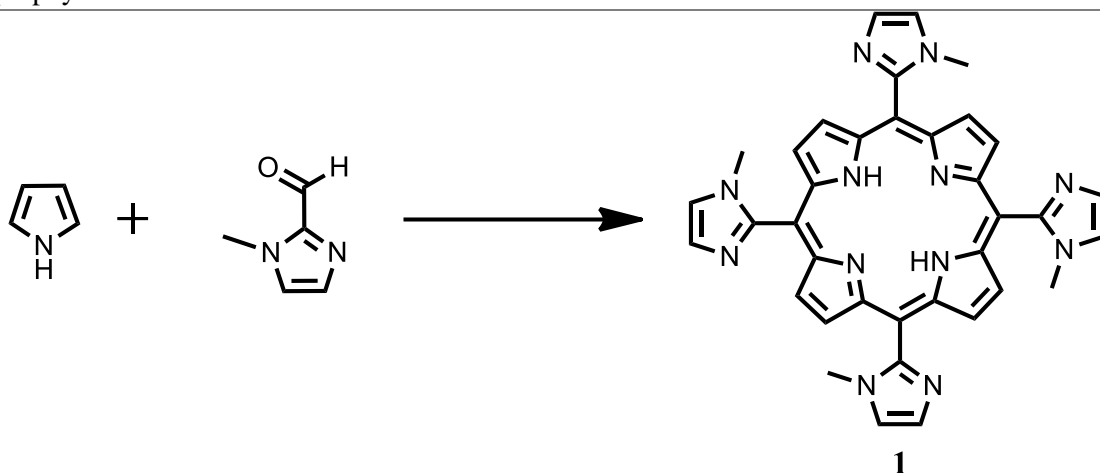
In the Catalysis & Fine Chemistry laboratory, tetra and bis-imidazolyl porphyrins (**1** and **2**, respectively) have been recently synthesized under milligram scale.⁸ Their zinc complexes were cationized using a large excess of methyl iodide and have shown excellent activity against Gram-negative bacteria and biofilms.⁸⁻⁹ and consequently, as mentioned before, this was the starting point of our studies.

One of the main goals of this work is to expand the family of the *meso*-imidazolyl based porphyrins for future preparation of chlorins and aPDI clinical transposition. Our first approach was to overcome the challenge for the preparation of the designed photosensitizers (tetra and bis-imidazolyl porphyrins **1** and **2**) in the amounts and purity that would open the way for their future transposition to pharmaceutical industrial synthesis.

3.1. Tetra-substituted imidazolyl-porphyrins

The studies began with the optimization of porphyrin **1** synthesis, in a laboratory scale, by selecting the most suitable synthetic methodology that will allow its easy transposition to multi-gram scale. These results are presented in Table 3.1. The multi-gram scale optimization studies were carried out at PorphyChem, Dijon laboratory and the results are shown in Table 3.2.

Table 3.1: Process optimization for synthesis of 5,10,15,20-tetra(1-methylimidazol-2-yl)porphyrin **1**.



#	Method	Concentration (mol/L)	Time	Purification	Yield
1	Two-step Lindsey, 1989 ⁵	0.01	24 h	-	0 %
2	Two-step Balaban, 2020 ⁶	0.0039	24 h	-	0%
3	One-pot Nitrobenzene Pereira-Gonsalves 1991 ³	0.20	2 h	Two silica gel adsorption chromatographies	19 %
4	One-pot Nitrobenzene/MW Pineiro- Gonsalves 2007 ¹⁰	0.20	20 minutes	Alumina plug	21 %

Our first approach to synthesize porphyrin **1** was based on the two-step Lindsey's methodology firstly reported in 1989.⁵ In a typical experiment, 1-methylimidazol-2-carboxyaldehyde was dissolved in chloroform and nitrogen was bubbled for ten minutes. Then, an equimolar amount of freshly distilled pyrrole was added dropwise followed by addition of catalytic amounts of $\text{BF}_3\text{Et}_2\text{O}$. To follow the cyclization step, the oxidation of the porphyrinogen toward the desired porphyrin was performed using 2,3-dichloro-5,6-dicyanobenzoquinone (DDQ) as oxidant. So, at timepoints 1 h, 3 h, 4 h, 5 h, 22 h and 24h, aliquots were removed from the reaction and an excess of DDQ was added. The solution was heated up to 60 °C for 30 minutes. A band at 460 nm (in general open chain

dipyrromethenes) was observed and the evolution of the reaction was monitored by TLC using silica as stationary phase and methanol:dichloromethane (20:80) as eluent. Under these conditions we observed that a spot migrated, but when we put the TLC plate under TFA vapors, it did not turn green (typical color of porphyrin di-cation), leading us to consider that it was not the desired product. Therefore, the reaction was stopped (Table 3.1, entry 1).

The second attempt was based on the two-step synthetic method recently described by Balaban⁶ using a set of non-polar aldehydes. To perform this, imidazol-2-carboxyaldehyde was added to ethanol and then the solution was bubbled with nitrogen. An equimolar amount of freshly distilled pyrrole was subsequently added dropwise. The solution was left in the dark, at 25 °C, with stirring, for 10 minutes. Finally, a catalytic amount of a diluted HCl solution (0.2 M; 30 mmol) was added. Timepoints were made after 1 h, 3 h, 5 h, 6 h, 22 h and 24 h. For these timepoints, aliquots were removed from the solution, extracted with chloroform, washed with distilled water and then a saturated solution of water was added. Once this process was done, excess of DDQ was added along with triethylamine for acid neutralization. UV-vis spectrum was performed but the typical Soret band at 420 nm was not observed (Table 3.1, entry 2). These disappointing results led us to conclude that these reaction conditions may avoid the cyclization step probably due to nitrogen atom protonation prior to condensation. These non-promising results led us to pursue the synthetic studies based on previously described one-pot methodologies that use weaker acids both as solvents and catalysts.

We started with the evaluation of the nitrobenzene method³ to promote the condensation of 1-methylimidazol-2-carboxyaldehyde with pyrrole (0.2 mol/L) using an acetic acid/nitrobenzene (2:1) mixture as solvent. The temperature was raised to 150 °C and the reaction was left under reflux for 2 hours. After cooling down, the solvents were evaporated *via* distillation, under vacuum. An adsorption column chromatography was then performed using silica gel as stationary phase and dichloromethane:hexane (1:1) as the first eluent. Once the remaining nitrobenzene was removed, the eluent's polarity was gradually changed from 10:0.1 (dichloromethane to methanol) till 10:1 proportion. The product was not pure and a second purification was required, using again silica gel as stationary phase and dichloromethane:methanol (10:1) as eluent. The desired 5,10,15,20-tetra(1-methylimidazol-2-yl) porphyrin **1** was obtained, with high purity, with 19 % isolated yield (Table 3.1, entry 3). It should be mentioned that no contamination with the correspondent chlorin was observed by analysis of the UV-Vis spectrum.

Finally, following the methodology firstly described by Pineiro and Gonsalves¹⁰ and based on microwave assisted synthesis, we carried out an experiment using a mixture of nitrobenzene:propionic acid as solvent and oxidant, under microwave irradiation. In a 50 mL flask, 1-methylimidazol-2-carboxyaldehyde was dissolved in a propionic acid/nitrobenzene (2:1) mixture and then equimolar amounts of pyrrole were added. The temperature ramp was set to 10 °C per minute with P_{max}=200 W to reach 175 °C within twenty minutes, with 22% stirring power. The temperature was then maintained at 175 °C for 20 minutes with P_{max}=125 W. After cooling, the solvents were evaporated before performing a short plug purification using alumina as stationary phase and the following combination of eluents: firstly, heptane to remove the remaining nitrobenzene, secondly, dichloromethane and finally dichloromethane with 3% of methanol. A purple fraction was recovered and after evaporation of the solvents, under vacuum, a simple recrystallization using methanol:diethyl ether as solvents (5:15) was enough to obtain the porphyrin with high purity. Using this more sustainable synthetic and purification procedures 21% isolated yield was obtained (Table 3.1, entry 4). From a critical analysis of Table 3.1, it is possible to conclude that the nitrobenzene/propionic acid method, under microwave irradiation, led to the highest yield and the simplest purification process. These results are not compared to the literature because, on the one hand, the powers used are not the same (320-640 W vs. 200W) and, on the other hand, no microwave-assisted synthetic methods can be found using imidazolyl aldehydes. Additionally, the concentration used in this reaction is transposed directly from the classical nitrobenzene method and is more concentrated than what we can find in the literature, which is a key point for large scale transposition.⁵

It should be emphasized that these nitrobenzene/acid methodologies when compared with Adler's process⁴ (using propionic acid without nitrobenzene) present the great advantage of the product not being contaminated with the respective chlorin. The classic nitrobenzene method has a more difficult purification process than the microwave process and this is one of the main reasons why the microwave approach was chosen for further process development to obtain a pilot lot (Figure 3.1). This process development includes the evaluation of other microwave methods, previously described in the literature, for the synthesis of **1** and the results are presented in Table 3.2.

Table 3.2: Optimization of the microwave synthetic process for tetra-imidazolyl porphyrin

#	One-pot methods	Temperature (°C)	Reaction time	Chlorin	Yield
1	Mw (propionic acid) ^a	175	20 minutes	Yes	~12%
2	Mw (nitrobenzene/ propionic acid) ^a	175	20 minutes	No	21%
3	Mw (water) ^b	180	10 minutes	Yes	~12%

a) Reaction conditions: pyrrole (5 mmol); aldehyde (0.510g; 4.62 mmol); volume (23 mL)

b) Reaction conditions: pyrrole (5 mmol); aldehyde (0.510g; 4.62 mmol); volume (0.2 mL)

First, we adapted the Adler's propionic acid method to the use of microwave irradiation.⁴ Thus, 1-methylimidazol-2-carboxyaldehyde (0.5 g; 4.6 mmol) was dissolved in 25 mL of propionic acid and 0.32 mL (5.0 mmol) of pyrrole were added in the microwave reactor, with a weflon magnet, setting the temperature to 175 °C at 125-200 W. After cooling we observed by UV-vis that a large amount of chlorin was formed. (Table 3.3, entry 1). Then, to be able to evaluate the reproducibility of the process we repeated the propionic acid/nitrobenzene method described above and once again we obtained 21% isolated yield. As shown in Figure 3.2, no chlorin formation was detected (Table 3.4, entry 2).

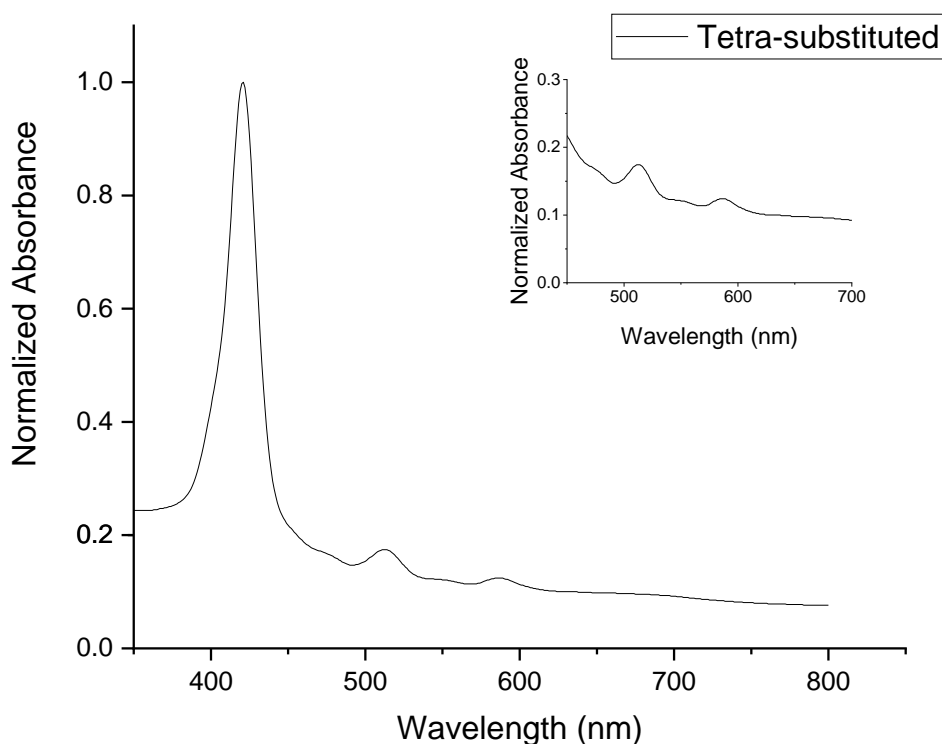


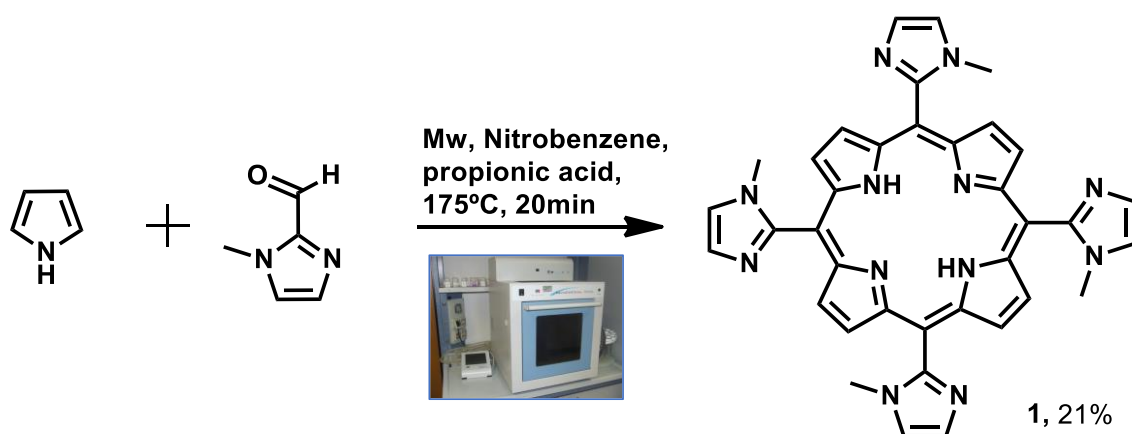
Figure 3.2: UV-vis spectrum of the reaction crude from aliquots of the microwave propionic acid/nitrobenzene reaction. No chlorin formation was observed.

Lastly, a mass of 0.5g (5 mmol) of 1-methylimidazol-2-carboxyaldehyde was added into a microwave tube with 0.34 mL of pyrrole (5 mmol) and 0.2mL of water. The tube was inserted into the microwave apparatus. The temperature was set at 185 °C with Pmax of 13 atm and a maximum potency of 300 W for 10 minutes. The solid was filtered from the aqueous phase and the mixture of compounds were dissolved in dichloromethane. A liquid-liquid extraction was performed using a sodium bicarbonate solution/ CH_2Cl_2 and finally CH_2Cl_2 /water. The porphyrin remains in the organic phase as demonstrated by UV-vis. The compound was purified using column chromatography with silica as stationary phase and the eluent was dichloromethane:methanol (10: 0.1 to 10:1). The solution was dried under vacuum overnight. However, it should be noted that chlorin formation was observed again (Table 3.5, entry 3).

From these results we can conclude that the method of choice to do the pilot scale is the propionic acid/ nitrobenzene under microwave irradiation. This decision is based on: i) high reproducibility; ii) low reaction time; iii) high yield; iv) higher concentrations

(0.20 M) than those from the literature; v) simple work-up; vi) high purity by simple recrystallization; vii) no chlorin formation.

Due to limitations on the maximum volume in the microwave apparatus and for safety reasons, we decided to maintain the reaction at this scale but repeat it four times before global lot purification. (This methodology is allowed by GLP)¹¹ After these replications, the solvents were evaporated before performing an alumina plug using heptane to remove the remaining nitrobenzene, then dichloromethane and finally dichloromethane with 3% methanol. The porphyrin was purified via recrystallization using methanol and diethyl ether (5:15) as solvents. After drying a mass of 0.451g was isolated with an overall yield of 21 %. Characterization data is present in Chapter 5. Scheme 3.1 shows the best synthetic route developed in this work.



Scheme 3.1: Best synthetic route to obtain porphyrin 1.

The ¹H-NMR spectrum of porphyrin 1 is presented in Figure 3.3. It is possible to observe the peaks at $\delta= 8.90-8.75$ (m, 8H _{β}), shown in blue, attributed to the beta hydrogens; 7.66-7.58 (m, 4H) and 7.45-7.41 (m, 4H), in yellow, from the hydrogens of the aromatic imidazolyl groups; 3.49-3.28 (m, 12H), in purple, showing the methyl groups and the inner hydrogens of the porphyrin -2.88 to -3.05 (m, 2H_{NH}) in green. This spectrum clearly shows that no chlorin peaks are observed namely at $\delta= -1$ to $\delta= -2$ ppm typical of the inner hydrogens nor at $\delta= 4$ to $\delta=5$ ppm typical of the four protons linked to the sp³ chlorin carbons.

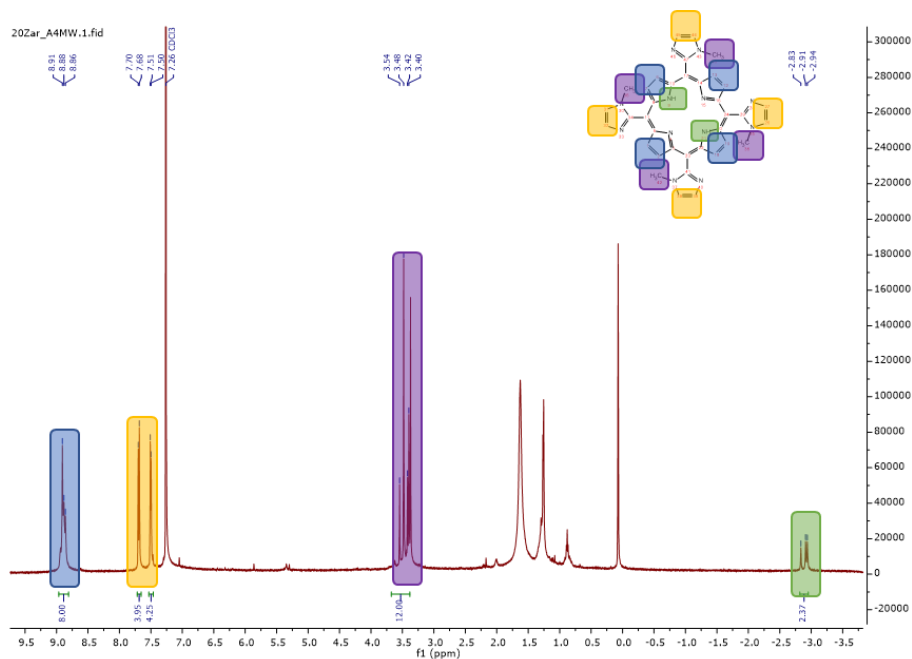
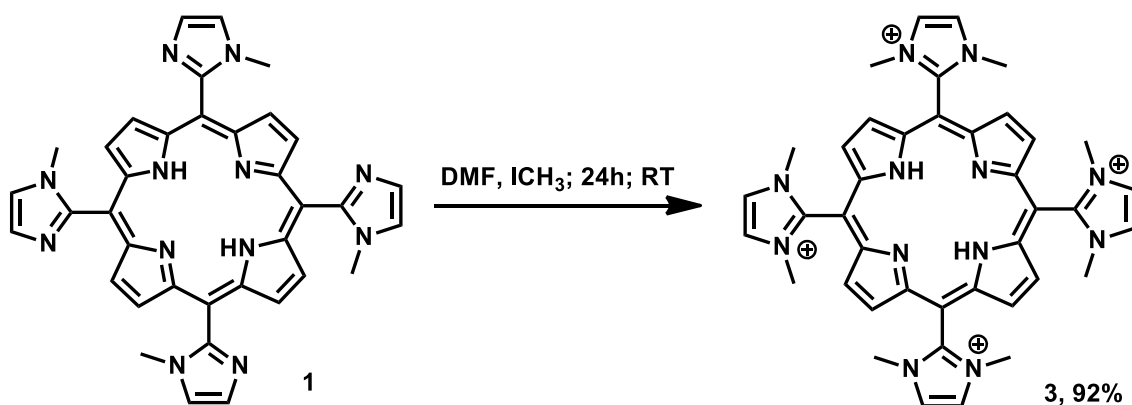


Figure 3.3: $^1\text{H-NMR}$ spectrum of tetra-*meso* imidazolyl porphyrin. In blue, the protons of the beta positions, in yellow the ones from the imidazolyl groups, in purple the methyl groups and in green the central protons of the porphyrinic ring.

It should be noted that the presence of multiplets instead of singlets corroborates the presence of several atropisomers as shown in the computational conformational analysis described in Chapter 2. To obtain the desired amphiphilic photosensitizer the tetra-cationization was performed with iodo-methyl in DMF, by adaptations of the procedures described in the literature.⁸ Scheme 3.2 shows the synthetic process used in this work to obtain the desired cationic 5,10,15,20-tetra(1-methyl)imidazolyl porphyrin, **3**.



Scheme 3.2: Cationization process of the 5,10,15,20-tetra(1-methyl)imidazolyl porphyrin using the method described in the literature.

The yield obtained (92%) is similar to the one previously described in the literature.⁸ For the workup, the product was precipitated using diethyl ether. A possible improvement of this reaction would be to use another aprotic solvent such as DME, that generally allows an easier work-up of the product. Due to time restrictions, our work focused on the di-substituted molecules as they showed better biofilm penetration results. In the future, tetra-substituted porphyrins should be subjected to further studies as they showed better results in photoinactivation of planktonic bacteria.⁸

In sum, the use of microwave irradiation for porphyrin synthesis, presents several advantages as discussed in Chapter 1, including lower time and energy consumption and easier work-up. However, this greener synthetic approach has some limitations for scale transposition associated with the volume of the microwave vials. At these high concentrations, using larger vials would allow the synthesis of porphyrins in a multigram scale faster than when using classical methods. For instance, using a MicroSYNTH Labstation batch scale-up pressure reactor it would be possible to use a 1 L vial allowing to safely have 500 mL of solvents. This would yield about 1.5 g of compound in only 20 minutes of reaction. To obtain the first pilot lot, it is estimated that about 10 g of this compound would be necessary, which would imply about 7 repetitions in 1 L flasks, which is possible to do within one week of work.¹²

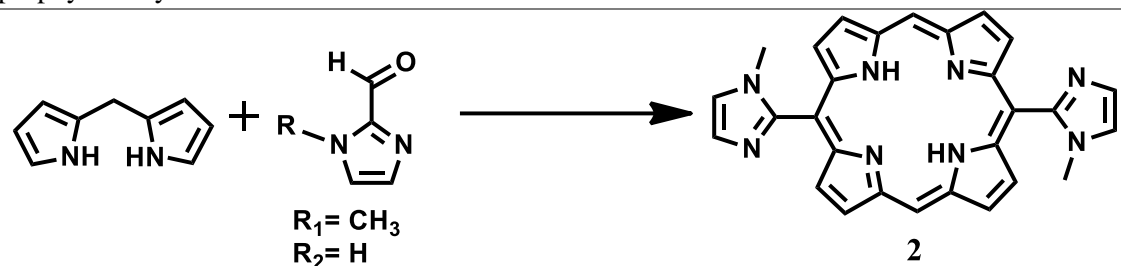
3.2. Scale-up of 5,15-bis-imidazolyl porphyrins

Another promising molecule that was previously studied in the Catalysis & Fine Chemistry laboratory is the Zn(II)-5,15-bis-imidazolyl porphyrin complex that showed one of the best results described in the literature so far to promote the photoinactivation of multi-resistant Gram-negative bacteria and biofilms, using a 415 nm LED (1.35 J/cm²).⁸ This exciting result led us to pursue this studies with the optimization of its multigram-scale preparation aiming the synthesis of a large family of amphiphilic cationic derivatives that could be promising molecules for aPDI and other medicinal applications.

To select the most appropriate synthetic method before the transposition to multigram scale, the studies began with the synthesis of **2** in a laboratory scale, using again

short modifications of the previously described methods. These results are presented in Table 3.6.

Table 3.6: Selection of the most promising synthetic method for 5,15-bis(1-methylimidazol-2-yl)porphyrin **2** synthesis

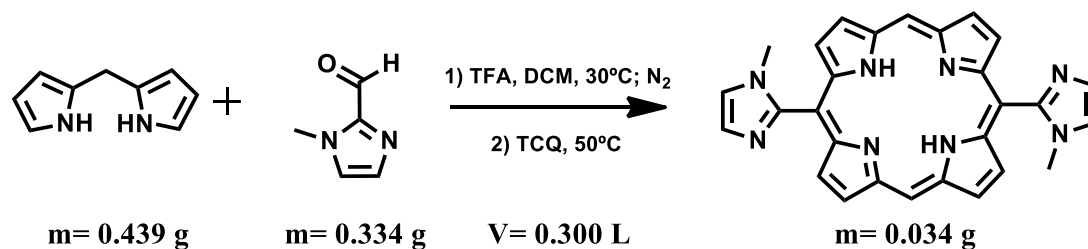


Entry	Method	R	Concentration (mol/L)	Time	Purification	Yield
1	Two-step Balaban, 2020 ⁶	R ₁ , R ₂	0.0039	17 h	-	0 %
2	Lindsey Two-step optimized in C&FC ⁷	R ₁	0.010	4 h	Silica gel adsorption chromatography and Flash chromatography	19%
3	Two-step (small scale) ⁵	R ₁	0.0052	24 h	Alumina plug	11.9%
4	Two-step (larger scale) ⁵	R ₁	0.0052	24 h	Silica gel plug and alumina plug	16.8 %

Our first synthetic approach was based on the two-step method described by Balaban *et al.* in 2020.¹⁰ First, 1-methylimidazol-2-carboxyaldehyde and dipyrromethane were added to ethanol, previously bubbled with nitrogen. The solution was left in the dark, at 25 °C, with stirring, for 10 minutes before adding a diluted solution of HCl, as catalyst. Timepoints were made after 1 h, 3 h, 5 h, 6 h and 17 h. For these timepoints, aliquots were removed from the solution, extracted with chloroform, washed with distilled water and then with a saturated solution of water. Once this process was done, excess of DDQ was added along with triethylamine. UV-vis spectra were performed but the typical porphyrin Soret band was not observed (Table 3.3, entry 1). The same method

was repeated in another experiment but using imidazol-2-carboxyaldehyde as the starting reactant, but again no porphyrin formation was observed (Table 3.3, entry 1).

Then, we repeated the C&FC Lindsey optimized methodology. In a typical experiment, 1-methylimidazol-2-carboxyaldehyde was added to dipyrromethane dissolved in dichloromethane. The solution was left to degasify for 15 minutes and then a catalytic amount of TFA was added. The solution was left at room temperature, under stirring and inert atmosphere, for 3 hours, protected from light. DDQ was added to the reaction mixture and left for 1 hour at 50 °C, protected from light, under stirring. The solvent was evaporated, and ethyl acetate was added. The solution was neutralized with sodium hydrogen carbonate. This procedure was repeated several times, using fresh sodium bicarbonate solutions. To purify this compound, an adsorption chromatography was done using silica gel as the stationary phase and dichloromethane:methanol (10:1) as the eluent and then the compound was purified using Flash chromatography. After drying porphyrin **2** was obtained with 19% isolated yield. (Table 3.3, entry 2).



Scheme 3.3: two-step synthesis of 5,15-bis-imidazolyl porphyrin **2** in a milligram scale.

The complicated work-up led us to optimize the purification procedure. Thus, after performing the condensation/cyclization reaction of dipyrromethane (**0.439 g**) with 1-methylimidazol-2-carboxyaldehyde (**0.334 g**) in dichloromethane (**0.330 L**) as previously described the porphyrinogen oxidation was carried out with tetra-chloro-p-benzoquinone (1 g) instead of DDQ. The reaction was kept at 40°C for 1 hour. After neutralization with triethylamine (1 mL), the solvents were evaporated under vacuum. Then, the purification step was optimized. The silica column was substituted by a simple alumina plug purification, using chloroform as the eluent. Finally, the product was recrystallized using dichloromethane:heptane (5:15) as solvents. A mass of 0.034 g (11.9% yield) was obtained (Table 3.6, entry 3).

performed using chloroform as the eluent. The porphyrin **2** was recrystallized using dichloromethane:heptane as solvents. A mass of 1.6882 g (16.8% yield) was obtained (Table 3.6, entry 4). The compound was fully characterized (Chapter 5) and the $^1\text{H-NMR}$ and UV-vis spectra are presented in Figure 3.5 and Figure 3.6, respectively.

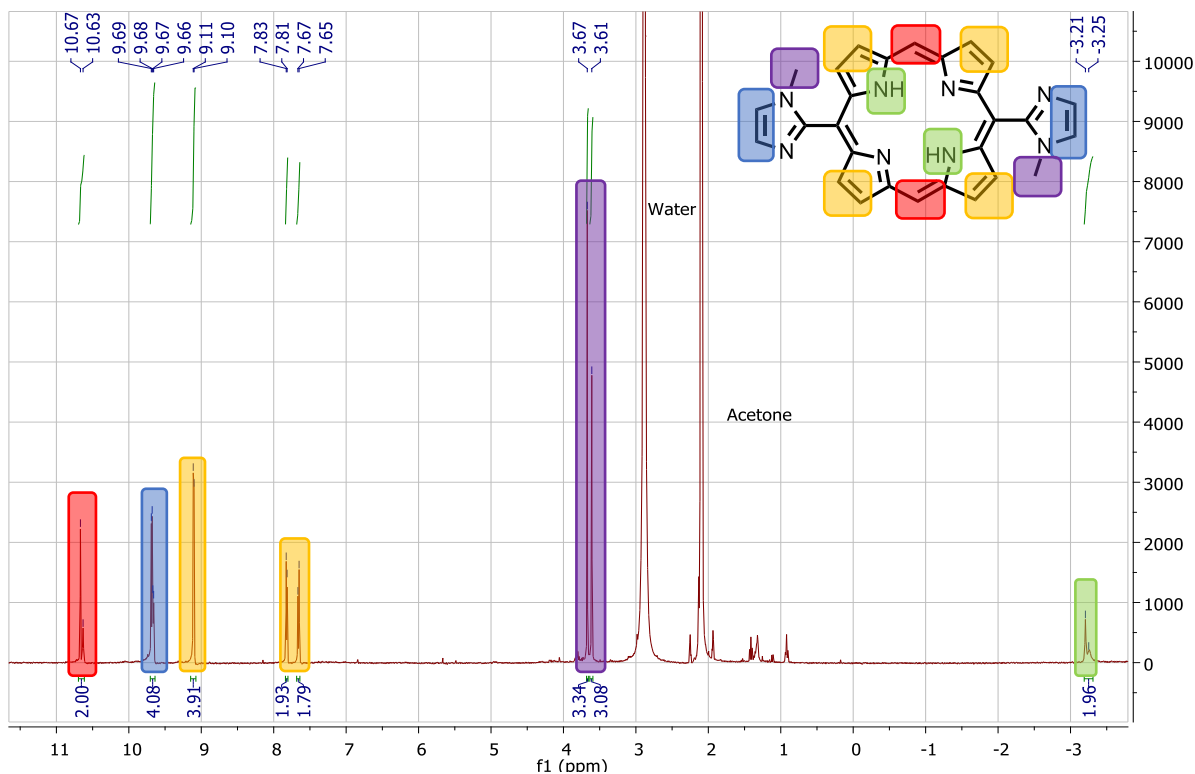


Figure 3.5: ^1H NMR spectrum of 5,15-bis(1-methylimidazol-2-yl) porphyrin using CD_3COCD_3 as solvent. In red the protons of the unsubstituted *meso* positions, in blue the protons of the imidazolyl, in yellow the protons of the beta positions, purple shows the methyl groups and green for the inner protons of the porphyrin.

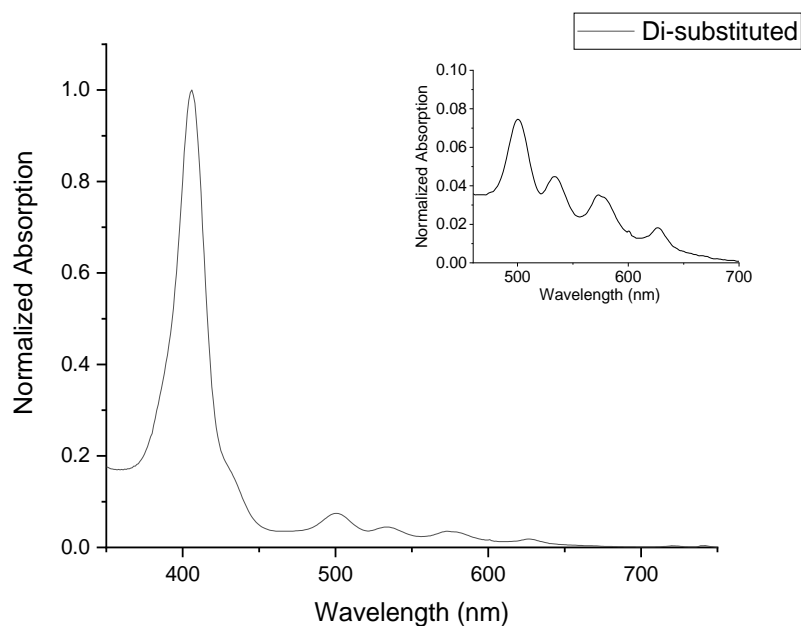
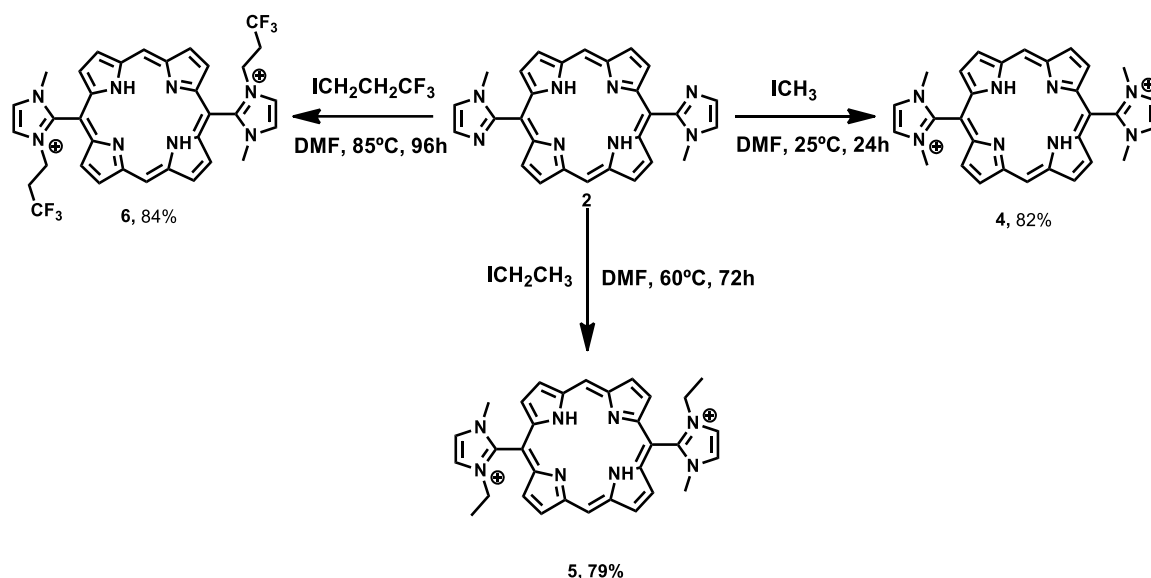


Figure 3.6: UV-vis spectrum of 5,15-bis(1-methylimidazol-2-yl) porphyrin in CH_2Cl_2 .

The $^1\text{H-NMR}$ spectra shows that the porphyrin was obtained with high purity. Highlighted in red, are the protons from the *meso* unsubstituted position, in blue the hydrogens of the imidazolyl group, yellow shows the protons of the central ring, in purple the 6 protons of the methyl groups and in green, the protons associated with the central nitrogens of the porphyrin. It is also possible to observe that there is some water present in the solution, as well as acetone and grease. Once again, no chlorine was observed.

From the UV-vis spectrum, it is possible to observe that the Soret band has a maximum at 406 nm, and the four Q bands appear at 500 nm 535 nm 573 nm and 627 nm, with a typical *etio*-type spectrum.

Once precursor **2** was obtained in high purity and quantity, it was possible to pursue with the synthesis of their biocompatible cationic derivatives, oriented by computational studies previously described, Scheme 3.5.



Scheme 3.5: Synthesis of cationic biocompatible porphyrins derived from porphyrin **2**.

The precursor **2** was dissolved in DMF and the selected alkyl-iodide (methyl-iodide, ethyl-iodide and 1,1,1-trifluoroethyl-iodide) was added. The reactions were maintained at optimized temperatures and times and their evolution was followed by TLC. It should be noted that the reaction kinetic is strongly dependent on the alkyl iodide structure, which required for each case an adjustment of the reaction's temperature and time. This may be explained by the changes in polarity of the solvent due to the large excess of alkyl iodide required for the $\text{S}_{\text{N}}2$ reactions or aryl alkyl decomposition. The use of iodo-trifluoroethyl did not give the desired cationic porphyrin (compound **2A-2E** described in Chapter 2) and to overcome this synthetic challenge, the iodo-trifluoroethyl was substituted by 1-iodo-3,3,3-trifluoropropyl.

The isolated yields were high and similar with the ones described in the literature.¹³ In all cases we obtain full transformation of the initial porphyrin, the lower isolated yields are explained by product loss during the work-up procedure. The cationic porphyrins **4-6** were fully characterized and data is presented in Chapter 5. The $^1\text{H-NMR}$ and mass spectrometry results are summarized in Table 3.7.

Table 3.7: Structural characterization of bis-imidazolyl porphyrins.

Porphyrin	¹ H NMR (400 MHz), δ (ppm)								ESI-MS m/z
2	10.67-10.63 (m, 2H _{meso})	9.69-9.67 (m, 4H _β)	9.11-9.10 (m, 4H _β)	7.83-7.81 (m, 2H _{imi})	7.67-7.65 (m, 2H _{imi})	3.67 (s, 3H _{Met})	3.61 (s, 3H _{Met})	-3.30 to -3.16 (m, 2H _{NH})	Experimental 471.20405 [M+H] ⁺ ; calculated [C ₂₈ H ₂₃ N ₈] ⁺ 471.20402
4	10.90 (s, 2H _{meso})	9.88-9.86 (m, 4H _β)	9.20-9.13 (m, 4H _β)	8.39 (s, 4H _{imi})	3.85 (s, 12H _{Met})	-2.20 (s, 2H _{NH})	--	--	Experimental 250.1218 [M-2I] ²⁺ /2; calculated [C ₃₀ H ₂₈ N ₈] ²⁺ /2 250.1213
5	10.78 (s, 2H _{meso})	9.74-9.73 (m, 4H _β)	9.05 (sl, 4H _β)	8.37 (d, J=2.2Hz, 2H _{imi})	8.29 (d, J=2.2Hz, 2H _{imi})	4.02 (q, J=7.3Hz, 4H _{CH₂})	3.72 (s, 6H _{Met})	1.19-1.16 (m, 6H _{Met})	Experimental 528.2743 [M-2I] ⁺ ; calculated [C ₃₂ H ₃₂ N ₈] ⁺ 528.2744
6	10.94 (s, 2H _{meso})	9.92-9.87 (m, 4H _β)	9.23-9.15 (m, 4H _β)	8.62-8.59 (m, 2H _{imi})	8.51-8.47 (m, 2H _{imi})	4.50-4.40 (m, 4H _{CH₂})	3.97-3.87 (m, 6H _{Met})	2.77-2.61 (m, 4H _{CH₂})	Experimental 664.2467 [M-2I] ⁺ ; calculated [C ₃₄ H ₃₀ F ₆ N ₈] ⁺ 664.2492
6	¹⁹ F NMR (400 MHz), δ -66.72 to -66.75 (m, 6F)								

* NMR Solvents: **2** (CD₃)₂CO; **4, 5, 6** CD₃OD.

The accurate mass spectra and the ^1H NMR show that the designed cationic biocompatible imidazolyl porphyrins were obtained with high purity. The multiplicity of the ^1H -NMR signals of porphyrins **2**, **5** and **6** and the observation of 2 spots on the TLC plates, confirm experimentally the presence of atropisomers, discussed for the chlorins derivatives in the computational discussion of Chapter 2. It should be noted that preliminary studies allowed the atropisomers of porphyrin **2** separation, using preparative silica flash chromatography and dichloromethane:methanol (1%) as eluent. This study opens the way or future complete isolation/characterization of atropisomers and consequently for their separate biological evaluation. According to EMA and FDA regulations, the use of these compounds in future clinical trials would require the complete isolation/characterization of each atropisomers of these molecules. Since compound **4** only has one conformer, it was chosen as the precursor for the chlorin synthetic process optimization (Chapter 4). To evaluate porphyrins **2**, **4**, **5** and **6** as potential photosensitizers for aPDI (Chapter 4), photophysical studies were performed, and are described below.

3.3. Photophysical studies of 5,15-bis imidazolyl porphyrins

As previously mentioned, the photophysical properties of photosensitizers are key for their use in aPDI. In this section, we present and discuss the results of photophysical characterization of porphyrins **2**, **4**, **5** and **6**, namely: absorption spectra (molar absorption coefficient), singlet oxygen quantum yield, fluorescence quantum yield (Table 3.8) and photostability.

The absorption spectra of the precursor porphyrin **2** and cationic porphyrins **4**, **5** and **6** were obtained using dichloromethane (**2**) and ethanol (**4**, **5** and **6**) as solvents. As an example, Figure 3.7 shows the absorption spectra of the precursors 5,15-bis(1-methylimidazol-2-yl) porphyrin **2**, and 5,15-bis(1,3-dimethylimidazol-2-yl) porphyrin, **4**.

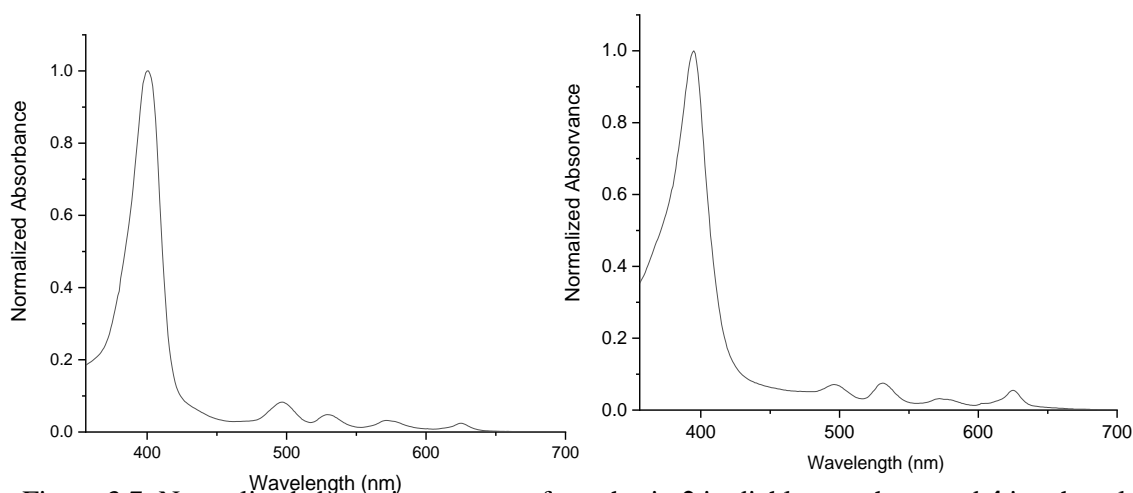


Figure 3.7: Normalized absorption spectra of porphyrin **2** in dichloromethane and **4** in ethanol.

As observed in Figure 3.7, in both cases a typical porphyrin spectrum is observed. As described by Gutterman, there is a Soret band ($\lambda=406$ nm (**2**), $\lambda=395$ nm (**4**)), a Q band $Q_y(0,1)$ ($\lambda=501$ nm (**2**), $\lambda=496$ nm (**4**)), a $Q_y(0,0)$ band ($\lambda=535$ nm (**2**), $\lambda=532$ nm (**4**)), a $Q_x(0,1)$ band ($\lambda=573$ nm (**2**), $\lambda=572$ nm (**4**)) and a $Q_x(0,0)$ band ($\lambda=627$ nm (**2**), $\lambda=625$ nm (**4**)). The pattern of these spectra are in accordance with the literature.⁸

To evaluate light absorption, a relevant parameter to describe a potential photosensitizer is the molar absorption coefficient that can be obtained from the Beer-Lambert law (equation 3.1).

$$A(\lambda) = \log \frac{I_{\lambda}^0}{I_{\lambda}} = \varepsilon(\lambda)lc \Leftrightarrow \varepsilon(\lambda) = \frac{A(\lambda)}{lc} \quad (3.1)$$

From this equation, it is possible to determine the molar absorption coefficient for each absorption peak of di-substituted porphyrins synthesized in this chapter. Solutions with well-defined concentrations were prepared using the appropriate solvent for compounds **2**, **4**, **5** and **6** (for details see Chapter 5). As a selected example, Figure 3.8 shows the graphical representation of the absorbance vs. the concentration for the Soret band of porphyrin **4**. To obtain this graphic, the solutions containing porphyrin **4** were prepared in ethanol with concentrations between 10^{-4} to 10^{-6} M and their absorption

spectra were recorded. Then, the maximums of the absorbances of each band were plotted against the concentration, where the slope of the linear fitting represents the molar absorption coefficients (ϵ), according to the Beer-Lambert law (equation 3.1). The values obtained for all the compounds can be found in Table 3.5.

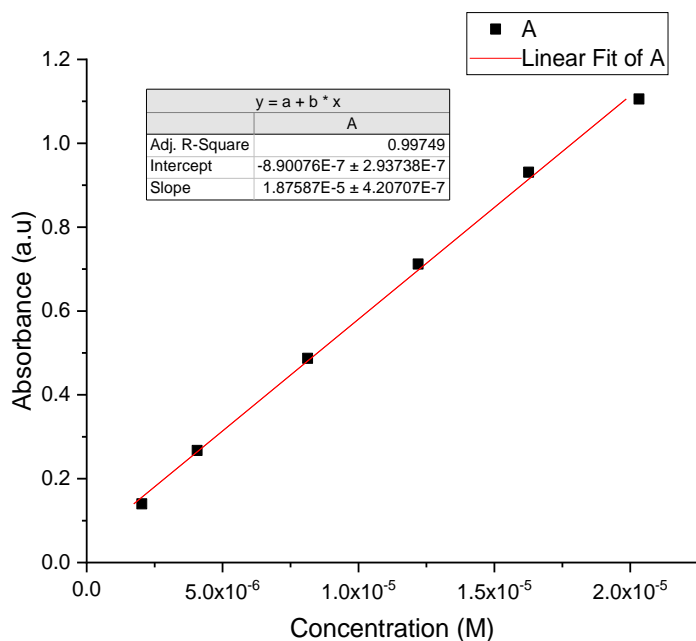


Figure 3.8: Plot of absorbance vs. porphyrin **4** concentration using ethanol as solvent for the Soret band ($\lambda_{\text{max}} = 395 \text{ nm}$).

All the values obtained both for the Soret bands and the Q bands are in accordance with the literature for di-substituted neutral and cationic *meso*-aryl porphyrins.^{8, 14}

To continue the photo-characterization of the new porphyrins, the fluorescent spectra and the fluorescent quantum yield of the same porphyrins were performed, using ethanol as solvent (Table 3.5). As a consequence of Kasha's rule,¹⁵ an ideal PS should have low fluorescence quantum yield (ϕ_F), which may lead to higher intersystem crossing and increase singlet oxygen quantum yield. To obtain ϕ_F data, we followed the methodology described by Parker *et al.*¹⁶ where the fluorescent spectrum is compared with a reference with known ϕ_F . Detailed description of this methodology is presented in Chapter 5. In this study, the reference was pure *meso*-tetraphenyl porphyrin (TPP) dissolved in toluene ($\phi_F = 0.11$).¹⁷ As selected example, Figure 3.9 shows the emission fluorescent spectra of neutral porphyrin **2** and cationic porphyrin **4**, using ethanol as solvent and the ϕ_F obtained are presented in Table 3.5.

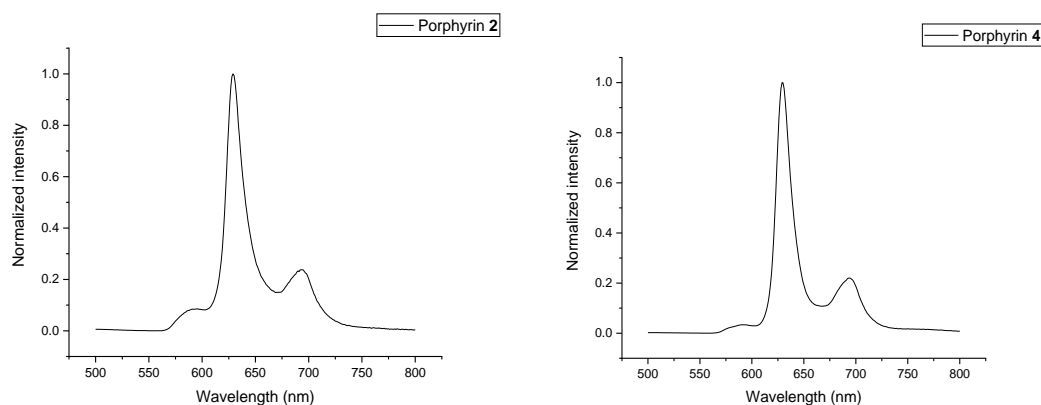


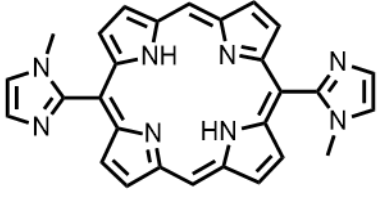
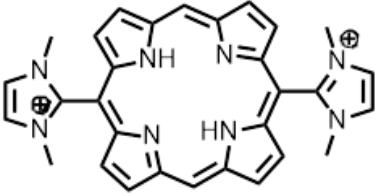
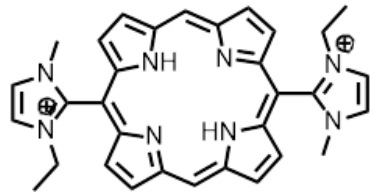
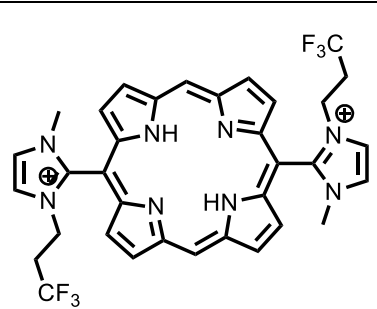
Figure 3.9: Emission fluorescence spectra of porphyrin **2** and cationic porphyrin **4** acquired in ethanol.

It should be noted that the effect of solvent was taken into consideration. From this data, we observe that independently of the porphyrin structure, these imidazolyl porphyrins present a quite low fluorescence quantum yield (0.1-0.2), suggesting that these are promising PSs.

Then, the singlet oxygen quantum yield (one of the most relevant quantum properties of an ideal PS) was calculated using methylene blue as reference ($\phi\Delta = 0.50$ in ethanol).¹⁸ The phosphorescence emission spectrum of the oxygen was obtained, at room temperature, after exciting the solution containing the desired porphyrin with the appropriate concentrations to obtain an absorbance of 0.3 at 625 nm. The steady state spectra of the samples were obtained and compared with the oxygen spectrum.

The $\phi\Delta$ for porphyrins **2**, **4**, **5** and **6** are summarized in Table 3.8. As expected, from this data, we observe a small effect of the porphyrin substituents on the $\phi\Delta$, being the best value obtained (0.70) for the cationic porphyrin with the shortest side chain, **4**, which, surprisingly, is in agreement with what was previously obtained for the corresponding zinc complex.⁸ In Chapter 4, we will present and discuss the correlation of these photophysical properties with *in vitro* antibacterial tests.

Table 3.8: Singlet oxygen yield ($\phi\Delta$) in ethanol, fluorescence quantum yield (ϕF) in ethanol and molar absorption coefficients in ethanol and dichloromethane.

Compound	λ (log ϵ)	ϕF	$\phi\Delta$
 <p style="text-align: center;">2</p>	406 (4.83); 501 (3.75); 535 (3.54); 573 (3.37); 627 (3.12) nm In CH ₂ Cl ₂	0.090	0.58
 <p style="text-align: center;">4</p>	395 (4.73); 496 (3.66); 532 (3.70); 572 (3.34); 625 (3.61) nm In ethanol	0.092	0.63
 <p style="text-align: center;">5</p>	396 (4.52); 497 (3.95); 531 (4.00); 572 (3.63); 625 (3.92) nm In ethanol	0.106	0.56
 <p style="text-align: center;">6</p>	395 (5.72); 498 (3.54); 533 (3.60); 572 (3.17); 626 (3.49) nm In ethanol	0.167	0.46

Finally, photostability studies were carried out. A LED emitting at 630 nm and total output power of $P = 5\text{mW}$ was employed. For these studies, photodecomposition was followed by UV-vis for three hours. This was performed in ethanol for the non-cationic porphyrin and in two different solvents for the cationic porphyrins (DMSO and water and a cell media) to be able to compare to the *in vitro* testing.

Photostability studies of porphyrins were carried out with irradiation at 625 nm and they show that 5,15-bis(1-methylimidazol-2-yl) porphyrin (**2**) exhibit ~10% photobleaching for light doses ~50 J in culture medium, but the 5,15-bis(1,3-dimethylimidazol-2-yl) porphyrin (**4**) which is a di-cationic photosensitizer, does

not photo-bleach in this medium, under our experimental conditions. The increase stability of the di-cationic photosensitizers can be understood considering that these photosensitizers generate reactive oxygen species that can produce their own oxidation, but the presence of positive charges stabilizes the photosensitizers against oxidation reactions by lowering the electronic density in the ring (see electronic structure calculations described in Chapter 2). Detailed experimental methodology is described in Chapter 5.

3.4. Conclusions

It is well established that to overcome the public health problems related to the multi-resistant microorganisms, it is necessary to develop new molecules and new therapies. Among them we highlight aPDI as the ultimate goal of this thesis. As discussed in the introduction of the thesis and in this chapter, one of the main conditions for achieving good results in the photo-destruction of bacteria and viruses is to have available methods for the large-scale synthesis of efficient photosensitizers, combined with the appropriate light sources. Knowing from the literature that cationic *meso*-imidazolyl porphyrins were very promising photosensitizers for aPDI we directed the studies described in this chapter towards developing methods for larger-scale synthesis of tetra- and bis-imidazolyl porphyrins, as these are simultaneously the precursors of cationic and amphiphilic porphyrins and chlorins.

Concerning the synthesis of *meso*-tetra-imidazolyl porphyrin we can conclude that the one-step process using an organic acid and nitrobenzene as solvent with conventional heating or by microwave irradiation allowed to prepare the porphyrin with isolated yields of 19% and 21%, respectively. However, the reaction performed with microwave irradiation at W=200 W and T= 175 °C yielded fewer polymeric side products, which facilitated the work-up. Thus, this method was selected to promote the repetition of the reaction (4 times), followed by purification in a single batch. This synthetic methodology allowed us to prepare 1.5 g of compound, using 100 mL of solvent. From the literature review we conclude that the methodology developed in this study will allow an easy transposition for a pilot scale if a 1L microwave vial is used. Finally, we can conclude

that the use of DMF as solvent and CH₃I electrophile allowed the preparation of tetramethyl cationic porphyrin **3** with 92% isolated yield. The synthesis of this porphyrin on a larger scale will certainly allow, in the future, the preparation of a new family of cationic amphiphilic porphyrins and their respective chlorins. Due to time limitations, it was out of the scope of these studies. Regarding the synthesis of bis-imidazolyl porphyrin **2**, a relevant precursor for the preparation of all the cationic photosensitizers described in the thesis, we can conclude that the two-step Lindsey method (cyclization /oxidation) was the one that allowed us to obtain the best yields of isolated product in the multi-gram scale (16.8%). However, the scale-up to the multigram level was performed at the PorphyChem's Laboratory due to reactor size limitations at the University of Coimbra. We point out that the transposition of this methodology to pilot scale is inherently associated with the need to use large reactors. Studies are underway in the C&FC laboratory for attempts at scale transposition using flow chemistry.

After full characterization of bis-imidazolyl porphyrin **2**, it was used as precursor for the synthesis of cationic porphyrins **4**, **5** and **6**, via S_N2 reactions with iodo-alkyls, with yields up to 84 %. From these studies we can conclude that the reaction rate depends significantly on the structure of the iodo-alkyl, with the reaction of methyl iodide being significantly faster. Studies on the use of microwaves to optimize these processes are underway in our laboratory. The procedures that were developed are likely to be accepted for GMP for future clinical trial development. The photosensitizers showed good properties for future applications in aPDI, including easy synthesis, high purity, modulated amphiphilicity, low fluorescent quantum yield, reasonable singlet oxygen quantum yield and high photostability. Their antibacterial activity is presented in Chapter 4. To obtain an ideal photosensitizer whose properties are described in Chapter 1, it is necessary to increase the absorption in the therapeutic window (600-800nm). This property is possible through the preparation of chlorin derivatives described in Chapter 4.

3.5. References

1. Senge, M. O.; Sergeeva, N. N.; Hale, K. J., Classic highlights in porphyrin and porphyrinoid total synthesis and biosynthesis. *Chemical Society Reviews* **2021**, *50* (7), 4730-4789.
2. Kuwahara, S. S., GLP and GMP in contract testing of drugs and biologics-what's the difference? *Journal of GXP Compliance* **2009**, *13* (2), 11-14.
3. Gonsalves, A. M. D. A. R.; Varejão, J. M. T. B.; Pereira, M. M., Some new aspects related to the synthesis of meso-substituted porphyrins. *Journal of Heterocyclic Chemistry* **1991**, *28* (3), 635-640.
4. Adler, A. D.; Longo, F. R.; Finarelli, J. D.; Goldmacher, J.; Assour, J.; Korsakoff, L., A simplified synthesis for meso-tetraphenylporphine. *The Journal of Organic Chemistry* **1967**, *32* (2), 476-476.
5. Lindsey, J. S.; Hsu, H. C.; Schreiman, I. C., Synthesis of tetraphenylporphyrins under very mild conditions. *Tetrahedron Letters* **1986**, *27* (41), 4969-4970.
6. Nowak-Król, A.; Plamont, R.; Canard, G.; Edzang, J. A.; Gryko, D. T.; Balaban, T. S., An efficient synthesis of porphyrins with different meso substituents that avoids scrambling in aqueous media. *Chemistry – A European Journal* **2015**, *21* (4), 1488-1498.
7. Littler, B. J.; Ciringh, Y.; Lindsey, J. S., Investigation of Conditions Giving Minimal Scrambling in the Synthesis of trans-Porphyrins from Dipyrromethanes and Aldehydes. *The Journal of organic chemistry* **1999**, *64* (8), 2864-2872.
8. Vinagreiro, C. S.; Zangirolami, A.; Schaberle, F. A.; Nunes, S. C. C.; Blanco, K. C.; Inada, N. M.; Da Silva, G. J.; Pais, A. A. C. C.; Bagnato, V. S.; Arnaut, L. G.; Pereira, M. M., Antibacterial photodynamic inactivation of antibiotic-resistant bacteria and biofilms with nanomolar photosensitizer concentrations. *ACS Infectious Diseases* **2020**, *6* (6), 1517-1526.
9. Gonçalves, N. P.; Santos, T., P.; Costa, G. P.; Monteiro, C. J.; Schaberle, F. A.; Alfar, S. C.; Abreu, A. C.; Pereira, M. M.; Arnaut, L. G. Atropisomers of halogenated tetraphenylbacteriochlorins and chlorins and their use in photodynamic therapy. 2016.
10. Nascimento, B. F. O.; Pineiro, M.; Gonsalves, A. M. D. A. R.; Silva, M. R.; Beja, A. M.; Paixão, J. A., Microwave-assisted synthesis of porphyrins and metalloporphyrins: a rapid and efficient synthetic method. *Journal of Porphyrins and Phthalocyanines* **2007**, *11* (02), 77-84.
11. European Commission. EudraLex - Volume 4 - Good Manufacturing Practice (GMP) guidelines https://ec.europa.eu/health/documents/eudralex/vol-4_en (accessed Jun 12, 2021).
12. Kappe, C. O.; Dallinger, D.; Shaun, M. S., Practical Microwave Synthesis for Organic Chemists: Strategies, Instruments and Protocols. 2009.
13. Carneiro, J.; Gonçalves, A.; Zhou, Z.; Griffin, K. E.; Kaufman, N. E. M.; Vicente, M. D. G. H., Synthesis and in vitro PDT evaluation of new porphyrins containing meso-epoxymethylaryl cationic groups. *Lasers in Surgery and Medicine* **2018**, *50* (5), 566-575.
14. Mandal, A. K.; Taniguchi, M.; Diers, J. R.; Niedzwiedzki, D. M.; Kirmaier, C.; Lindsey, J. S.; Bocian, D. F.; Holten, D., Photophysical properties and electronic structure of porphyrins bearing zero to four meso-phenyl substituents: new insights into seemingly well understood tetrapyrroles. *The Journal of Physical Chemistry A* **2016**, *120* (49), 9719-9731.
15. Kasha, M., Characterization of electronic transitions in complex molecules. *Discussions of the Faraday Society* **1950**, *9* (0), 14-19.
16. Parker, C. A.; Rees, W. T., Correction of fluorescence spectra and measurement of fluorescence quantum efficiency. *Analyst* **1960**, *85* (1013), 587-600.
17. Seybold, P. G.; Gouterman, M., Porphyrins: XIII: fluorescence spectra and quantum yields. *Journal of Molecular Spectroscopy* **1969**, *31* (1), 1-13.
18. Redmond, R. W.; Gamlin, J. N., A compilation of singlet oxygen yields from biologically relevant molecules. *Photochemistry and photobiology* **1999**, *70* (4), 391-475.

4. Cationic photosensitizers for photoinactivation of pathogens

Aiming to obtain photosensitizers with a high absorption in the therapeutic window, the studies pursued with the development of cationic amphiphilic chlorin photosensitizers derived from the previously described porphyrins. As mentioned before, for a new drug to be approved for clinical trials, it must consist of only one isomeric species. The regulations became more restricted after the consequences caused by thalidomide that was not enantiomerically pure in the 60's.¹ With this in mind, and from the critical analysis of the computational results (Chapter 2) and the experimental observations (Chapter 3), it was possible to settle that only the 1,3-dimethylimidazolyl porphyrin (**4**), presents these conditions. The synthetic methodologies described in the literature for preparation of *meso*-aryl chlorins were recently reviewed by Lindsey.² From these methods we can highlight the classic Whitlock process based on the reduction of porphyrins using activated p-toluenesulfonyl hydrazine.³⁻⁵ However, the final purification process is troublesome, due to the difficulty of separating the residual p-toluenesulfonic acid from the desired chlorins. Recently, and in parallel with these studies, a more sustainable approach for *meso*-aryl chlorin synthesis was described using hydrated hydrazine activated by a mechanical process.⁶

Considering the literature results and the C&FC experience in the use of catalytic process for hydrazine-hydrate reduction of hetero-aromatic compounds,⁷ in our work, we selected this approach to start the optimization of imidazolyl chlorin synthesis.

4.1. Synthesis, purification and characterization of chlorins

The reduction studies of porphyrins towards the chlorins started by evaluating the effect of solvent, amount of hydrazine and presence of palladium as catalyst. The qualitative results based on UV-vis analysis are presented in Table 4.1.

Table 4.1: Optimization of the reduction reaction of porphyrin 2 to its respective chlorin.

#	Solvent ^a	Time ^b	Catalyst	Hydrazine. H ₂ O (eq.)	Chlorin ^c	Bacteriochlorin ^c
1	DMF	2h	-	10+10	++	+
2	Xylene	2h	-	10+10	+++	+++
3	DMF/Argon	2h	-	30	++++	++
4	Xylene/Argon	2h	-	30	++++	+++
5	DMF	2h	Pd/C	40	+++++	+
6	Xylene	2h	Pd/C	40	+++	+++

a) Temperature:70°C. b) When left for a longer period of time and up to 18 hours, no evolution of the reaction is observed. c) based on the proportion of the areas of absorption bands at 650 nm and 550 nm.

The optimization studies of chlorin synthesis started with the evaluation of the effect of solvent. It is well-known that for a reduction experiment using hydrazine.H₂O, aprotic solvents are typically used. Therefore, we started by evaluating the effect of two solvents with different polarities (DMF and xylene) on the selectivity for preferential chlorin formation. (Table 4.1, entries 1,2).

In the first attempt, porphyrin 2 was dissolved in DMF in an open vessel, at 70 °C, and 10 equivalents of hydrazine.H₂O were added. After 1 h, some chlorin formation was observed. Then, 10 equivalents of hydrazine were added. The reaction was stopped after 2h and the product was isolated by precipitation with Et₂O. Small amounts of bacteriochlorin formation was observed (Table 4.1, entry 1). The reaction was repeated under the same reaction conditions but using xylene as solvent. Although the percentage

of chlorin increased, an equally high bacteriochlorin contamination was observed (Table 4.1, entry 2).

It should be mentioned that when leaving the reaction for longer periods (18 hours) no significant evolution of the reduction reaction was observed. Since these reactions were performed under open vessel, we hypothesized that a possible re-oxidation of the chlorin to the porphyrin may occur and another set of similar experiments was carried out, under Argon atmosphere (Table 4.1, entries 3, 4). The qualitative analysis of these results led us to conclude that a significant improvement of chlorin formation was obtained, still contaminated with the bacteriochlorin.

Then, based on recent Pereira's experience⁷ we decided to evaluate the use of Pd/C as catalyst for *in situ* generation of hydrogen from hydrazine. Once again, we evaluated the effect of solvent and the results are presented in Table 4.1 entries 5, 6. From the analysis of these results we concluded that the most selective synthetic approach for preparation of the desired chlorin **7**, is the one that uses DMF as solvent and a large excess of hydrazine (40 equivalents). These reaction conditions were selected to perform the work-up and purification of the desired chlorin. Thus, repeating the synthesis under these reaction conditions (but 10 times larger), the chlorin was precipitated with diethyl ether and the solid was isolated by filtration.

In this sense, more batches were prepared using these conditions, and an analytical method (Figure 4.1) was developed using High Performance Liquid Chromatography (HPLC) technique, as part of the API search process.

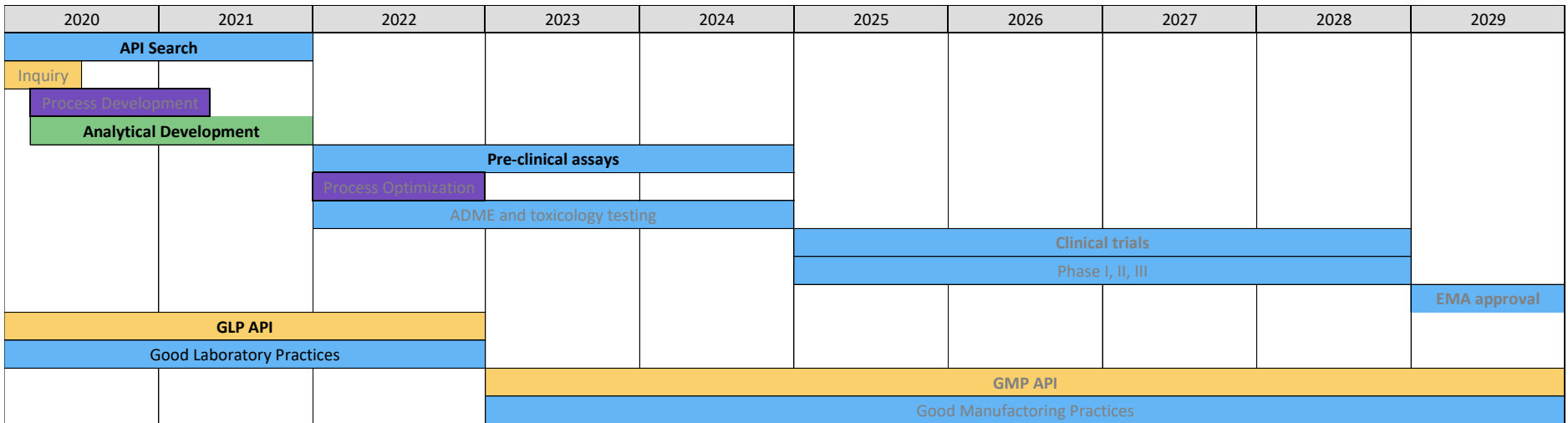


Figure 4.1: Drug discovery pipeline, highlighted is the analytical development phase, that typically takes 10 months during the API search.

Once optimized, we expected that this method will be transposable to flash preparative chromatography. The greatest challenge in this purification was the separation of the porphyrin from the chlorin since they have similar polarities and, as previously observed, their separation can be very difficult.⁸ Several attempts were made to do this optimization namely, selecting the best solvents, gradient, and volume injected. Table 4.2 shows selected experiments of the analytical HPLC optimization procedures.

Table 4.2: High Performance Liquid Chromatography experimental method development for chlorin 7.

#	Injected volume (μL)	Flow (mL/min)	Retention time (min)	Methanol (%)	Acetate buffer (pH=9) (%)	Acetonitrile (%)	Separation
1	50	1.0	13-17	50	0	50	● ○ ○ ○ ○
2	50	1.0	5-7	70	0	30	● ○ ○ ○ ○
3	50	0.8	9-20	60-83	40-17	0	● ● ○ ○ ○
4	30	0.8	10-18	60-83	40-17	0	● ● ● ○ ○
5	50	0.8	12-22	60-70	40-30	0	● ● ○ ○ ○
6	50	0.8	5-28	60-70	40-30	0	● ● ● ● ○
7	10	0.8	9-28	60-70	40-30	0	● ● ● ● ●

Red: no separation observed, orange: separation of atropisomers, yellow: separation of one atropisomer of the porphyrin and the rest of the solution; light green: separation of the atropisomers and porphyrin/chlorin; dark green: separation of all compounds.

The study for HPLC optimization started with reverse phase TLC plates and the best separation was observed using a mixture of methanol:acetonitrile (1:1). Accordingly, in the first attempt to promote HPLC separation, the eluents used were methanol:acetonitrile (1:1). The volume injected was 50 μ L and the flow was set to 1.0 mL/min. Under these chromatographic conditions a large peak was observed, with a maximum at 14.6 minutes, and no peak separation was detected (Table 4.2, entry 1). In the second attempt, a ratio methanol:acetonitrile (2:1) was used with the same flow and injected volume. Under these conditions, the retention time lowered to 7 minutes and again no separation was observed (Table 4.2, entry 2). From a careful analysis of the spectra of each HPLC peak we concluded that some protonation of the inner nitrogens of the chlorin had occurred. In this sense, an ammonium acetate buffer with a pH 9 was prepared. For safety reasons, the flow was lowered to 0.8 mL/min while using this buffer. The first separation was performed starting with 60 % methanol and 40 % buffer solution. The program was set to change the eluent gradually, increasing 2% of methanol per minute and maintaining that eluent for 2 minutes, up to 83% methanol and 17% buffer (Table 4.2, entry 3). Using these conditions, a better peak separation was observed. The same procedure was applied to an injection with only 30 μ L of solution and the separation improved (Table 4.2, entry 4).

Figure 4.2 depicts the percentage of methanol with the timings used to change the eluent percentage for entries 5-7 of Table 4.2. The other eluent used was the buffer. In black, the elution for entry 5 of Table 4.2 and in blue entries 6 and 7. For entry 7, only a change in the injection volume (10 μ L instead of 50 μ L) was made and the best separation was obtained. Figure 4.3 shows the HPLC graphics of the starting point (entry 1, Table 4.2) and best experiment (entry 7, Table 4.2).

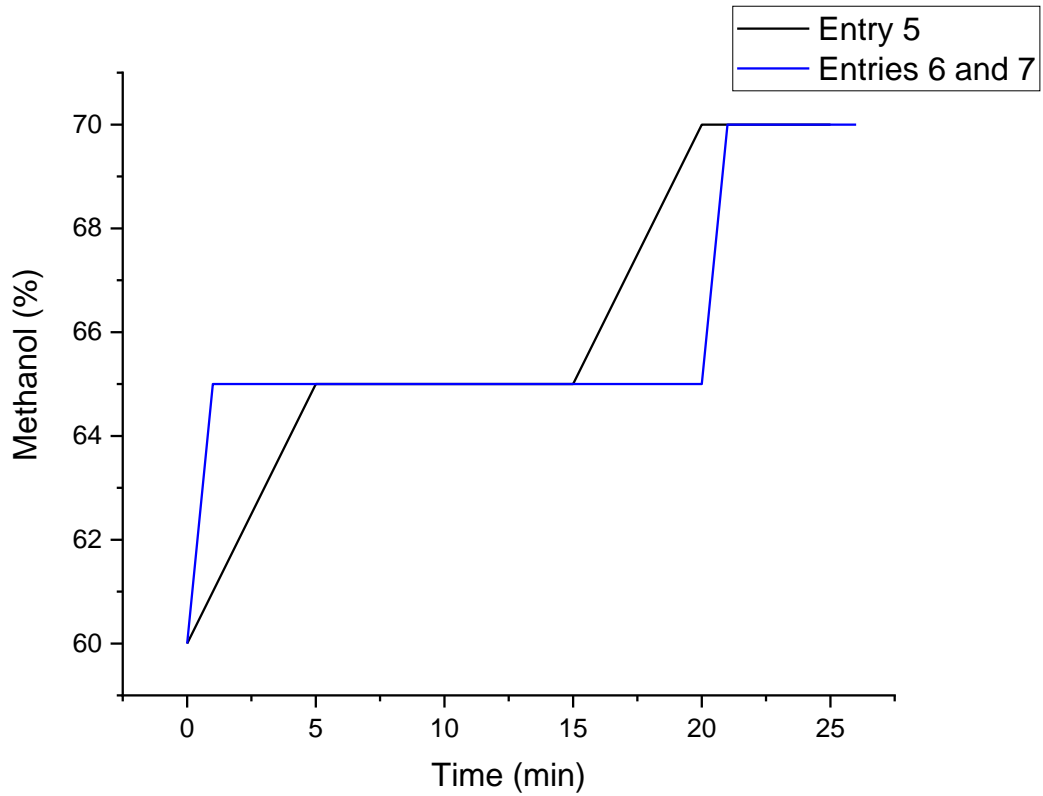


Figure 4.2: Optimization of the elution in the HPLC method for chlorin 7. In black entry 5, starting with 60% methanol and 40% buffer and finishing with 70% methanol and 30% buffer. In blue, entries 6 and 7 using the same elution with different timings.

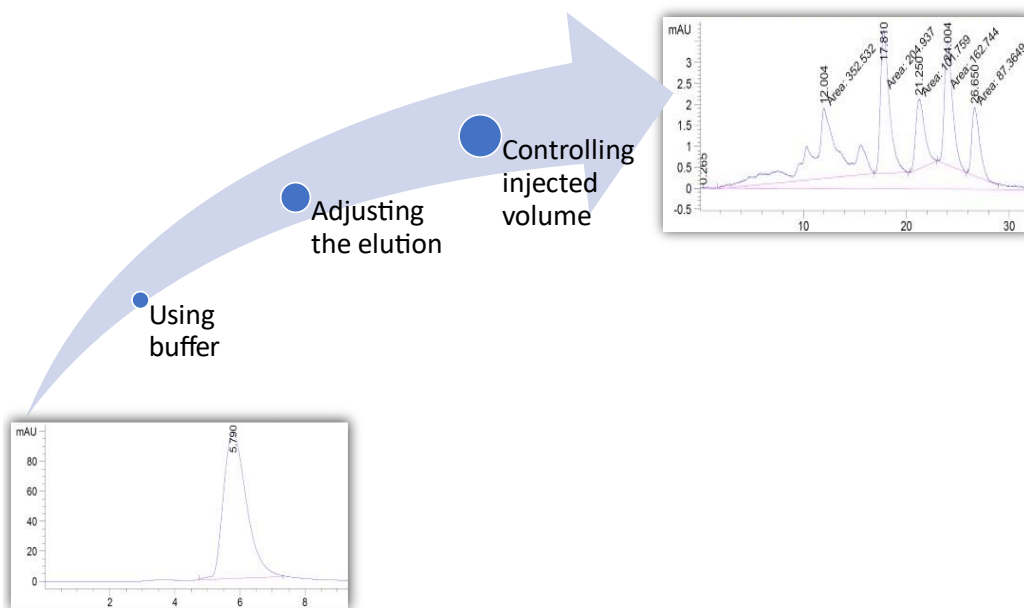






















Figure 4.3: HPLC method optimization overview

These conditions were transposed to flash chromatography purification. A small optimization in the loading of the sample was performed and the results are shown in Table 4.3.

Table 4.4: Optimization of the flash chromatography purification of chlorin 7.

#	Flow (mL/min)	Load	Number of columns	Separation
1	5	0.3 mL	1	    
2	2	0.3 mL	1	    
3	2	0.3 mL	2	    
4	2	Dry load	2	    

Red: no separation observed, orange: separation of atropisomers, yellow: separation of an atropisomer of the porphyrin and the rest of the solution; light green: separation of the atropisomers and porphyrin/chlorin; dark green: separation of all compounds.

For the flash chromatography purification, the flow rate, the type of loading and the number of columns to perform the separation were evaluated. The studies started with a flow set to 5mL/min, the loading was performed using 0.3mL of chlorin dissolved in methanol and only one column. Under these conditions, no separation was observed (Table 4.3, entry 1). After lowering the flow to 2mL/min, some improvement in the separation was achieved and some atropisomers were separated, but not the porphyrin from the chlorin (Table 4.3, entry 2). When using two columns, the separation was further improved and one of the atropisomers of the chlorin was separated from the rest of the mixture (Table 4.3, entry 3). Finally, we decided to try a dry loading process, using the same eluents and the same number of columns. These chromatographic conditions allowed for the best separation of the compounds (Table 4.3, entry 4).

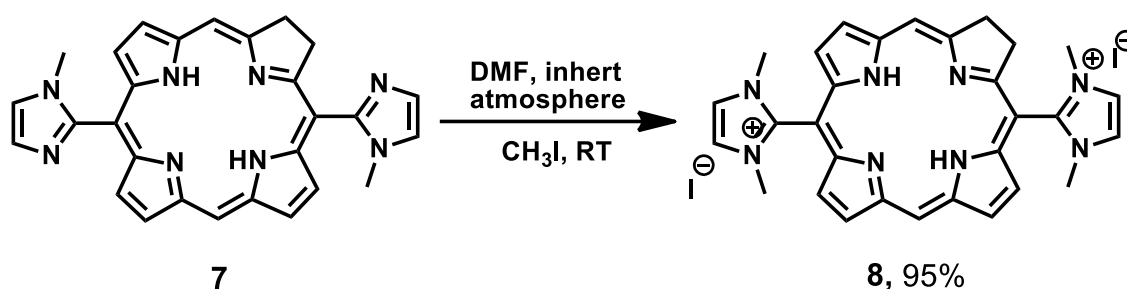
Then, and surprisingly, the product drying was another great challenge. First, it was dried by solvent evaporation, under vacuum, and due to the use of 40°C for water evaporation oxidation of the chlorin molecule occurred as was observed by UV-vis. This purification process yielded 31% of isolated chlorin contaminated with 20% porphyrin. Therefore, as an alternative we tried to lyophilize the product after methanol evaporation. However, the solid obtained from this method was insoluble in all solvents (dichloromethane, methanol, ethanol, DMF, acetone and DMSO) where the non-dried chlorin was soluble.

Table 4.5: Structural characterization of 5,15-bis-imidazolyl chlorins in (CD₃)₂CO.

Chlorin	¹ H NMR (400 MHz), δ (ppm) ^a						ESI-MS m/z
7	10.12-10.11 (m, 1H _{meso}) 9.42-9.41 (m, 1H _{meso})	9.31-9.29 (m, 1H _β) 9.13-9.11 (m, 2H _β) 8.88-8.87 (m, 1H _β) 8.52-8.51 (m, 1H _β) 8.37-8.36 (m, 1H _β)	7.74-7.51 (m, 4H _{imi})	4.84-4.79 (m, 2H _β) 4.67-4.61 (m, 2H _β) 4.27-4.21 (m, 1H _β)	3.69-3.57 (m, 6H _{Met})	-1.49 (s, 1H _{NH}) -1.80 (s, 1H _{NH})	<i>obtained</i> 473.2182 [M+H] ⁺ ; <i>calculated</i> [C ₂₈ H ₂₄ N ₈] ⁺ 472.2124
8	10.29 (s, 2H _{meso})	9.53-9.51 (m, 4H _β)	8.92-8.91 (m, 2H _β)	8.44-8.42 (m, 4H _{imi})	4.40-4.38 (m, 4H _β)	3.85-3.83 (m, 12H _{Met})	<i>obtained</i> 251.1283 [M- 2] ²⁺ /2 ; <i>calculated</i> [C ₃₀ H ₃₀ N ₈] ²⁺ /2 251.1291

a) Contaminated with 20% of the corresponding porphyrin.

Then, to enhance their biocompatibility, the cationization process, *via* SN₂ reaction with an excess of iodomethane and DMF as solvent, was performed. After precipitation with diethyl ether, 95 % isolate yield was obtained, Scheme 4.1. As expected, the ¹H NMR spectra also presents the signals typical of chlorin (80 %) and porphyrin (20 %) porphyrin. This was the sample used in the biological assays described below.



Scheme 4.2: Cationization of the 5,15-bis-imidazolyl chlorin, under inert atmosphere.

Photophysical characterization

Photophysical studies of chlorins **7** and **8** (absorption spectra, fluorescent quantum yield, singlet oxygen quantum yield and photostability) were performed using the methodologies described in Chapter 3 for the porphyrins and the results obtained are presented in Table 4.4.

After cationization and purification, the chlorin still contained about 20% porphyrin. Therefore, the determination of the molar absorption coefficients were not performed and the ratio of the peaks (Soret band – 100%) are presented in Chapter 5. The UV-vis spectrum is shown in Figure 4.4, and a relative percentage of the bands is shown in table 4.5.

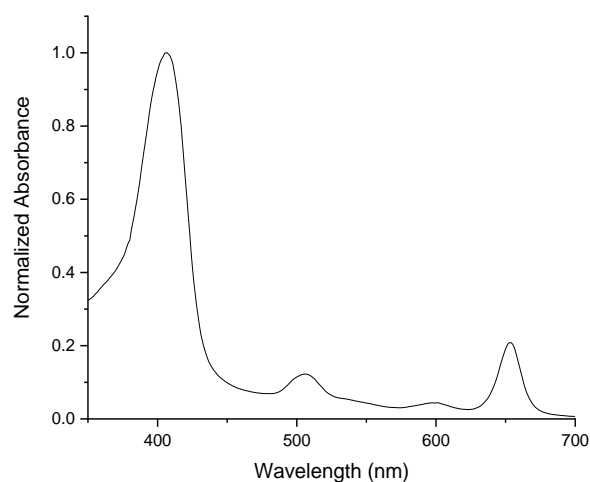
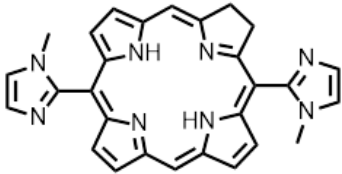
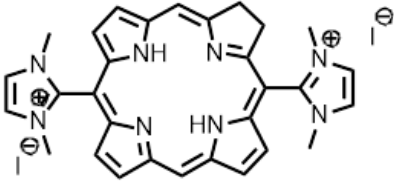


Figure 4.4: UV-vis spectrum of a) chlorin **7** in CH₂Cl₂.

Table 4.6: Singlet oxygen yield ($\phi\Delta$) in ethanol, fluorescence quantum yield (ϕF) in ethanol and molar absorption coefficients in ethanol and dichloromethane.

Compound	λ max (relative %)	$\phi\Delta$	ϕF
 <p style="text-align: center;">7</p>	406 (100) 506 (51) 528 (34) 589 (21) 645 (81) nm In CH ₂ Cl ₂	0.85	0.158
 <p style="text-align: center;">8</p>	395 (100) 500 (7) 537 (4) 570 (2) 644 (12) nm In ethanol	0.69	0.159

The fluorescence of chlorins **7** and **8** was determined in ethanol with optical absorption ca. 0.01 at 652 nm. The samples were excited at 652 nm, using oxazine-170 as reference in ethanol ($\phi F=0.579$)⁹ and fluorescent quantum yields of 0.158 and 0.159 were obtained for **7** and **8** respectively. It should be noted that no significant differences in the fluorescent quantum yields were observed upon cationization.

Then we obtained the singlet oxygen quantum yields using the same methodology described in Chapter 3 for the porphyrin precursors and the results are presented in Table

4.5. The results obtained for $\phi\Delta$ are higher for chlorins **7** (0.85) and **8** (0.69), than the corresponding porphyrin **2** (0.57) and **4** (0.63), which is a very promising property for the application of these chlorins as PS.

Another important property for development of an ideal PS is the photostability and the results in DMSO and culture media for chlorins **7** and **8** are presented in Figure 4.5.

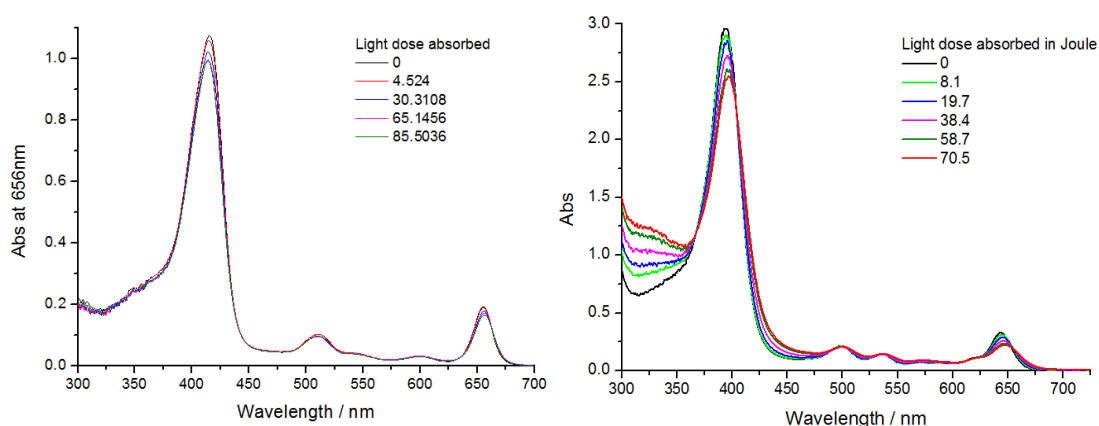


Figure 4.5: Chlorin **7** in DMSO and **8** in water and DMSO for photostability testing.

The UV-visible spectra of chlorin **7** in DMSO and chlorin **8** in culture media are presented in Figure 4.5. Photodecomposition studies with illumination at 650 nm for the chlorins show that 5,15-bis(1-methylimidazol-2-yl) chlorin exhibit ~10% photobleaching for light doses ~50 J in culture medium, but the di-cationic 5,15-bis(1,3-dimethylimidazol-2-yl) chlorin diiodide, does not photo-bleach in this medium under our experimental conditions.

These studies demonstrated that these compounds present high photostability, high solubility in culture media, a strong absorption in the therapeutic window (650nm), have moderate fluorescence quantum yields and high singlet oxygen quantum yield, which are excellent properties for aPDI of pathogens. With these promising photochemical properties in mind, a collaboration for photoinactivation of bacteria and viruses was viable and the proof-of-concept to enter the pre-clinical assays is described in the next section. According to Figure 4.1, this is the next step in the drug discovery pipeline.

4.2. Biological studies

The following results were obtained in collaboration with University of Coimbra Hospital Center (CHUC), Center for Neuroscience and Cell Biology (CNC) and the Faculty of Pharmacy from the University of Coimbra.

aPDI of SARS-CoV-2

The clinical relevance of aPDI with chlorin **8** was investigated using clinical samples of SARS-CoV-2 collected from the nasopharynx of Covid-19 patients admitted in the CHUC, after their informed consent, according to a protocol approved by the CHUC ethical committee. The SARS-CoV-2 samples were transported in the appropriate media to a biosafety-II lab where they were split in control experiments of virus alone (V), virus exposed only to light (L), virus exposed only to chlorin **8**, and virus exposed to chlorin **8** (estimated concentration: 0.3 μ M) and light 4.9 J/cm². The illumination was completed less than 15 min after the addition of chlorin **8** to SARS-CoV-2. The amount of SARS-CoV-2 in the samples was evaluated by RT-qPCR using a calibration curve to quantify the reduction of the viral titer with the treatment. Figure 4.6 shows that the viral titer drops below the sensitivity of our RT-qPCR equipment (viral titer decrease by >99.999%). It is important to emphasize that RT-qPCR detects the RNA of the virus.

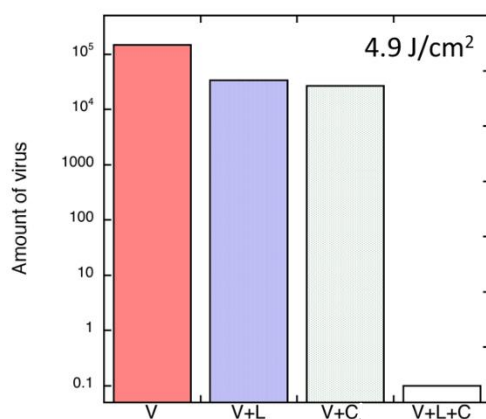


Figure 4.6: aPDI of clinical samples. Concentration of chlorin **8**: 0.3 μ M, light dose: 5 J/cm². V = virus only; V+L = virus and light for 8 min; V+C = virus and chlorin **8** for 8 min V+L+C = virus, chlorin **8** and light for 4 min; Data by Paulo Santos

Nasal photo-disinfection of SARS-CoV-2 with chlorin **8** can be performed in seconds with viral amplification inhibitions >99.999% without toxicity. This prophylactic

approach to Covid-19 can reduce substantially the viral load and offer a better change for speedy recovery of patients. Moreover, aPDI is a broad-spectrum approach to the inactivation of viruses, possibly targeting viral membrane components, the S protein and viral RNA. This approach is less likely to be susceptible to mutation in the virus or to induce mutations. It can be expected to have broad applications in the inactivation of known enveloped viruses and of viruses that may cross species barriers in the future.

aPDI of *E. coli*

Porphyrins

Figure 4.7 shows the structures of the porphyrins synthesized in Chapter 3 whose efficacy was studied against *E. coli* strains.

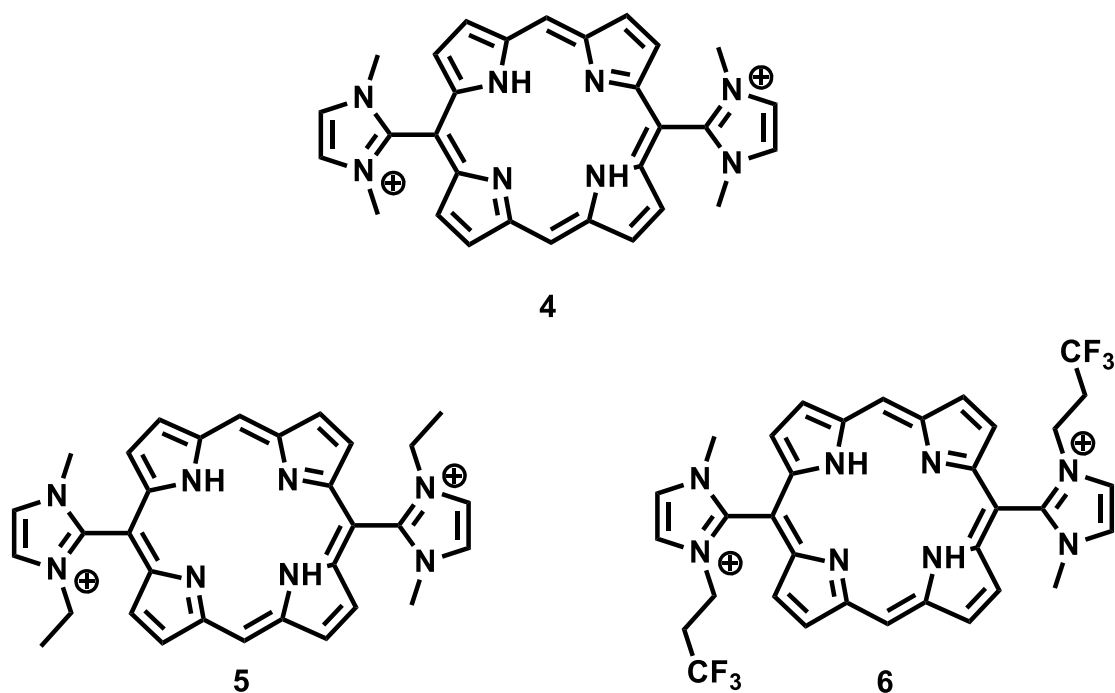


Figure 4.7: Structures of the porphyrins studied for aPDI, synthesized in Chapter 3.

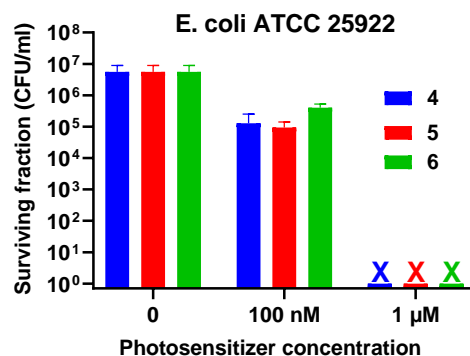


Figure 4.8: aPDI in planktonic cultures of laboratory strains of bacteria (*E. coli* ATCC 25922) using cationic photosensitizers 4-6 in different concentrations, using 1.36 J/cm² light dose. Illuminated with a blue light LED (415 nm, 4 mW/cm²).

The 5,15-bis-imidazolyl cationic porphyrins containing methyl (4), ethyl (5) and CF₃ (6) substituents were tested in the photoinactivation of Gram-negative bacteria (*E. coli*) in planktonic cultures. Figure 4.8 presents the results obtained. For the photoinactivation of *E. coli*, 100 nM of photosensitizer is not enough to produce significant inactivation (1 log CFU reduction). With a concentration of 1 μM, using 1.36 J/cm² illuminated at 415 nm, a total inactivation of *E. coli* (7 log CFU) was possible with all three cationic porphyrins. These results are in agreement with those found in the literature for similar compounds.¹⁰

As suggested in Chapter 2, these results point out the importance of using cationic photosensitizers with longer hydrophobic chains and the development of a separation process of the atropisomers.

Chlorins

As mentioned before, the development of photosensitizers capable of absorbing light in the therapeutic window is very important. Chlorins have a great absorption in this window, as described in this chapter. Although porphyrins have a good activity against bacteria as shown in Figure 4.8, they have to be illuminated at 415 nm, where their molar absorption coefficient is about 50 times higher than in the therapeutic window (600-800 nm). Although these results are interesting, too many biological endogenous chromophores absorb light at these wavelengths, which would greatly reduce the activity of these molecules in a clinical setting. In this sense, due to their high molar absorption coefficients, chlorins allow for a more efficient illumination in the therapeutic window and are studied in this section.

Due to PS **5** and **6** having atropisomers, which require a separation method to be developed, in the interest of time, chlorin 5,15-bis(1,3-dimethyl)imidazolyl was chosen to perform the photoinactivation of *E. coli* ATCC 25922 (non-resistant strain) and a resistant strain (243) multi-resistant to b-lactam, fluoroquinolones and tetracycline antibiotics. For the photoinactivation of de *E. coli* ATCC 25922, using chlorin **8** at a concentration of 1 μM , an average reduction of 1.5 log CFU for a light dose of de 2.5 J/cm^2 , was observed and a reduction of 2 log CFU for a light dose of 5 J/cm^2 , when irradiating with a LED at 650 nm (Figure 4.9). When using a higher concentration (10 μM), both light doses led to the total inactivation of *E. coli* (7 log CFU). Some dark toxicity is observed at these concentrations (1 log).

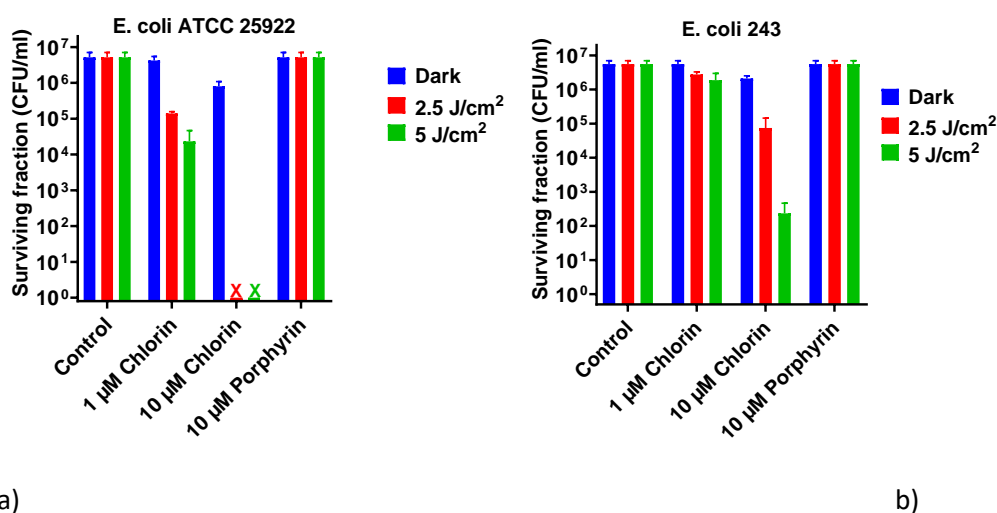


Figure 4.9: a) PDI in planktonic cultures of a laboratory type *E. coli* (ATCC 25922) and b) a multi-drug resistant *E. coli* 243, using 5,15-bis(1,3-dimethyl)imidazolyl) chlorin and the correspondent porphyrin for comparative purposes. (Illuminated with a red LED (659 nm, 7.2 mW/cm^2)

It should be noted that for similar concentrations to the chlorin, using porphyrin **4** as a PS with irradiation at 659 nm did not lead to any phototherapeutic effect in any of the bacterial strains, due to its low molar absorption coefficient at this wavelength.

Finally, photoinactivation studies using the multi-resistant *E. coli* 243 strain were performed. With chlorin concentrations of 1 μM , less photoinactivation was observed at 2.5 J/cm^2 and 5 J/cm^2 . Nonetheless, using a concentration of 10 μM of photosensitizer, the photoinactivation was dependent on the light dose. At 2.5 J/cm^2 , 1.5 log CFU inactivation was observed and at 5 J/cm^2 , 4 log CFU reduction was achieved. Once again, using the corresponding porphyrin did not produce any antimicrobial photoinactivation.

These studies clearly show the great advantages of using 5,15-bis(1,3-dimethylimidazol-2-yl) chlorin, with a high absorption in the therapeutic window for future transposition for the *in vivo* studies, where light penetration is a determining factor for efficient photoinactivation of microorganisms that cause topical infections.

4.3. Conclusions

The experimental work that gave rise to the writing of this MSc thesis culminated with *in vitro* pre-clinical development of a process to obtain the lead photosensitizer 5,15-dimethylimidazolyl chlorin (**8**) for potential aPDI application. Its synthesis, chemical and photophysical characterization, analytical development and preliminary biological assays against *E. coli* and SARS-CoV-2 were herein described.

It is well established that authorization by EMA or FDA for a new molecule to be submitted to clinical trials requires the development of a pilot synthesis under GMP conditions. Thus, the selection of chlorin **8** as lead compound was based on the following assumptions: i) Among the cationic imidazolyl porphyrins synthesized in Chapter 3 the 5,15-(1,3-dimethyl)imidazolyl porphyrin was the only one that met the requirement of absence of atropisomers, observed both by computational (Chapter 2) and experimental (Chapter 3) studies; ii) In this thesis we have developed, in PorphyChem laboratories a method for the synthesis of the porphyrin 5,15-(1-methyl)imidazolyl in multi-gram scale and with high purity, which ensures the availability of the necessary precursor for the synthesis of chlorin **8**; iii) the Pd/C hydrazine.H₂O reduction method described in this thesis allowed the synthesis of biocompatible chlorin **8**, which after flash chromatography purification, was obtained in 95 % isolated yield in the form of a single isomer with 80 % purity; iv) chlorin **8** shows high absorption in the therapeutic window has a low fluorescence quantum yield (0.159), shows high singlet oxygen quantum yield (0.71), has high photostability and low phototoxicity in the dark; a 4 log CFU inactivation of multi-resistant bacteria *E. coli* 243 was observed using chlorin **8** as photosensitizer at 10 μ M concentration; total inactivation of SARS-CoV-2 virus was achieved after inoculation with **8** and irradiation with 5 J/cm² under 0.3 M concentration. This concentration proved to be non-toxic for mammalian cells under the same conditions.

In sum, the studies developed in this MSc thesis have successfully fulfilled all requirements of *in vitro* pre-clinical development of a new drug (Figure 4.1), allowing a smooth transition to the GMP level, required for clinical transposition. This new photosensitizer **8** and the relevant collaborations established with Coimbra Hospital, Faculty of Pharmacy and CNC (Center for Neuroscience and Cell Biology) will certainly pave the way, in a near future, for the transposition to *in vivo* pre-clinical and clinical trials for photoinactivation of both multi-resistant bacteria and viruses, including SARS-CoV-2, at nasal level.

4.4. References

1. Ridings, J. E., The Thalidomide Disaster, Lessons from the Past. In *Teratogenicity Testing: Methods and Protocols*, Barrow, P. C., Ed. Humana Press: Totowa, NJ, **2013**; pp 575-586.
2. Taniguchi, M.; Lindsey, J. S., Synthetic chlorins, possible surrogates for chlorophylls, prepared by derivatization of porphyrins. *Chemical Reviews* **2017**, *117* (2), 344-535.
3. Whitlock, H. W.; Hanauer, R.; Oester, M. Y.; Bower, B. K., Diimide reduction of porphyrins. *Journal of the American Chemical Society* **1969**, *91* (26), 7485-7489.
4. Pineiro, M.; Pereira, M. M.; Rocha Gonsalves, A. M. d. A.; Arnaut, L. G.; Formosinho, S. J., Singlet oxygen quantum yields from halogenated chlorins: potential new photodynamic therapy agents. *Journal of Photochemistry and Photobiology A: Chemistry* **2001**, *138* (2), 147-157.
5. Pereira, M. M.; Abreu, A. R.; Goncalves, N. P. F.; Calvete, M. J. F.; Simões, A. V. C.; Monteiro, C. J. P.; Arnaut, L. G.; Eusébio, M. E.; Canotilho, J., An insight into solvent-free diimide porphyrin reduction: a versatile approach for meso-aryl hydroporphyrin synthesis. *Green Chemistry* **2012**, *14* (6), 1666-1672.
6. Pineiro, M.; Gomes, C.; Peixoto, M., Mechanochemical in situ generated gas reactant for the solvent-free hydrogenation of porphyrins. *Green Chemistry Letters and Reviews* **2021**, *14* (2), 339-344.
7. Aroso, R. T.; Guedes, R. C.; Pereira, M. M., Synthesis of computationally designed 2,5(6)-benzimidazole derivatives via Pd-catalyzed reactions for potential E. coli DNA gyrase B inhibition. *Molecules* **2021**, *26* (5), 1326.
8. Pineiro, M.; Carvalho, A. L.; Pereira, M. M.; Gonsalves, A. M. d. A. R.; Arnaut, L. G.; Formosinho, S. J., Photoacoustic measurements of porphyrin triplet-state quantum yields and singlet-oxygen efficiencies. *Chemistry – A European Journal* **1998**, *4* (11), 2299-2307.
9. Rurack, K.; Spieles, M., Fluorescence Quantum Yields of a Series of Red and Near-Infrared Dyes Emitting at 600–1000 nm. *Analytical Chemistry* **2011**, *83* (4), 1232-1242.
10. Vinagreiro, C. S.; Zangirolami, A.; Schaberle, F. A.; Nunes, S. C. C.; Blanco, K. C.; Inada, N. M.; Da Silva, G. J.; Pais, A. A. C. C.; Bagnato, V. S.; Arnaut, L. G.; Pereira, M. M., Antibacterial Photodynamic Inactivation of Antibiotic-Resistant Bacteria and Biofilms with Nanomolar Photosensitizer Concentrations. *ACS Infectious Diseases* **2020**, *6* (6), 1517-1526.

5. Experimental section

This chapter is divided into 6 sections. First are presented the computational analysis details, then the solvents and reagents, then instrumentation used throughout the experiments. Then, the experimental part associated with Chapter 3, followed by the experimental section of Chapter 4 and, finally, the experimental description of the photophysical characterization.

5.1. Computational analysis

Calculations. Molecular structures were optimized at the DFT level of theory, using the B3LYP hybrid functional¹⁻³ and the standard 6-31G(d,p) basis set. *Vibrational analysis* was performed to identify the *nature of the stationary points*. Calculations were performed by combining Gaussian 09⁴ and Gamess⁵ program packages. Gamess was used for geometry optimization while electron density maps were calculated with Gaussian. All calculations refer to the isolated molecules. The electronic densities of the chlorins with substituents are presented. Calculations were also performed to assess charge densities of alternative di-cationic photosensitizers of small size.

5.2. Solvents and reagents

All solvents were dried according to standard procedures. All reagents were used as delivered by Sigma-Aldrich-Merck, Acros, Fluorochem and PorphyrChem. Products such as chlorins sensitive to air were used under argon atmosphere and vacuum.

Deuterated chloroform, methanol and acetone were used to obtain ¹H-NMR spectra. The chloroform was neutralized using grade I basic alumina.

The control of the reactions was done using Thin Layer Chromatography (TLC), using aluminum plaques covered with silica gel 60 with a fluorescence indicator UV254. TLC plaques coated with silica gel C₁₈ with fluorescence indicator UV254 were used for the cationic photosensitizers.

The purification of the compounds was performed using silica gel (granulometry 0.040-0.063 μm), reverse phase C₁₈ silica gel (40-63 μm) or grade 1 basic alumina oxide (40-300 μm). In adsorption chromatography or flash chromatography, granulometry F0025, reverse phase C₁₈, were used.

Solvent purification:

-Dichloromethane, n-hexane and ethyl acetate

The solvent was left to reflux for two hours in the presence of calcium chloride anhydride and pumice, then they are distilled under the appropriate temperature. The solvents were passed through a short grade I basic alumina column to remove the remaining water and acid.

5.3. Instrumentation

I- Ultraviolet-Visible Spectroscopy

UV-vis spectra were recorded on Hitachi U-2001 or Shimadzu 2100 spectrophotometers using spectroscopic grade solvents.

II- Fluorescence Quantum yield

The fluorescence studies were performed at room temperature, in a *Horiba-Jobin-Ivon SPEX Fluorog 3-22* fluorimeter, equipped with a xenon 450W. Quartz cells were used, with an optical path of 1cm. Corrections were done for the wavelength of the system. For the chlorins, the instrument used was spectrometer PerkinElmer LS 45.

III- Mass Spectrometry

The mass spectra (ESI-FIA-TOF or MALDI) obtained at PorphyChem were obtained using the Applied Biosystems Voyager DE-STR spectrometer, equipped with a nitrogen laser ($\lambda=337$ nm). The matrix used in the assays was trans-2-[3-(4-tert-Butylphenyl)-2-methyl-2-propenylidene] malononitrile (DCTB).

The mass spectra ESI-TOF were performed using the spectrometer *Bruker Microtof* and the MALDI-TOF using *Bruker Autoflex* at the unit of mass spectrometry at the University of Santiago de Compostela.

IV- Nuclear Magnetic Resonance

The ^1H and ^{19}F NMR spectra were recorded on a 400 Bruker Avance III NMR spectrometer (400.101 and 376.5 MHz, respectively), using tetramethyl silane ($\delta = 0.00$ ppm) and TFA ($\delta = -76.55$ ppm) as internal standard. The multiplicity is indicated as follows: s - singlet, sl - large singlet, d - doublet, t - triplet, q - quartet, dd - double doublet, m – multiplet.

V- Ultra-sounds

The dissolution of some of the compounds was carried out inside an Ovan ultrasonic bath was used.

VI- High Performance Liquid Chromatography

HPLC methods were optimized using the HPLC system Agilent 1100 series with an automatic injector.

VII- Microwave

The reactions using microwaves were performed using the equipment CEM Discover® 600635 SP, using a gas addition kit (Discover® Gas Addition) connected to the gas line of the department of chemistry of the University of Coimbra. Appropriate 10mL glass tubes were used and a Teflon magnet. At PorphyChem, a Milestone MicroSYNTH labstation with a fibre optic probe for temperature control and vials of 50 mL were used.

VIII- Centrifuge

The Selecta Centromix-BLT centrifuge was used for certain samples.

IX- Flash chromatography

The reaction products were purified using a PuriFlash XS 420® flash chromatography equipment equipped with a UV diode array detector (Interchim, Montluçon, France). HP silica F0025 columns (0.15 μm) were used as stationary phase.

X- Muffle furnace

The samples were dried using the muffle furnace SNOL 8.2/1100 LHM01 at 100°C.

XI- Heidolph Rotavac G1

To evaporate the solvents, a Heidolph Rotavac G1 was used at the adequate temperature and rotation speed.

XII- pH meter

The pH of the buffer solutions used was measured using Mettler Toledo SevenCompact™ pH meter that was calibrated before use with the appropriate stock solutions.

XIII- Singlet Oxygen Quantum Yield

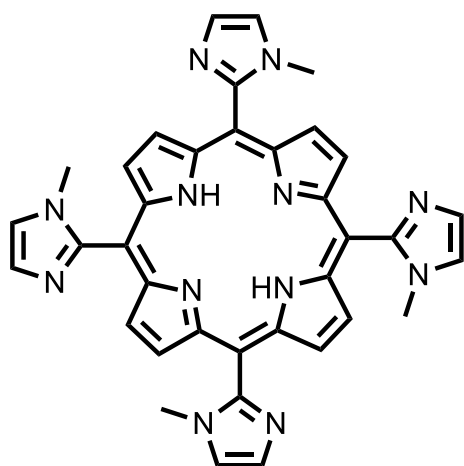
The quantum yield to form singlet oxygen was determined by collecting the steady state phosphorescence spectrum of oxygen in the spectrofluorometer Horiba Fluorolog. The phosphorescence was collected using a photomultiplier Hamamatsu R5509-42.

5.4. Porphyrin synthesis

5,10,15,20-tetra(1-methylimidazol-2-yl)porphyrin (1)

Nitrobenzene method: The porphyrin was synthesized with some modifications of the nitrobenzene method described in the literature.⁶ 1-methylimidazol-2-carboxyaldehyde (0.510 g; 4.62 mmol) was introduced into a 50 mL round bottom flask and a glacial acetic acid/nitrobenzene mixture (15 mL/7 mL) was added, followed by drop wise addition of pyrrole (0.32 mL; 5.00 mmol), under stirring, at room temperature (25 °C). The solution was maintained at 150 °C for 2 hours. Once the reaction mixture cooled down, the solvents were removed *via* low-pressure distillation. The work-up was carried out by washing the product with a concentrated solution of sodium bicarbonate. The organic phase was dried using anhydrous sodium sulphate, which was then filtered off and the solvent evaporated. The product was re-dissolved in dichloromethane and purification using adsorption column chromatography was performed using silica gel as stationary phase and dichloromethane:hexane (1:1) as the starting eluent. Once the remaining nitrobenzene was removed, the eluent's polarity was gradually changed from 10:0.1 to 10:1 (dichloromethane to methanol). The eluent was then changed to dichloromethane, methanol and ethanol (10:1:1) to finish the column. The solvent was evaporated, and the product was kept in the dark. The final product was obtained with a 19% yield (0.136 g).

Microwave method: In a 50 mL reactional flask, 1-methylimidazol-2-carboxyaldehyde (0.510 g; 4.62 mmol), 15 mL of propionic acid, 8 mL of nitrobenzene and 0.32 mL (5.00 mmol) of pyrrole were added. The mixture underwent microwave irradiation with Pmax=125W for 20 minutes at 175 °C with 22% stirring power. After repeating the reaction 4 times, the solvents were evaporated before performing a plug with alumina using heptane to remove the rest of the nitrobenzene, then dichloromethane and, finally, 3% methanol. A recrystallization was performed using methanol and diethyl ether. The product was obtained with a 21% yield (0.451 g).



¹H NMR (400 MHz, CDCl₃) δ, ppm: 8.90-8.75 (m, 8H_β), 7.66-7.58 (m, 4H), 7.45-7.41 (m, 4H), 3.49-3.28 (m, 12H), -2.88 to -3.05 (m, 2H_{NH})

ESI-MS m/z: obtained 631.2787 [M+H]⁺; calculated for [C₃₆H₃₁N₁₂]⁺ 631.2789

UV-Visible (CH₂Cl₂) λ_{max} (log ε): 420 (5.31); 513 (4.14); 587 (3.67); 658 (3.59) nm.

5,15-bis(1-methylimidazol-2-yl)porphyrin (2)

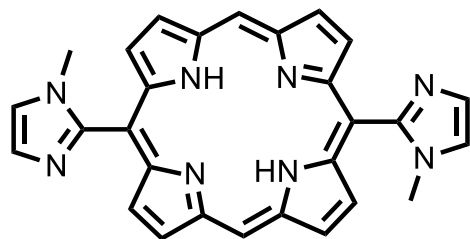
1-methylimidazol-2-carboxyaldehyde (0.334 g; 3 mmol) was added to 0.439 g (3 mmol) of dipyrromethene and dissolved in 300 mL of dichloromethane. The solution was left to degasify for 15 minutes using argon/vacuum system (3 times). Once degasified, 153 μL (2 mmol) of TFA were added. The solution was left at room temperature with a magnet and under vacuum, for 3 hours, protected from light.

2,3-Dichloro-5,6-dicyano-*p*-benzoquinone (DDQ) (2.041 g; 6 mmol) was added to the reaction mixture and left for 1 hour, protected from light, under stirring. The solvent was evaporated, and ethyl acetate was added. The solution was left in sodium bicarbonate with agitation overnight. This procedure was repeated for four days, using fresh sodium bicarbonate solutions. The solution was then filtered, and a TLC was performed using dichloromethane and methanol (10:1) as the eluent.

To purify this compound, an adsorption chromatography was done using silica gel as the stationary phase and dichloromethane:methanol (10:1) as the eluent. The product was obtained with a 11.9% yield (0.034 g).

Scale-up of 5,15-bis(1-methylimidazol-2-yl) porphyrin (2)

Dipyrromethane (13.27 g; 89 mmol) was dissolved in 17.2 L of dichloromethane and introduced onto a 20 L reactor. Then, 1-methylimidazol-2-carboxyaldehyde (9.99 g; 89 mmol) was added. The solution was bubbled with nitrogen along 15 minutes. After this period, trifluoroacetic acid (TFA) (4.20 mL; 56 mmol) was added. The solution was left with stirring at room temperature (25 °C), for 24 hours, protected from light. The oxidation was performed with tetrachloro-*p*-benzoquinone (28.56 g; 114 mmol). The reaction mixture was left at room temperature, for 2 hours under stirring, protected from light. The temperature was then risen to 60 °C and left for 1 h. Finally, triethylamine (31.96 mL; 228 mmol) was added and the reaction was maintained under stirring, for another 30 minutes. The solvent was evaporated to dryness. The crude was dissolved in the minimum amount of dichloromethane (100 mL) and a silica gel plug was performed, using initially dichloromethane as eluent and finally a mixture of dichloromethane/methanol (methanol up to 10%). The product was recrystallized from a mixture of dichloromethane:heptane. 5,15-bis(1-methylimidazol-2-yl)porphyrin was obtained in 16.8% yield (1.6 g).



¹H NMR (400 MHz, (CD₃)₂CO), δ, ppm: atropisomer mixture 10.67-10.63 (m, 2H), 9.69-9.67 (m, 4H), 9.11-9.10 (m, 4H), 7.83-7.81 (m, 2H), 7.67-7.65 (m, 2H), 3.67 (s, 3H), 3.61 (s, 3H), -3.30 to -3.16 (m, 2H).

ESI-MS m/z: obtained 471.2041 [M+H]⁺; calculated for [C₂₈H₂₃N₈]⁺ 471.2040

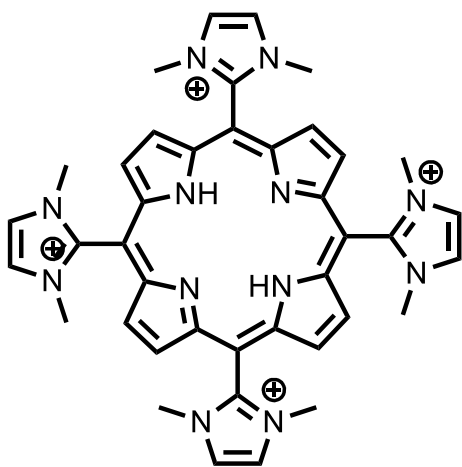
UV-Visible (CH₂Cl₂) λ_{max} (log ε): 406 (4.83); 501 (3.75); 535 (3.54); 573 (3.37); 627 (3.12) nm.

Synthesis of cationic porphyrins

General method: In a round bottom flask, the porphyrin was inserted with a large excess of the alkyl iodide in DMF, at a specific temperature depending on the alkyl iodide used (see Scheme 3.5). The evolution of the reaction was followed by TLC. The final product was precipitated using diethyl ether or *n*-pentane.

5,10,15,20-tetra(1,3-dimethylimidazol-2-yl)porphyrin tetraiodide (3)

Following the general procedure, the 5,10,15,20-tetra(1-methylimidazol-2-yl) porphyrin (30 mg; 0.0476 mmol) was dissolved in DMF (0.12 mL) and iodomethane (2.2 mL; 35.3 mmol) was added. The reaction was left, at room temperature, for 24 hours, under inert atmosphere, with stirring. The product was precipitated using diethyl ether. The spectroscopy data is according to the literature.⁷⁻⁸ The product was obtained with a 92% yield (0.030 g).



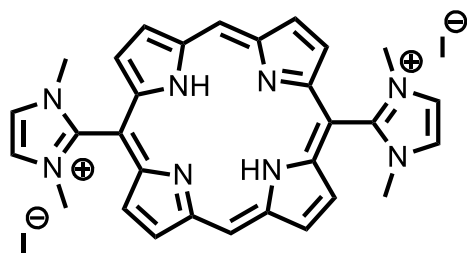
¹H NMR (400 MHz, DMSO) δ , ppm: 9.35 (sl; 8H), 8.53 (sl; 8H), 3.75 (sl; 24H), -3.21 (sl; 2H).

ESI-MS m/z: obtained 172.5908 [M-4I]⁴⁺/4; calculated for [C₄₀H₄₂N₁₂]⁴⁺/4 172.5908.

UV-Visible (H₂O) λ_{\max} (log ϵ): 407 (5.22); 507 (4.17); 541 (3.73); 579 (3.79); 630 (3.78) nm.

5,15-Bis(1,3-dimethylimidazol-2-yl)porphyrin diiodide (4)

Following the general procedure, the 5,15-bis(1-methylimidazol-2-yl) porphyrin (100 mg; 0.21 mmol) was dissolved in DMF (0.35 mL) and iodomethane (1.36 mL; 22 mmol) was added and the reaction was left with stirring at 30°C for 24h. After precipitation with diethyl ether porphyrin **4** was obtained in 82 % yield (0.074 g). The spectroscopic data was according to the literature.⁷



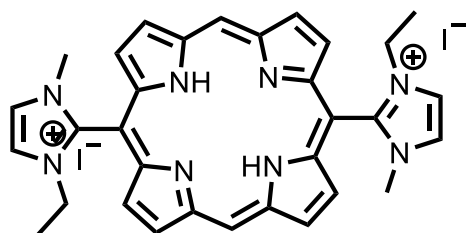
¹H NMR (400 MHz, CD₃OD) δ, ppm: 10.90 (s, 2H), 9.88-9.86 (m, 4H), 9.20-9.13 (m, 4H), 8.39 (s, 4H), 3.85 (s, 12H), -2.20 (s, 2H).

ESI-MS m/z: obtained 250.1218 [M-2I]²⁺/2; calculated for [C₃₀H₂₈N₈]²⁺/2 250.1213

UV-Visible (ethanol) λ_{max} (log ε): 395 (4.73); 496 (3.66); 532 (3.70); 572 (3.34); 625 (3.61) nm.

5,15-bis(1-methyl-3-ethylimidazol-2-yl)porphyrin diiodide (5)

Following the general procedure, the 5,15-bis(1-methylimidazol-2-yl) porphyrin (100 mg; 0.21 mmol) was dissolved in DMF (0.35 mL) and iodoethane (1.75 mL; 22 mmol) was added and the reaction was left with stirring at 70°C for 72h. After precipitation with diethyl ether **5** was obtained in 79 % (0.087 g) yield.



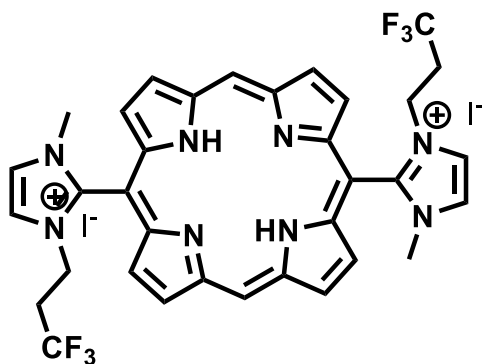
¹H NMR (400 MHz, CD₃OD) δ, ppm: 10.78 (s, 2H), 9.74-9.73 (m, 4H), 9.05 (sl, 4H), 8.37 (d, *J*=2.2Hz, 2H), 8.29 (d, *J*=2.2Hz, 2H), 4.02 (q, *J*=7.3Hz, 4H), 3.72 (s, 6H), 1.19-1.16 (m, 6H);

ESI-MS m/z: obtained 528.2743 [M-2I]⁺; calculated for [C₃₂H₃₂N₈]⁺ 528.2744

UV-Visible (ethanol) λ_{max} (log ε): 396 (4.52); 497 (3.95); 531 (4.00); 572 (3.63); 625 (3.92) nm.

Synthesis of 5,15-bis(1-methyl-3-(1,1,1-trifluoropropyl)imidazol-2-yl)porphyrin diiodide(6)

Following the general procedure, the 5,15-bis(1-methylimidazol-2-yl)porphyrin (50 mg; 0.11 mmol) was dissolved in 0.4 mL of DMF and 1,1,1-trifluoropropyl iodide (0.05 mL; 42 mmol) was added and the reaction was left with stirring at 85 °C for 4 days. After precipitation with a mixture of CH₂Cl₂ and n-pentane, **6** was obtained in 84% yield (0.061 g).



^1H NMR (400 MHz, CD_3OD) δ 10.94 (s, 2H), 9.92-9.87 (m, 4H), 9.23 – 9.15 (m, 4H), 8.62-8.59 (m, 2H), 8.51-8.47 (m, 2H), 4.50-4.40 (m, 4H), 3.97-3.87 (m, 6H), 2.77-2.61 (m, 4H).

^{19}F NMR (400 MHz, CD_3OD) δ -66.72 to 66.75 (m, 6F).

ESI-MS m/z: obtained 664.2467 $[\text{M}-2\text{I}]^+$;
calculated or $[\text{C}_{34}\text{H}_{30}\text{F}_6\text{N}_8]^+$ 664.2492

UV-Visible (ethanol) λ_{max} (log ϵ): 395 (5.72); 498 (3.54); 533 (3.60); 572 (3.17); 626 (3.49) nm.

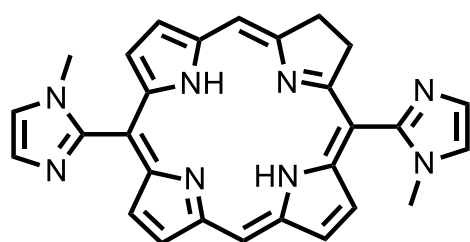
5.5. Chlorin synthesis

Synthesis of 5,15-bis(1-methylimidazol-2-yl)chlorin (7)

Hydrazine method: The 5,15-bis(1-methylimidazol-2-yl)porphyrin (100 mg; 0.2 mmol) was dissolved in dimethyl formamide (DMF) (2.5mL). Then, C/Pd (5%) (10 mg) and hydrazine ($\text{NH}_2\text{NH}_2 \cdot \text{H}_2\text{O}$) (0.70 mL; 0.014 mmol) were added. The reaction was monitored by UV-vis. Once the reaction was completed, the palladium was filtered off and the crude was washed with dichloromethane/water. The organic layer was dried using anhydrous sodium sulfate and the solvent was evaporated. Then, the solid was recrystallized from dichloromethane/diethyl ether and dried under vacuum. To separate the chlorin from the porphyrin, a Flash chromatography was performed using methanol and an ammonium acetate buffer (1 L distilled water, 800 mg of ammonium acetate and the pH 9 was adjusted using a 30% solution of NaOH 1M). Two F0025 (32 g), reverse phase columns. The elution steps are described in Table 5.1. 91 mg (91% yield) of 5,15-bis (1-methylimidazol-2-yl) chlorin was obtained with 80% purity. Therefore, the NMR spectra contains the peaks of porphyrin (20%) as well as the chlorin peaks described below.

Table 5.1: Elution steps used for the purification of chlorin 7.

N°	Time	Flow Rate	%A	%B	%C
01	40:12	2.0	70	30	00
02	50:12	2.0	70	30	00
03	51:12	2.0	75	25	00
04	59:12	2.0	75	25	00
05	01:02:02	2.0	90	10	00
06	01:02:05	5.0	90	10	00
07	01:04:12	5.0	100	00	00
08	01:05:31	5.0	88	00	12
09	01:05:34	10.0	88	00	12
10	01:14:12	10.0	10	00	90
11	01:19:12	10.0	10	00	90
12	01:30:12	10.0	10	00	90
13	01:35:12	10.0	10	00	90



¹H NMR (400 MHz, (CD₃)₂CO), δ, ppm: 10.12-10.11 (m, 1H), 9.42-9.41 (m, 1H), 9.31-9.29 (m, 1H), 9.13-9.11 (m, 2H), 8.88-8.87 (m, 1H), 8.52-8.51 (m, 1H), 8.37-8.36 (m, 1H), 7.74-7.51 (m, 4H), 4.84-4.79 (m, 2H), 4.67-61 (m, 1H), 4.27-4.21 (m, 1H), 3.69-3.57 (m, 6H), -1.49 (s, 1H), -1.80 (s, 1H).

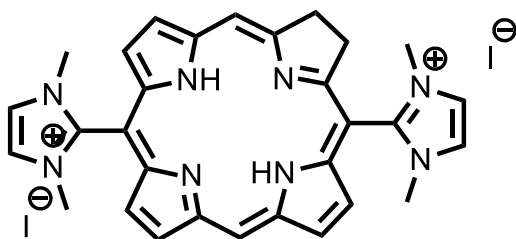
ESI-MS: obtained 473.2195 [M+H]⁺; calculated for [C₂₈H₂₄N₈]⁺ 472.2124

UV-Visible (CH₂Cl₂) λ_{max} (relative %): 406 (100); 506 (51); 528 (34); 589 (21); 645 (81) nm.

Synthesis of cationic chlorins

Synthesis of 5,15-bis(1,3-dimethylimidazol-2-yl)chlorin diiodide (8)

5,15-bis(1-methylimidazol-2-yl)chlorin (100 mg) was dissolved in DMF (0.5 mL) and a large excess iodomethane (1.8 mL; 29 mmol) was added. The reaction was maintained at 30°C for 24h, under argon atmosphere. The progression of the reaction was followed by thin layer chromatography (TLC). The product was precipitated with diethyl ether and the solid was filtrated and dried under vacuum. The 5,15-bis(1,3-dimethylimidazol-2-yl)chlorin diiodide was obtained in 95% yield.



¹H NMR (400 MHz, (CD₃)₂CO), δ, ppm:

10.29 (s, 2H), 9.53-9.51 (m, 4H), 8.92-8.91 (m, 2H), 8.44-8.42 (m, 4H), 4.40-4.38 (m, 4H), 3.85-3.83 (m, 12H).

ESI-MS m/z: obtained 251.1283 [M]²⁺/2; calculated for [C₃₀H₃₀N₈]²⁺/2 251.1291.

UV-Visible (CH₂Cl₂) λ_{max} (relative %): 395 (100); 500 (7); 537 (4); 570 (2); 644 (12) nm.

5.6. Photochemical characterization studies:

UV-vis spectroscopy

The molar absorption coefficients of the samples were obtained using quartz cells with an optical path of 1 cm. They were obtained using the appropriate solvent at 5 different concentrations for the Soret and five for the Q bands. A calibration curve was obtained in order to calculate the molar absorption coefficient, using the Beer-Lambert law ($A = \epsilon lc$), where A is the absorbance, ϵ is the molar absorption coefficient, l is the length of the optical path and c is the concentration of the solution.

Generally, a stock solution with a concentration of 10^{-4} was prepared and solutions with concentrations ranging from 10^{-5} to 10^{-7} were prepared using the stock solution. The absorbances were then noted to calculate the molar absorption coefficient.

Fluorescent quantum yield

Fluorescence experiments were performed in a spectrometer PerkinElmer LS 45. Porphyrin samples were excited at 420 nm, using Tetraphenylporphyrin (TPP) as a reference in toluene, $\phi F = 0.11$,¹⁰ with optical absorption ca. 0.01 at Soret band. Fluorescence of samples was determined in ethanol, applying a correction factor for the refractive index in the determination of fluorescence quantum yield. Chlorin samples were excited at 652 nm, using oxazine 170 as reference in ethanol, $\phi F = 0.579$.⁹ The absorbance of samples and reference were ca. 0.01 at 652 nm.

Fluorescence quantum yield were determined by integrating the emission spectra, in wavenumber scale, following the equation 5.1:

$$\phi F(\text{sample}) = \frac{\text{Area}(\text{sample})}{1 - 10^{-\text{Abs}(\text{sample})}} * \frac{1 - 10^{-\text{Abs}(\text{ref})}}{\text{Area}(\text{ref})} * \frac{\eta^2(\text{sample})}{\eta^2(\text{ref})} * \phi F(\text{ref}) \quad (5.1)$$

The area refers to the integration of the fluorescence spectra, Abs to the absorbance in the appropriate wavelength and η to the refraction index in the solvent where the sample is dissolved.

Singlet oxygen quantum yield

The quantum yield to form singlet oxygen was determined by collecting the steady-state phosphorescence spectrum of oxygen in the spectrofluorometer Horiba Fluorolog. The phosphorescence was collected using a photomultiplier Hamamatsu R5509-42, with voltage set at 1750 volts, cooled to 193 K in a liquid nitrogen chamber. The cutoff filter Newport 10LWF-1000-B was used to avoid fluorescence light.

Methylene blue was employed as a reference, $\phi\Delta = 0.50$.¹¹ Excitation was either 625 nm for porphyrins or 650 nm for chlorins. Optical absorption in both wavelengths was ca. 0.3. All samples were prepared in ethanol.

The calculation of the yield was performed using equation 5.2.

$$\phi\Delta(\text{sample}) = \frac{\text{Slope}(\text{sample})}{1 - 10^{-\text{Abs}(\text{sample})}} * \frac{1 - 10^{-\text{Abs}(\text{ref})}}{\text{Slope}(\text{ref})} * \frac{\eta^2(\text{sample})}{\eta^2(\text{ref})} * \phi\Delta(\text{ref}) \quad (5.2)$$

Photostability assays

In order to determine the photodegradation quantum yield, 3mL of solutions either in DMSO or water or cell culture medium were irradiated by LED light sources. A LED emitting at 630 nm and total output power of $P = 5\text{mW}$. A LED emitting at 660nm and total output power of $P = 13\text{mW}$ was employed for chlorins. The solutions were kept stirring during the experiment and optical absorption spectra recorded in function of irradiation time for 3 hours. The light doses used to induce photodegradation were corrected considering the overlap between the spectra of light sources and those of optical absorption.

5.7. Bibliography

1. Becke, A. D., Density-functional exchange-energy approximation with correct asymptotic behavior. *Physical Review A* **1988**, 38 (6), 3098-3100.
2. Becke, A. D., Density-functional thermochemistry. III. The role of exact exchange. *The Journal of Chemical Physics* **1993**, 98 (7), 5648-5652.
3. Lee, C.; Yang, W.; Parr, R. G., Development of the Colle-Salvetti correlation-energy formula into a functional of the electron density. *Physical Review B* **1988**, 37 (2), 785-789.
4. Frisch, M. J.; Trucks, G. W.; Schlegel, H. B.; Scuseria, G.; Robb, M. A.; Cheeseman, J. R.; Scalmani, G.; Barone, V.; Mennucci, B.; Petersson, G. A.; Nakatsuji, H.; Caricato, M.; Li, X.; Hratchian, H. P.; Izmaylov, A. F.; Bloino, J.; Zheng, G.; Sonnenberg, J. L.; Hada, H.; Ehara, M.; Toyota, K.; Fukuda, R.; Hasegawa, J.; Ishida, M.; Nakajima, T.; Honda, Y.; Kitao, O., N., H.; Vreven, T.; Montgomery, J. A.; Peralta, J. E.; Ogliaro, F.; Bearpark, M.; Heyd, J. J.; Brothers, E.; Kudin, K. N.; Staroverov, V. N.; Kobayashi, R.; Normand, J.; Raghavachari, K.; Rendell, A.; Burant, J. C.; Iyengar, S. S.; Tomasi, J.; Cossi, M.; Rega, N.; Millam, J. M.; Klene, M.; Knox, J. E.; Cross, J. B.; Bakken, V.; Adamo, C.; Jaramillo, J.; Gomperts, R.; Stratmann, R. E.; Yazyev, O.; Austin, A. J.; Cammi, R.; Pomelli, C.; Ochterski, J. W.; Martin, R. L.; Morokuma, K.; Zakrzewski, V. G.; Voth, G. A.; Salvador, P.; Dannenberg, J. J.; Dapprich, S.; Daniels, A. D.; Farkas, O.; Foresman, J. B.; Ortiz, J. V.; Cioslowski, J.; Fox, D. J. *Gaussian 09*, Gaussian Inc., Wallingford, CT, USA. , **2009**.
5. Schmidt, M. W.; Baldrige, K. K.; Boatz, J. A.; Elbert, S. T.; Gordon, M. S.; Jensen, J. H.; Koseki, S.; Matsunaga, N.; Nguyen, K. A.; Su, S.; Windus, T. L.; Dupuid, M.; Montgomery, J. A. *Gamess, Journal of computational chemistry*, **1993** 1347-1363;.
6. Gonsalves, A. M. d. A. R.; Varejão, J. M. T. B.; Pereira, M. M., Some new aspects related to the synthesis of meso-substituted porphyrins. *Journal of Heterocyclic Chemistry* **1991**, 28 (3), 635-640.
7. Vinagreiro, C. S.; Zangirolami, A.; Schaberle, F. A.; Nunes, S. C. C.; Blanco, K. C.; Inada, N. M.; da Silva, G. J.; Pais, A. A. C. C.; Bagnato, V. S.; Arnaut, L. G.; Pereira, M. M., Antibacterial Photodynamic Inactivation of Antibiotic-Resistant Bacteria and Biofilms with Nanomolar Photosensitizer Concentrations. *ACS Infectious Diseases* **2020**, 6 (6), 1517-1526.
8. Maximiano, R. V.; Piovesan, E.; Zílio, S. C.; Machado, A. E. H.; de Paula, R.; Cavaleiro, J. A. S.; Borissevitch, I. E.; Ito, A. S.; Gonçalves, P. J.; Barbosa Neto, N. M., Excited-state absorption investigation of a cationic porphyrin derivative. *Journal of Photochemistry and Photobiology A: Chemistry* **2010**, 214 (2), 115-120.
9. Rurack, K.; Spieles, M., Fluorescence Quantum Yields of a Series of Red and Near-Infrared Dyes Emitting at 600–1000 nm. *Analytical Chemistry* **2011**, 83 (4), 1232-1242.
10. Seybold, P. G.; Gouterman, M., Porphyrins: XIII: fluorescence spectra and quantum yields. *Journal of Molecular Spectroscopy* **1969**, 31 (1), 1-13.
11. Redmond, R. W.; Gamlin, J. N., A compilation of singlet oxygen yields from biologically relevant molecules. *Photochem Photobiol* **1999**, 70 (4), 391-475.